DISSERTATION ZUR ERLANGUNG DES DOKTORGRADES
DER FAKULTÄT FÜR CHEMIE UND PHARMAZIE
DER LUDWIG-MAXIMILIANS-UNIVERSITÄT MÜNCHEN

Sensory Monitoring and Laser-Induced Initiation of Primary Explosives: Impact Sensitivity and Laser-Induced Decomposition Studies on Sensitive Peroxides

Emre Ünal
aus
Siegburg, Deutschland

2024

Erklärung

Diese Dissertation wurde im Sinne von §7 der Promotionsordnung vom 28. November 2011 von Prof. Dr. Thomas M. Klapötke betreut.

Eidesstattliche Versicherung

Diese Dissertation wurde eigenständig und ohne unerlaubte Hilfe erarbeitet.

Siegburg, den 18.10.2024

Emre Ünal

Dissertation eingereicht am: 18.10.2024

Erstgutachter: Prof. Dr. Thomas M. Klapötke

Zweitgutachter: Prof. Dr. Peter-Michael Kaul

Mündliche Prüfung am: 17.02.2025

Contents

Part I

Introduction

Energetic Materials

Energetic materials (EMs) are compounds or mixtures of substances that contain both fuel and an oxidizer. When these materials react, they release thermal energy and produce a large amount of gas. The initiation of these substances can be triggered by mechanical, thermal, electrostatic, or optical influence. A distinction is made between materials that are capable of exploding and those that are hazardous due to their potential to explode [1].

EMs are not only used for military purposes, but also for civilian applications, such as in airbags, fireworks or explosives in mining. It has been a long way from the initial invention of the first explosives to their widespread use today. In 220 B.C., the Chinese accidentally discovered black powder. Centuries later, in the 13th and 14th centuries, the monk Roger Bacon and the German Berthold Schwarz researched the explosive for the first time in Europe. The military use of black powder began at this time. In 1846, nitroglycerine was discovered by Ascanio Sobrero. Alfred Nobel reduced the sensitivity of the highly sensitive nitroglycerine, thus making it possible to use the substance. The so-called dynamite was developed. Alfred Nobel also played an important role in the progress in the history of initial substances. His findings made it possible to reliably initiate dynamite by replacing black powder with mercury fulminate. This was replaced at the beginning of the 20th century by lead azide, which is still used today [2, 3].

In the following years, as demand increased, other explosives were developed and synthesised, many of which are still in use today. This led to the development of trinitrotoluene, triaminotrinitrobenzene and hexogen (RDX), for example. The focus in the development of energetic materials changed over time. In addition to reliability, the safe handling of the substances was often at the centre of research when it came to their commercial/military use. During the Second World

War, for example, the use of polymer-bound explosives was favoured, resulting in the production of Semtex, a mixture of nitropenta (PETN) and RDX bound with styrene-butadiene rubber. Today, the focus of the development of energetic materials is on environmentally friendly research into materials in terms of sustainability and the improvement of existing properties (e.g. shorter initiation times for special military applications).

1.1 Classification of Energetic Materials

1.1.1 Primary Explosives

Primary explosives ,or also called primaries, are substances that have a significantly faster transition from combustion or deflagration to detonation than secondary explosives. They are highly sensitive to thermal, electrostatic and mechanical impact. Despite this, primary explosives have a significantly lower power than secondary explosives [4, 1].

The main application of primary explosives is the initiation of secondary substances. The resulting shock wave of the initial substances is often sufficient to initiate the main charge. It is not always necessary for the primary to generate a shockwave to initiate the secondary explosive. In the case of priming charges, the primary substance acts as a sensitizer, enabling the ignition of a propellant, for example, by deflagrating without causing detonation. Examples of common primaries are lead azide, lead styphnate and silver azide. Certain explosives, such as hexamethylene triperoxide diamine (HMTD) and triacetone triperoxide (TATP), are not used in industrial or military applications due to their high reactivity and unpredictable behavior [5, 6, 7, 8, 9, 10].

TATP

TATP is an extremely sensitive and reactive compound, notable for its straightforward synthesis and the broad availability of its precursor substances. It is formed through an acid-catalyzed reaction involving a common organic solvent and a strong oxidizing agent. The reaction can be catalyzed by various acids that are easily obtainable, making the process accessible even to those with minimal

chemical expertise. The combination of its simple production and the widespread availability of its starting materials has led to its utilization in unauthorized and hazardous contexts. Due to its high explosive potential and the challenges associated with its detection by conventional security systems, this compound has been implicated in numerous illicit activities. Handling it is particularly dangerous, as it is highly sensitive to mechanical impact, friction, and temperature changes, which can lead to accidental detonation. The compound's instability presents significant risks during both synthesis and storage, posing challenges even for experienced professionals. Studies on its decomposition have shown that it can rapidly degrade into volatile and potentially harmful by-products, complicating its safe handling and forensic examination. Due to the instability and unpredictable nature of the compound its analysis is challenging, thus increasing the risks associated with its use. As a result, it is considered a major concern in terms of safety and security [11, 12, 13].

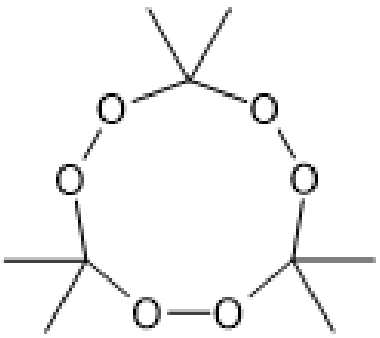

Figure 1.1: Structure formula of TATP

HMTD

HMTD is a highly reactive organic peroxide known for its sensitivity and significant explosive power. The compound is produced through an acid-catalyzed process involving hexamine and hydrogen peroxide, with citric acid or hydrochloric acid typically serving as the catalysts. Due to the ease of obtaining these materials, HMTD has become accessible even to those with minimal chemical expertise. This accessibility, combined with the straightforward synthesis process, has led to its use in various unauthorized activities. HMTD has been associated with several prominent incidents, including the thwarted Los Angeles airport bombing

attempt in 1999 and the London bombings of 2005 [6, 5, 7, 9].

However, HMTD is not adopted by military forces due to its extreme sensitivity to physical stimuli, such as impact, friction, and heat, which can easily trigger an accidental explosion. This high reactivity makes HMTD dangerous to handle, posing significant risks during both production and storage. Research into the decomposition of HMTD has shown that it breaks down over time into volatile by-products, which is particularly important for forensic identification. The compound's instability and the associated difficulties in handling and analysis create substantial challenges for forensic experts, making it a significant concern for both safety and security.

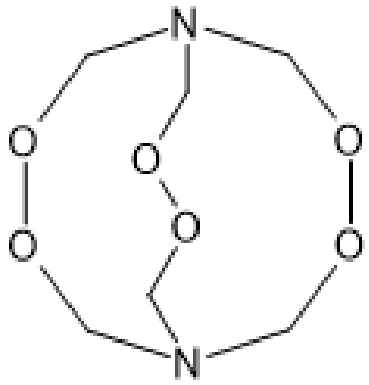

Figure 1.2: Structure formula of HMTD

1.1.2 Secondary Explosives

The term secondary explosive covers all substances that are used to create an explosive effect and which must be initiated by the detonation impact of a primary. Compared to primary explosives, they are relatively insensitive, which means that they can also be handled on a larger scale. They form the actual detonating effect and performance in explosives technology [1].

Secondary explosives can be categorized into booster explosives and high explosives. The distinction lies in the fact that booster explosives are more easily initiated and are designed to transmit and amplify the shock wave from the primary explosive to the main charge. PETN is a commonly used booster explosive in various applications. In contrast, the main charge, typically a high explosive

like RDX, is more difficult to initiate directly [14, 4, 15].

1.2 Explosion

Explosions are dynamic processes fundamentally driven by the natural tendency of gases to expand rapidly and are characterized by the spontaneous release of energy. These events involve a rapid chemical reaction that simultaneously generates substantial quantities of gas and heat. The swift expansion of gases results in a powerful force that can cause significant physical disruption.

In the study of explosions, a distinction is made between two types of explosive reactions: detonation and deflagration. These classifications are based on the specific speed of sound in the material at which the reaction front propagates and the nature of the energy release. Each type has distinct characteristics and implications for the effects and damage caused by the explosion [16].

Detonation

In a detonation, the decomposition reaction occurs at velocities well above the speed of sound, typically ranging from 1500 to 9000 m/s. This rapid reaction is intrinsically linked to a shock wave, characterized by sudden and extreme increases in both pressure and temperature. Detonation can be triggered either by the direct transfer of energy from an initial explosive material or by the accelerating combustion of the substance, where a deflagration progresses into a detonation. The intense conditions generated by the shock wave are responsible for the substantial destructive force associated with detonation [1].

Deflagration

Deflagration is a decomposition reaction that takes place at subsonic speeds, meaning below the specific speed of sound in the material. It can be described as a fast-burning process within the material, where the reaction is self-sustained by the heat it produces, and the resulting gases flow in the opposite direction to the advancing reaction front. Depending on the method of initiation or the specific burning conditions, deflagration can sometimes transition into detonation [1].

1.3 Ignition and Initiation of Energetic Materials

The initiation of explosives and the ignition of energetic materials can be triggered in various ways, including heat, shock, or mechanical impact. These mechanisms can lead to outcomes such as ignition, deflagration, or detonation, depending on the intensity of the initiating force. Each explosive material has a specific ignition temperature, which depends on whether the heat generated during the reaction exceeds the heat lost to its surroundings [17, 18].

The initiation process is primarily thermal, with shockwaves causing adiabatic compression that results in significant heat generation. Mechanical impacts, friction, or electrical inputs like electrostatic discharge (ESD) also convert their respective energies into heat, leading to the formation of small, localized hotspots. These hotspots can reach temperatures as high as 900°C, especially when caused by the adiabatic compression of gas bubbles within the explosive material. These bubbles play a key role in both liquid and solid explosives [19].

Frictional heating can also produce hotspots, especially when small, hard crystals or crystalline needles within the explosive are deformed or broken. The energy released in these processes may generate hotspots, but not all of them will lead to ignition or detonation. Whether a reaction is sustained depends on whether sufficient heat is generated before it dissipates. Typically, secondary explosives require temperatures around 400°C within a hotspot to initiate, so materials with lower melting points are less likely to be initiated by such mechanisms [20].

For liquid explosives, hotspots caused by the adiabatic compression of gas bubbles can also lead to initiation, though these hotspots are very short-lived. Friction between crystals can generate enough heat to form hotspots, particularly in materials with lower thermal conductivity. In primary explosives, initiation by impact usually results from inter-crystalline friction, while in secondary explosives, impact initiation often arises from gas bubbles between crystals that exist only briefly, around 10^{-6} seconds [21].

Understanding these mechanisms is crucial for the safe handling and application of explosives. This knowledge is instrumental in designing materials that are both stable and capable of controlled reactions, supporting advancements in

the field of energetic materials [22, 23].

1.3.1 Laser Initiation

A widely utilized and modern approach to initiating explosives is through laser initiation, which offers distinct advantages over traditional methods. In a military context, one significant benefit is the extremely short duration in which the laser pulse interacts with the explosive material. Laser initiation induces the detonation of the explosive through the interaction of the laser beam with the energetic material, with key factors such as laser power, wavelength, pulse duration, and spot size playing crucial roles [24].

This technique provides substantial benefits over conventional initiation methods, including immunity to electromagnetic interference, precise control over the initiation process, and the ability to detonate explosives that are otherwise less sensitive. Laser-induced detonation generally occurs through one of three primary mechanisms: direct interaction with the explosive, rapid heating of a thin film in contact with the explosive, or the ablation of a thin metal foil to create a high-velocity flyer plate that impacts the explosive. In the first mechanism, the laser beam directly interacts with the explosive material, causing the material to absorb the laser energy and subsequently heat up. This energy absorption can result in the formation of hotspots within the material, which then ignite and propagate a reaction wave. The efficiency of this mechanism is influenced by factors such as the laser's wavelength, pulse duration, and the physical characteristics of the explosive, including its density and specific surface area. The second mechanism involves the rapid heating of a thin metal film that is in contact with the explosive. The laser energy causes the metal film to heat up rapidly, transferring this heat to the explosive and thereby initiating a reaction. While this method allows for controlled detonation, its reliability can vary depending on the type of explosive. The third mechanism, which is particularly effective for insensitive explosives, involves the use of laser-driven flyer plates. In this approach, a thin metal foil is ablated by the laser, creating a high-speed flyer plate that strikes the explosive and generates a shock wave, leading to detonation. This method is currently considered the most practical and effective for detonating insensitive explosives due to its reliability and effectiveness in operational scenarios [25, 26].

In summary, the findings from the previous investigations suggest that laser initiation is predominantly a thermal process, although the precise mechanisms and the factors influencing them remain incompletely understood. Typically, a thermal mechanism implies that laser light is absorbed by the material and subsequently converted into heat, possibly through processes like internal conversion.

At lower laser power levels, ranging from approximately 10^{-1} to 10 W, explosives tend to undergo a deflagration-to-detonation transition (DDT) after being heated to their auto-ignition temperatures. However, at higher laser powers, typically around 100 W or more, shock initiation of the explosive occurs, and the DDT process is no longer observed.

Hafenrichter et al. identified four distinct regimes of laser initiation, each defined by the surface power density, or irradiance. At low power densities, the material reaches a steady-state temperature without triggering ignition, as the heat dissipates before auto-ignition can occur. As the power density increases to the kW/cm^2 range, ignition begins to take place, though the delay times are relatively long, on the order of milliseconds, due to significant heat conduction away from the ignition site.

At even higher power densities, in the mW/cm^2 range, the material reaches its auto-ignition temperature rapidly, before substantial heat dissipation can occur, resulting in much shorter ignition delay times on the order of microseconds. Finally, at extremely high power densities, in the gW/cm^2 range, the explosive is shock-initiated by laser-induced ablation of the surface, leading to ignition delay times in the ns range. This progression of behaviour with increasing power density highlights the complex and multifaceted nature of laser initiation in energetic materials [27].

1.4 Testing methods

1.4.1 Impact Sensitivity

The drop hammer test is a fundamental method for assessing the impact sensitivity of explosives. In this test, a weight is dropped from a specified height onto a sample to determine the energy required to induce a reaction, such as ignition or detonation. Due to its straightforward nature and efficiency, the drop hammer

test is widely employed for the preliminary evaluation of explosives. Its simplicity and speed are particularly advantageous, as the procedure involves only a drop weight, a height-adjustable fixture, and the sample material, allowing for rapid testing and quick results. This test is versatile and can be applied to various forms of explosives, including single crystals, powder coatings, pressed pellets, gels, polymer-bonded explosives (PBX), and propellants, making it a valuable tool for assessing a wide range of energetic materials.

However, the drop hammer test has certain limitations. One significant drawback is its inability to provide detailed insights into the nature and severity of the reaction it triggers. While the test can indicate the occurrence of a reaction, it does not differentiate between different types of decomposition, such as detonation and deflagration. This lack of specificity can be a limitation when more detailed analysis of explosive behavior is required.

Another issue with the drop hammer test is the variability of results, which can arise from differences in test methods and operator handling. Factors such as sample preparation, precise alignment of the apparatus, and subjective interpretation of the results can introduce inconsistencies, affecting the reliability and reproducibility of the test outcomes. Furthermore, the BAM drop hammer, a specific variant used for characterizing explosives, may yield limited insights into impact sensitivity due to the potential for sample ignition by adiabatic compression during the preparation process.

Recent studies suggest that by equipping drop hammers with a variety of sensors, it is possible to extract significantly more information than the traditional binary yes/no outcome. For instance, integrating microphones to capture emitted sound or employing optical measurement techniques such as spectrometry or high-speed imaging has enhanced our understanding of explosive initiation. These advanced measurement methods have allowed for the detection and visualization of phenomena such as hotspots, providing a deeper insight into the mechanisms of explosive initiation [28, 29, 30].

1.4.2 Optical Initiation

Laser systems are widely employed to characterize various properties of energetic materials. A key objective is to evaluate how sensitive different explosives

are to laser energy, determine the optimal laser parameters, and assess the reliability of detonation under diverse conditions. These evaluations typically involve the use of pulsed high-power lasers, including Nd:YAG, CO_2, and excimer lasers, which provide the necessary energy to initiate reactions in the explosive materials. Another area of research focuses on determining the initiation thresholds of energetic materials. These studies contribute to advancements in the detection and neutralization of such substances. Crucial parameters that must be carefully controlled during these experiments include the wavelength of the laser, pulse duration, beam spot size, and the presence of confining materials. Research has indicated that the physical characteristics of the explosives, such as density and purity, as well as the presence of dopants, play significant roles in influencing the ignition threshold. Understanding how these factors interact with laser parameters is essential for accurately determining the sensitivity and detonation reliability of various explosives under a range of conditions [31, 32, 33].

1.5 Multivariate Statistics

Multivariate statistics involves the analysis of multidimensional data to uncover relationships and patterns within complex datasets. This statistical approach is especially valuable in challenging fields such as explosives detection, where it enhances the accuracy and reliability of identifying hazardous substances by integrating and analyzing data from various sources. In the realm of explosives detection, multivariate statistics is applied primarily in two key areas: sensor array-based detection and spectroscopy-based detection.

In sensor array-based detection, arrays of sensors generate intricate data patterns when exposed to different substances. By applying multivariate techniques, such as Principal Component Analysis (PCA) or Partial Least Squares Discriminant Analysis (PLS-DA), researchers can effectively distinguish between explosive and non-explosive materials based on the responses from these sensors. For instance, sensor arrays can detect trace residues of explosives by analyzing the collective outputs of the sensors, with multivariate statistical methods facilitating the classification and identification of the detected substances.

In spectroscopy-based detection, multivariate statistical methods are com-

bined with advanced spectroscopic techniques, such as Fourier Transform Infrared Spectroscopy (FTIR) and Laser-Induced Breakdown Spectroscopy (LIBS). These techniques yield spectral data that represent the molecular composition of the samples under investigation. Multivariate statistics are employed to analyze these spectral data, enabling the differentiation between various types of explosives. For example, FTIR spectra of different explosive materials can be processed using PCA and other clustering techniques to pinpoint the most discriminative spectral regions, thereby allowing for the accurate identification and classification of explosives.

PCA is a key method in this context, used to reduce the dimensionality of a dataset while preserving the majority of its variance. PCA achieves this by transforming the original variables into a new set of uncorrelated variables, known as principal components, which are ordered according to the amount of variance they explain in the data. This reduction in dimensionality simplifies the visualization and interpretation of complex datasets, enabling researchers to focus on the most significant components.

On the other hand, Linear Discriminant Analysis (LDA) is a technique primarily used for classification tasks. LDA works by finding a linear combination of features that maximizes the separation between two or more classes of objects or events. Specifically, LDA seeks to maximize the ratio of between-class variance to within-class variance, thereby ensuring optimal separability between the different classes in the dataset. This approach is particularly useful for distinguishing between explosive and non-explosive materials, contributing significantly to advancements in security and forensic science.

Overall, the application of multivariate statistical methods in explosives detection has greatly enhanced the ability to accurately and reliably identify hazardous materials. By leveraging the power of techniques such as PCA and LDA, researchers can analyze complex data more effectively, leading to improved safety and efficacy in both security measures and forensic investigations [34, 35].

1.6 Motivation

The in-depth study of explosives initiation mechanisms is fundamental to ensuring the safe handling and application of energetic materials across various fields, including military operations, mining, and security. One particularly challenging area is the precise and controlled initiation of energetic materials using laser radiation in conjunction with sensor-based monitoring systems. This approach raises numerous questions, especially when dealing with sensitive initiators. Current research on detection methodologies focuses on the influence of the laser source, emphasizing the importance of controlled energy coupling into the materials under investigation, even when specific absorption coefficients are not fully known.

To address this challenge, one potential solution involves the application of specialized coatings with well-defined absorption coefficients onto the materials. Techniques such as drop-coating, spray-coating, and others can be employed for this purpose. By carefully selecting laser parameters in conjunction with these coatings, it is possible to achieve controlled local initiation within critical geometrical constraints, thereby preventing the bulk material from undergoing detonation or deflagration. The gases and physical phenomena emitted during the reaction can then be analyzed to study the material and the processes occurring during initiation.

Additionally, the research aims to expand traditional testing methods, such as the drop hammer test used for assessing impact sensitivity, by incorporating analyses of the detonation reactions that occur.

To improve the understanding of how explosives respond to different load conditions, recent research has integrated a wide range of sensors into test setups. These sensors play a crucial role in enhancing safety measures and lowering the risk of unintended detonations. By applying multivariate statistical techniques to preprocess sensor data, the consistency of sensitivity test outcomes can be substantially increased. This approach not only allows for more accurate forecasting of reaction behaviour but also aids in identifying explosives based on their distinct physical reaction profiles.

Part II

Summary and Conclusion

Sensory monitoring of primary explosives via drop hammer impact tests

Investigating the aging effects on the impact Sensitivity of hexamethylene triperoxide diamine (HMTD) using modern sensor systems

This paper investigates the impact sensitivity of hexamethylene triperoxide diamine (HMTD), focusing on how the sensitivity and response behaviour evolve with ageing of the material. The study utilises a special drop hammer setup equipped with optical and acoustic sensors to monitor the responses of HMTD samples subjected to mechanical impact. These sensors provide detailed data on the onset and intensity of explosive reactions, allowing for the assessment of HMTD sensitivity at different stages of aging.

The research shows that the sensitivity of HMTD changes significantly with ageing. Freshly synthesised HMTD exhibits a different impact sensitivity to aged samples, with the aged material showing altered sensitivity and response characteristics. The study also takes into account the influence of mechanical factors, such as the size of the spheres used in the drop hammer tests. Larger balls, which have a larger surface area, tend to trigger more violent reactions, which emphasises the mechanical aspects of the sensitivity test.

In addition to the impact sensitivity tests, chemical composition of the HMTD samples was analysed using proton transfer reaction time-of-flight mass spectrometry (PTR-ToF-MS). This technique enabled the identification of decomposition products and provided information on the chemical changes that occur

during the ageing of HMTD.

The results of this study are important for the safe handling and storage of HMTD as they provide a deeper understanding of how ageing affects the explosive properties of HMTD. This research also emphasises the importance of considering both chemical and mechanical factors in sensitivity testing, providing valuable data for the development of protocols for the safe handling of explosives.

Ignition of primary peroxide explosives with a ns-pulsed laser

Investigation of laser-initiation of graphite spray-coated TATP accompanied by sensor-safe surveillance and analytical monitoring using Microphone and PTR-ToF-MS

The paper titled delves into the controlled initiation of TATP using laser radiation, with a particular focus on monitoring and analysing the resulting reactions. TATP, known for its extreme sensitivity and frequent use in improvised explosive devices, presents significant challenges in safety and detection, making it a critical subject of research.

The primary objective of this study is to understand how various laser parameters, including power levels and the application of a graphite coating, affect the initiation and decomposition of TATP. The graphite coating, chosen for its known absorption properties, is applied to see if it allows for more controlled energy input from the laser, thereby preventing a full-scale detonation and instead inducing partial reactions that can be safely monitored and analysed.

To achieve this, TATP was synthetised and prepared for experimentation, with some samples being coated with graphite. These samples were then subjected to irradiation using a pulsed Nd:YAG laser at different power levels. Throughout the experiments, a sensitive microphone and PTR-ToF-MS were used to monitor acoustic signals and analyse the gases emitted during the laser-induced reactions. Additionally, Raman spectroscopy was employed to verify the purity of the TATP

samples.

The findings reveal that the graphite coating has a significant impact on the behavior of TATP when exposed to laser irradiation. Specifically, the coated samples exhibited a higher frequency of partial reactions at lower power levels compared to their uncoated counterparts. This suggests that the graphite coating facilitates more localized energy absorption, which leads to controlled initiation rather than complete detonation. The data collected by the microphone showed variations in reaction intensity and occurrence based on the laser's power and the presence of the coating. Moreover, the PTR-ToF-MS analysis indicated differences in the chemical composition of the gases released during TATP's decomposition, reinforcing the conclusion that the graphite coating plays a crucial role in modulating the explosive reaction.

In conclusion, the study demonstrates that applying a graphite coating to TATP allows for more controlled initiation under laser irradiation, reducing the risk of full detonation and enabling safer handling and analysis. The results suggest that this technique could be valuable in developing improved detection and safety protocols for sensitive explosives like TATP. The research also points to the need for further studies on different coating materials and laser parameters to optimize the controlled initiation of explosives.

Investigation of laser initiation of graphite-coated TATP and HMTD with regard to the influence of coating thickness accompanied by sensor-safe surveillance using a microphone

This work explores the laser initiation of graphite-coated Triacetone Triperoxide (TATP) and Hexamethylene Triperoxide Diamine (HMTD) with a focus on understanding the influence of coating thickness on the controlled initiation of these sensitive explosives. By employing laser radiation in conjunction with sensor-based monitoring, the study aims to achieve controlled local initiation without triggering full detonation or deflagration.

The research involved synthesising TATP and HMTD, applying graphite coat-

ings of varying thicknesses to these explosives, and then irradiating them with a pulsed Nd:YAG laser at different power levels. The coated samples were closely monitored using a sensitive microphone to capture acoustic signals during the laser interaction. The study investigated how the thickness of the graphite coating influences the initiation threshold and the subsequent reaction behavior of the explosives.

The findings indicate that graphite coatings can significantly affect the initiation process, with thicker coatings leading to more controlled energy absorption and reduced risk of unintended detonation. The study's results contribute to the development of safer methods for handling and analysing highly sensitive explosives, emphasising the importance of coating materials and laser parameters in controlling explosive reactions.

Sensory Monitoring for Breakthrough Detection in Mobile Laser Cutting of Various Materials in the Context of IED Disposal

This work details the development of a mobile laser cutting system designed for the safe and efficient disposal of improvised explosive devices (IEDs) while preserving forensic evidence. The research, conducted in collaboration with various partners, focuses on integrating advanced sensor technologies into the laser cutting process to ensure precision and safety. The study explores the laser cutting of different materials, including those containing explosives, to determine optimal cutting parameters and sensor configurations.

The laser cutting system, which employs a pulsed Nd:YAG laser, is designed to be mounted on robotic platforms, allowing bomb disposal teams to operate from a safe distance. The system's sensors, including microphones, photodiodes, and infrared cameras, monitor the cutting process in real-time, providing feedback on material breakthroughs and ensuring that the cutting process does not ignite the explosive charge. The system's effectiveness in cutting various materials, such as plastics and metals, is evaluated, with special attention to the impact of laser parameters like fluence and pulse energy.

The study concludes that the integration of sensory monitoring into the laser cutting system significantly enhances its capability to safely handle and dispose of IEDs. The research also highlights the need for further optimization and testing, particularly regarding the system's ability to cut through different materials and its application in real-world scenarios. Overall, the project represents a significant advancement in the field of explosive disposal, offering a safer and more controlled approach to neutralizing hazardous devices.

Part III

Results and Discussion: Drophammer Experiments

Sensor-monitored impact sensitivity investigations on HMTD of different ageing stages with accompanying PTR-TOF measurements of the substances

by

Matthias Muhr, Emre Ünal, Phillip Raschke, Thomas M. Klapötke, Peter Kaul

DOI: 10.1080/07370652.2023.2295280

as published in
Journal of Energetic Materials 2023, 23, 1-23
(doi:10.1080/07370652.2023.2295280)

The work presented in this publication was conducted in collaboration with Mr. Matthias Muhr, with my personal contribution accounting for approximately 50 %. My main focus was on performing the analysis, synthesizing the substance, and setting up the hardware. This involved both the construction and refinement of the experimental setup, as well as the execution and optimization of the measurements. A particular emphasis was placed on adapting the methods to effectively capture the signals from HMTD.

Abstract: Hexamethylene triperoxide diamine (HMTD) is a commonly used homemade explosive due to its simple synthesis and availability of reactants. However, its impact sensitivity may vary significantly depending on synthesis methods and possibly substance ageing, presenting safety concerns during handling. In this study, two batches of HMTD, one stored for 3 months and one freshly synthesized, were investigated. Analytical techniques including Raman spectroscopy and PTR-ToF were utilized for the HMTD specimen. A custom-designed drop hammer based on OZM's Ball Impact Tester, equipped with optical and acoustic sensors, was employed to evaluate impact sensitivity and chemical reaction process. The setup was tested and validated with HMTD, TATP and lead azide and silver azide. Extracted features of sensor data were subjected to multivariate statistical analysis (LDA, PCA) to assess the impact of ageing to impact sensitivity and reaction characteristics. The study aimed to determine the correlation between substance composition and reaction behaviour. The results contribute to the understanding of the influence of ageing on the response and mechanical sensitivity of HMTD as well as the batch-to-batch variation.

4.1 Introduction

Although HMTD has no industrial or military use, HMTD) has been the subject of many technical and scientific studies as an organic peroxide explosive. The substance has been analysed in many studies using spectroscopic, colorimetric methods as well as sensitivity tests [1, 2, 3, 4, 5]. Good results have been obtained, which facilitate the detection and identification of the substance [3, 6, 7]. Nevertheless, this substance has been used in numerous illegal terrorist activities in recent years [8, 9]. The reason for this is the easy availability of the reactants, as well simple synthesis [10]. Due to the different synthesis routes as well as other processing methods, the resulting product can vary in its morphology and chemical composition. An important parameter for safe handling of explosives is the impact sensitivity, which is determined with the drop hammer experiment [11, 12, 13, 14]. The smallest energy required for ignition is determined by varying the energy of the drop weight by adjusting mass or height of it. The test gives a purely binary result and is dependent on the operator's perception [13].

Guhne et al. found out that good and more realistic results than conventional test device geometry can be achieved in initiation tests with the Ball Impact Tester from OZM (BIT). In this test setup, the sample is ignited by a steel ball falling vertically on the sample [11]. Another major disadvantage is that no information is gained about the course of the reaction or the violence. The problems and issues associated with impact sensitivity have been studied in a variety of applications. Drop hammer devices were equipped with sensors. The glass anvil drop hammer was used in several publications [15, 12, 16]. With these and other measurements using high-speed cameras, spectrometers and other physical sensors, it was possible to investigate various reaction processes and the formation of hot spots. A major problem in all initiation experiments with explosives is poor reproducibility between different laboratories due to different setups [17]. For this reason, measurements were carried out with a drop hammer similar to the BIT with sensory monitoring and data evaluation using with multivariate statistics [18]. The results show that a classification is possible despite a large scattering of the data. Experiments were also carried out on the thermal initiation in which the data were evaluated using multi-variate statistics and could be classified [19]. The evaluation by means of multi-variate statistics makes it possible to determine characteristics and specific values for substances and reactions. This is a great advantage in contrast to the conventional purely binary evaluation. In this study, a drop hammer based on the ball impact tester (BIT) developed by OZM [18] was constructed and equipped with various sensors. The sensor system comprised three infrared (IR) and three visible (VIS) diodes with distinct sensitivities, along with a microphone and a piezo shock sensor. Two batches of Hexamethylene triperoxide diamine (HMTD) were synthesized and subsequently subjected to a water-methanol washing process [10, 20]. One batch was prepared three months earlier to enable measurement at different ageing stages of HMTD. The primary objective was to validate the sensor system, which involved the evaluation of four ignition substances during experimentation. Data analysis involved extracting features from the collected data and assessing them using multivariate statistics. Subsequently, the impact sensitivities of the two batches of HMTD were determined, and the corresponding sensor responses were evaluated. The study also investigated the influence of ageing on the impact sensitivity and the reaction progression. Additionally, HMTD was initiated with different spheres

possessing equal energy to examine the impact type's influence on the reaction course. To monitor the samples, HMTD was measured using a Proton Transfer Reaction-Time of Flight (PTR-TOF) device. The headspace of the sample was analysed using this method. Furthermore, Raman spectroscopy was employed to measure the HMTD samples.

4.2 Experimental

4.2.1 Synthesis

HMTD

Caution. HMTD is a strong explosive compound and requires experienced personnel. HMTD was synthesized according to the methodology outlined by [21, 22]. In a three-necked flask with a magnetic stirrer, 1.40 g (10 mmol) hexamethylenetetramine was dissolved in 4.6 ml (50 %) H_2O_2 and cooled to $\sim$0°C (ice/NaCl) in an ice bath. With stirring, 2.3 g (10.94 mmol) of citric acid monohydrate was added stepwise. The solution was further stirred for 8 hours and then stored at 24 °C in a refrigerator at 4 °C. The product was then washed first with 100 ml of distilled water and then with 50 ml of methanol using a vacuum sucker and dried. The yield was 0.58 g ($\sim$25%).

TATP

30 wt% of hydrogen peroxide was added to a flask, utilizing a small stirring rod. The flask was tightly sealed with parafilm and subsequently positioned in a t in a tempered ice bath. Pure acetone was introduced into the flask containing the hydrogen peroxide, and the two substances were allowed to thoroughly mix for a minimum of 15 minutes. Following this, sulfuric acid was added to the mixture. The combined solution was left undisturbed for a duration of 24 hours, after which it underwent purification from DADP (Diacetone diperoxide) through treatment with hot methanol (recrystallisation). Subsequently, the substance was subjected to washing with distilled water to remove impurities [23]. The substance was checked for the presence of TATP and DADP using Raman spectroscopy (Analytical Methods).

4.2.2 Analytical Methods

Raman

To analyse the sample and to ensure that the synthesis product contains mainly HMTD and TATP including the expected by-products, Raman measurements were performed with a FirstDefemder R; RM3706. The measurements were taken with the standard parameters of the instrument and compared and evaluated with the instrument's internal substance database. PTR-ToF For the measurements with the time-of-flight mass spectrometer with proton transfer reaction (PTR-ToF-MS), an Ionicon 2000 with a thermal desorption unit is used. This system consists of a reaction chamber, a drift tube, a time-of-flight mass spectrometer and an ion source. The thermal desorption unit is integrated into the system to facilitate the analysis of volatile compounds. The aim of the measurements is to ensure that they are HMTD and common by-products and decomposition products, as in the Raman measurements, and to determine how the ratios of the contents can be compared between the old and the new batch. For the measurements, 5 mg of the sample was filled into a vial and then enriched in the thermal desorption unit. The vial was filled and left to stand for 30 minutes to allow the volatile substances to accumulate in the gas phase. The suction tube of the device is then held in the vial and the sample is measured.

Sample Preparation

Four different explosives were tested during the measurements: TATP ($C_6H_{12}O_4$), HMTD ($C_6H_{12}N_{12}O_6$), lead azide ($Pb(N_3)_2$), and silver azide (AgN_3) were measured. The azides were purchased from DyniTec GmbH and were of industrial quality. The peroxides were synthesized according to the chapter on Synthesis. In the case of HMTD, two batches were prepared, one 3 months old at the time of measurement and the other a few days old. This serves to compare different ageing stages. Both batches were dried and stored at 30 % RH and 18 °C.

For the calibration measurements, TATP, silver azide, and lead azide were measured in addition to HMTD. Salt was also measured to investigate the influence of the ball impact on the microphone and the piezo crystal and to distinguish it from the signal of the explosive. In addition, blank measurements were carried

out. Sample preparation was standardized for all substances by first storing the sample in a climate chamber at 30 % RH and 18 °C for at least 24 hours.

Drop hammer

Building upon the promising outcomes of previous investigations [18], a drop hammer based on OZM's BIT (Ball Impact Tester) was constructed. This drop hammer demonstrated suitability for testing primary explosives including sensory monitoring. The test procedure involves a steel ball of specified weight being dropped onto the sample from a predetermined height. If the kinetic energy of the ball surpasses a certain threshold, the sample ignites, indicating a positive result. It comprises a steel base plate and a head part with an electromagnet. The electromagnet controls the release of the ball. The head part can be adjusted continuously along an aluminium rod. The sample is placed on a ceramic plate located on the base plate. An exemplary sketch of the structure can be seen in Figure 4.1.

Distinguishing itself from the OZM BIT, this setup incorporates a ceramic base plate instead of steel. This change was made to prevent cavities from forming on the plate after repeated tests, as such cavities could potentially impact the test results. Another distinction lies in the manner of ball release. In the OZM BIT, the ball rolls over a ramp, acquiring rotation and making ignition possible through friction. Additionally, the ball experiences horizontal acceleration, making it necessary to employ camera monitoring to ensure accurate impact on the sample. In the current setup, however, the ball is secured by an electromagnet, resulting in purely vertical acceleration and eliminating ball rotation. Impact energies ranging from 4.4 mJ to 233.8 mJ can be achieved using this configuration. Then, according to the sample preparation of BIT [11], sample was placed on the base plate of the drop hammer. It was applied 5 mg of the sample with a measuring spoon during the preparation. The sample was then smoothed to a thickness of 0.3 mm using a slide and rail, leaving a clotted layer. Table 4.1 shows the area and displaced volume of the ball at a sample height of 0.3 mm.

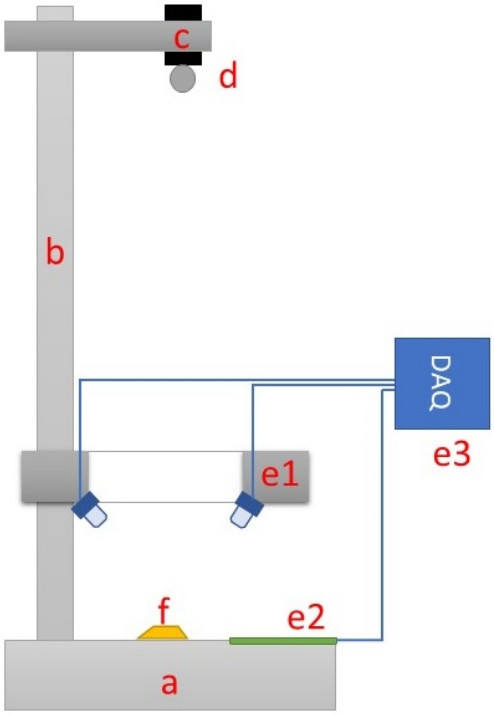

Figure 4.1: Setup drop hammer: a: baseplate, b: rod, c: electro magnet, d: ball, e1-3: sensors and data acquisition, f: sample

Table 4.1: Used ball sizes and heights, area and dispatched volume for ball size comparison.

Ball-size [mm]	Mass [g]	Area [mm^2]	Vol. [mm^3]
6	0.88	5.37	0.82
8*	2.01	7.26	1.10
10	4.08	9.14	1.35
15	23.08	27.99	4.21

4.2.3 Sensor array

To monitor the reactions, the drop hammer was equipped with various optical and acoustic sensors. For the IR range, a pre-amplified IR sensor (PDAPC3 - Thorlabs) and two IR diodes with downstream non-inverting amplifier with different gain levels were used. For the visible range a pre-amplified sensor (PDAPC1-Thorlabs) and two additional differently amplified VIS diodes (Conrad Electronic TRU COMPONENTS 1000nm 3004M1C) were used. Due to the redundant photodiodes, both large signals, as expected for azides and the like, and small signals, as for peroxides, can be detected. The acoustic sensors used were a MEMS microphone (ELV MEMS1) for sound and a piezo shock sensor (TE Connectivity Vibration Sensor) for baseplate vibration. The analogue signals from the sensors are measured and recorded using a DAQ board (Meilhaus RedLab 1608FS-PLUS) with a sampling rate of 100 kS/s. The entire setup is shielded for noise reduction and housed in an enclosure that is shielded against interference signals and the reaction gases can be exhausted.

4.2.4 Measurement Parameters

The second series of measurements investigated the influence of ball size on ignition and reaction behaviour, using samples exclusively from the new batch of HMTD. For these experiments, measurements were conducted using two balls of different sizes (10 mm, 40 cm, 4.08 g; 8 mm, 80 cm, 2.01 g), with the same energy level (16 mJ) corresponding to the respective height and repeated 10 times for each configuration. The data were evaluated following the same approach as in the first series of measurements. The aim here is to find out whether there is a trend between the size of the impact body and the intensity of the reaction. The third part of the paper deals with the comparison of the impact sensitivity of the two batches of HMTD and whether or how ageing affects the impact sensitivity of the material. In addition, the characteristics of the reactions are to be compared and whether differences arise due to ageing, the type of combustion of the sample. The heights of 40 cm, 30 cm, 25 cm and 20 cm were measured with the 6 mm sphere (0.88 g) in 10 trials each. The 10 mm sphere was used, because with this weight of the sphere a large energy range as well as an exactly sufficient reso-

Table 4.2: Impact sensitivities from literature of used samples.

Compound	E50 impact sensitivity (BIT) [mJ]	E16.6 impact sensitivity (BIT) [mJ]	Impact sensitivity 1-of-6 (BAM) [mJ]
HMTD	6*	4*	60**
TATP	18*	13*	<1000*
LA	n.d.	37*	2500–4000**
SA	n.d.	29*	<1000 to 3000*

lution to small energies is realisable at the construction. The resulting energies are 1.72 mJ, 2.16 mJ, 2.6 mJ, 3.5 mJ and 5.2 mJ. In addition to recording the sensor reactions, it was also documented whether the samples reacted completely, partially or not at all. Whether a sample was only partially reacted was checked by checked visually. The energy was gradually reduced until none of the 10 samples ignited. The evaluation of these measurements took into account both the raw data and the multivariate statistical analysis.

4.2.5 Pre-processing and Statistics

The measurements underwent pre-processing and analysis using a Python script [24] to obtain the sensor responses. To extract and present substance-specific characteristics from the measurements, 10 distinct features were derived from each measurement for every sensor. The features are namely the Y-position of the peak, the width of the peak at the base, the height of the peak when crossing the threshold, the height of the signal when falling below the threshold, the width of the peak, the width of the peak at half height, the half-height of the peak when rising, the half-height of the peak when falling, the integral of the peak, the slope when rising as well as when falling. Due to the excessive number of dimensions represented by the 80 extracted features, graphical analysis becomes challenging. To address this, principal component analysis (PCA) was employed to reduce the dimensions. The data was first pre-processed using a unit vector, and then three principal components were calculated using the default parameters of Scikit-learn PCA library [25]. This reduction in dimensionality helps to identify any apparent clusters within the data representation. By analysing the loadings, we can determine which extracted features are valuable for characterising and identifying substances, and which features are redundant or unnecessary. Additionally, the Scikit-learn library [25] was utilized, employing singular value decomposition as a solver, to perform linear discriminant analysis (LDA) on the entire dataset of extracted features. LDA, being a supervised method, not only enables the exploration of substance-specific clusters in the data but also facilitates the determination of a regressor function. This regressor function allows for the identification of unknown samples. To assess the accuracy of the regressor function, cross-validation was conducted using the leave-one-out procedure. In

this process, each measurement is successively used as a test dataset across all measurements, ensuring comprehensive evaluation despite the relatively small dataset.

4.3 Results and Discussion

In this section, we commence by presenting and assessing the analytical methods employed for data analysis. Subsequently, we proceed to discuss the validation measurements, ageing tests, and finally, the investigations conducted to ascertain the impact of ball size. Each of these aspects is discussed independently and in a sequential manner.

4.3.1 Analytical Methods

Raman

Figure 4.2 shows the data of the Raman measurements of old TATP (top), the new HMTD (middle) and old HMTD (bottom). Looking at the measurement of the TATP, there is a high overlap of the reference spectrum with the measured spectrum. The evaluation shows that the data are 100 % consistent with TATP. A search was also made for DADP (diacetone diperoxide), but this could not be found. When looking at the HMTD measurements, no significant differences can be seen between the old and the new batch. In both analyses, the substance is assigned 100 % as HMTD.

PTR-ToF

When analysing the PTR-ToF data, the focus was on the HMTD-relevant fragments. For both samples, the mass peaks of the relevant fragments were analysed and plotted logarithmically. In Figure 4.3, the fragments relevant for HMTD are plotted against each other. The method used only allows a limited quantitative analysis of the components, but trends in the proportions can be estimated. Table 4.3 lists the fragments with probable names of the molecules and fragments. In the old batch, the peaks of trimethylamine and dimethylformamide stand out,

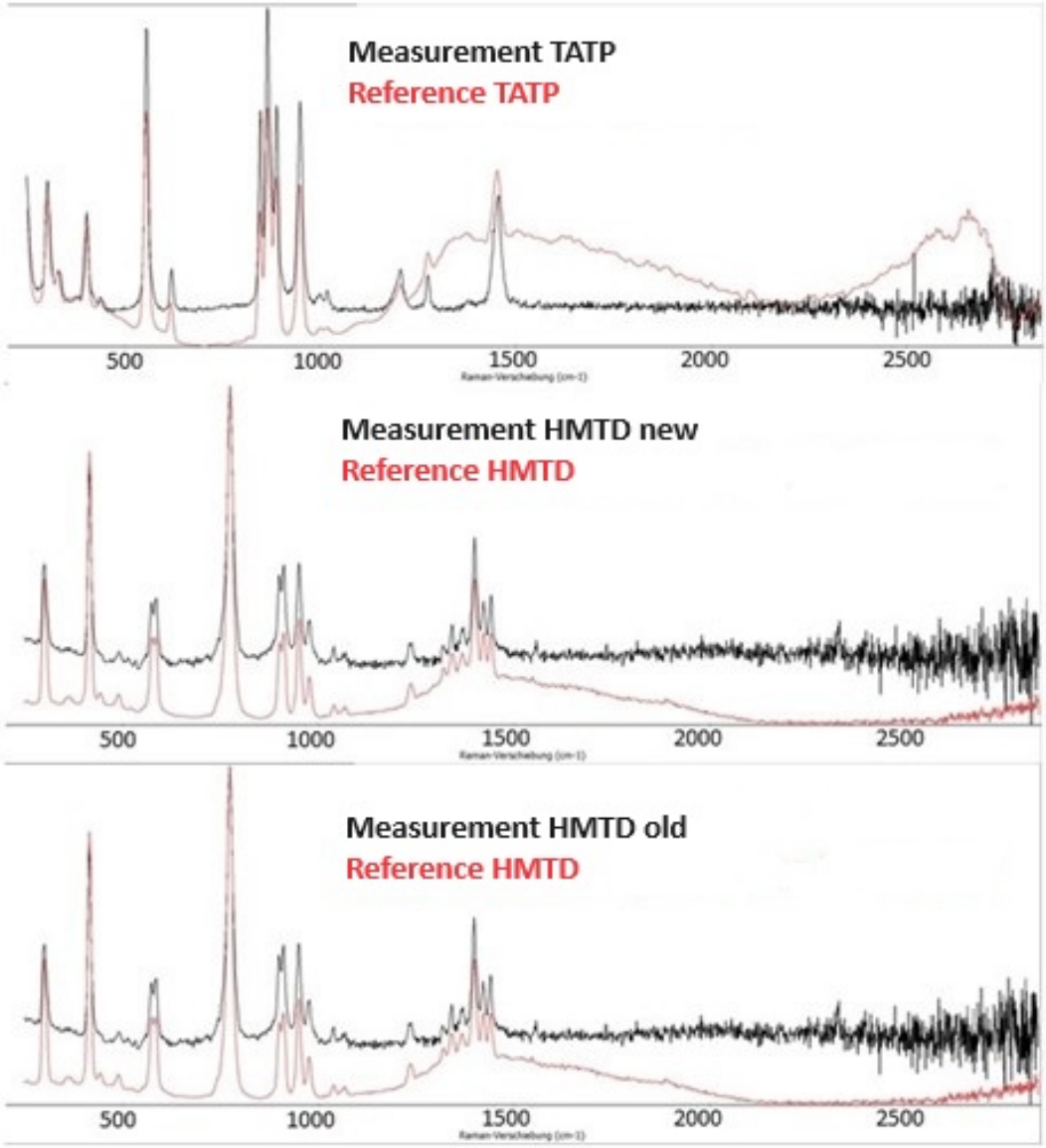

Figure 4.2: Raman spectra of TATP, old and new HMTD, the diagrams show the measured spectrum as well as the spectrum of the sought substance from the library of the instrument

Table 4.3: Predicted molecules and fragments of PTR-ToF

Fragment [m/z]	Name
46.029	Formamide
60.081	Trimethylamine
61.028	Acetic acid
74.060	Dimethylformamide
179.140	HMTD–Formaldehyde
209.077	HMTD

which indicates that this substance is formed during decomposition. This is consistent with observations from the literature. In general, it can be seen that substances that appear in measurements carried out in the literature can also be seen in these [10]. The results of the measurements show on the one hand that the synthesised substance is HMTD, and also that the composition of the substance changes over time.

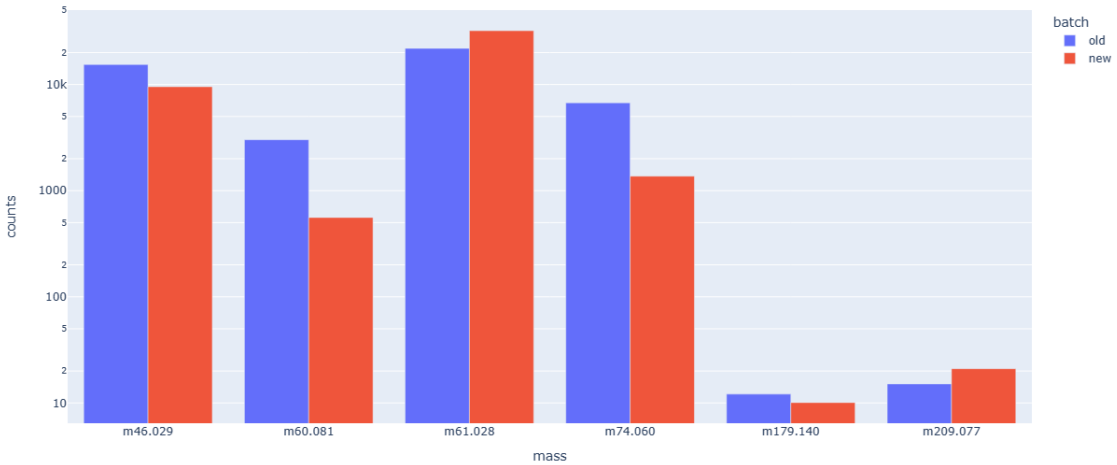

Figure 4.3: Cintegrals of selected molecular fragments of old and new HMTD, logarithmically plotted

4.3.2 Validation measurements

In the following, the features "Micro_integral" and the feature "piezo_integral" are discussed as examples, as an evaluation of all features would go beyond the scope of this article. These features represent the integrated signal above the threshold of the respective sensors. This was extracted as in Pre-processing and Statistics. Diagrams show the mean value including standard deviation of the extracted features for each sample. The feature "Micro_integral" was analysed to assess its effectiveness in differentiating explosives. Figure 4.3 illustrates the clear signals observed for the measured explosives. The mean values for AgN_3, HMTD, $Pb(N_3)_2$, and TATP were found to be 0.10 V, 0.23 V, 2.1 V, and 0.17 V, respectively. Conversely, the blank measurements and those with salt exhibited significantly smaller signals, with the salt measurement presenting the lowest signal intensity due to the attenuating effect of the substance. The signal from the large sphere is more pronounced due to the stronger impact on the ceramic plate. However, it is important to note that the standard deviations associated with the explosive samples were substantial, surpassing the corresponding mean values.

The feature "piezo_integral" was investigated to assess its discriminatory ability in the classification of explosives and to identify substance-specific trends. Figure 4.4 shows the analysis performed with this feature (mean values of the substances). Distinct signals were observed for the azide compounds. This phenomenon can be attributed to the higher power compared to peroxide-based explosives [13]. The structure-borne sound generated by the reactions propagates to the piezoelectric sensor and leads to the detected signals. However, the peroxides, especially TATP and HMTD, had relatively low signals whose intensities hardly differed from the blank measurements. This can be attributed to the nature of their reactions, which lead to less pronounced transmission of structure-borne sound.

Interestingly, the blank measurements had comparatively high signals. This can be attributed to the fact that the ball hits the base plate without encountering any resistance or braking effect. On the other hand, the presence of salt resulted in the smallest mean value of all substances examined. This can be attributed to the dampening effect of the substance, which softens the impact and reduces the resulting signal intensity.

When analysing the standard deviations related to the feature “piezo_integral”, it can be seen that the values are smaller compared to features such as the “microphone_integral”, but still too high to prevent an effective classification based on this feature alone. Therefore, additional features or complementary analytical methods are needed to improve the accuracy and reliability of explosives classification using the entire dataset.

When evaluating the features of the optical sensors, it becomes apparent that the azides produce clear optical signals through away. However, the emission of light during the decomposition of the peroxides is very sporadic. This greatly increases the standard deviation of these features and shows that none of these features are suitable for denoting the substances.

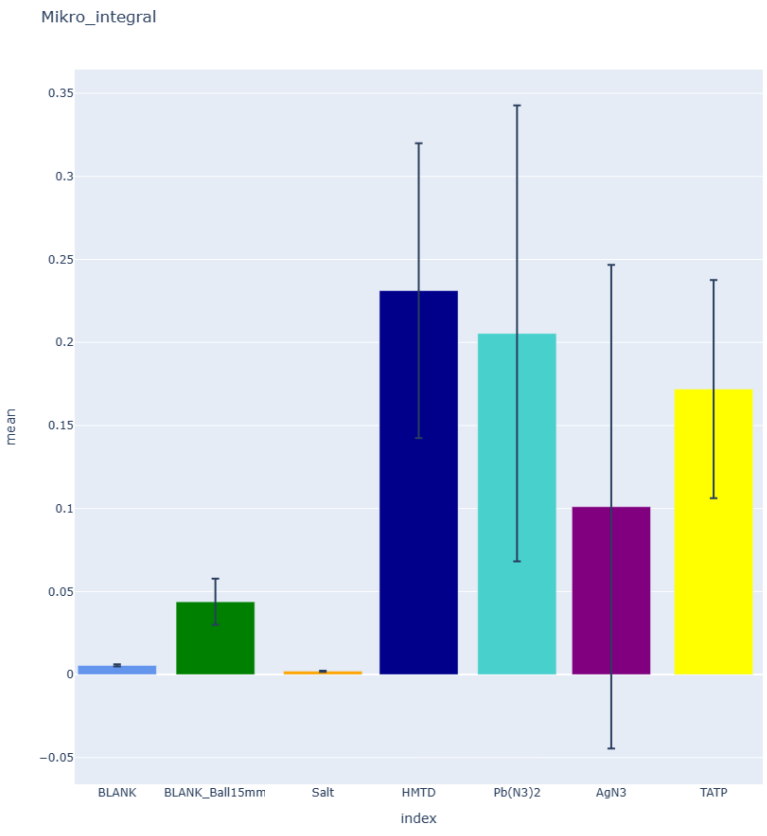

Figure 4.4: Mean of the Micro_integral feature for every sample including standard deviation for validation measurements

Principal Component Analysis (PCA) was utilized to derive three principal

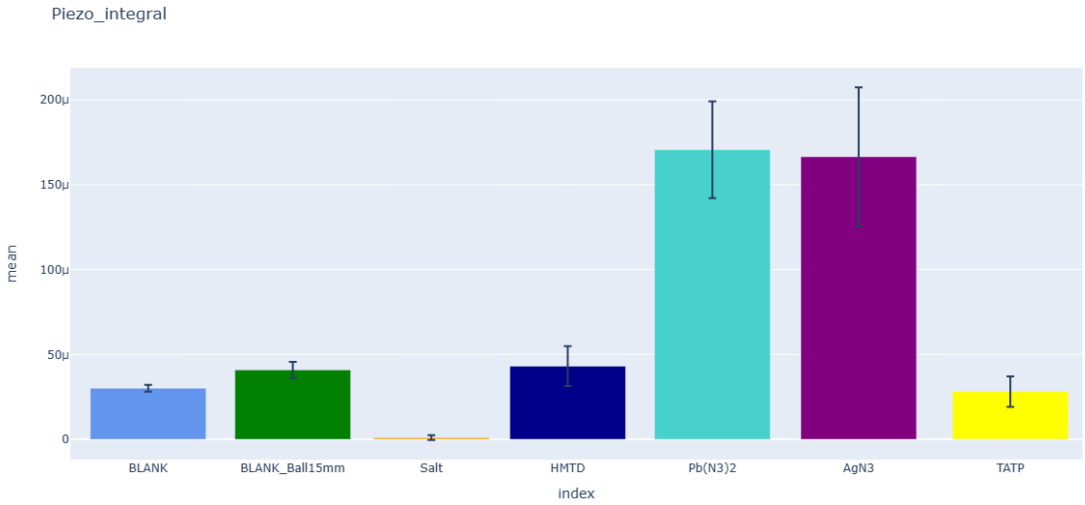

Figure 4.5: Mean of the piezo_integral feature for every sample including standard deviation for validation measurements

components from the initial set of 80 features. As an unsupervised method, PCA enables the reduction of data dimensions and offers insights into data separability. Figure 4.3 illustrates a plot of the three principal components obtained. Upon examining the plot, it becomes apparent that the point clouds corresponding to HMTD and TATP measurements exhibit overlap. This suggests that the classification of these substances is limited within the series of measurements conducted. Notably, TATP displays a notably smaller scattering range compared to HMTD, aligning with the observations made regarding the average micro_integral feature values. When considering the blank measurements and those involving salt, distinct and well-defined clusters are observed. These clusters indicate clear separability between these groups, reflecting their distinctive characteristics.

The point clouds associated with the azide compounds are particularly striking. They exhibit substantial scattering, consistent with the observations made regarding the extracted features. Notably, the azide measurements distinctly separate from all other point clouds, emphasizing their unique characteristics. Overall, the PCA analysis provides valuable insights into data separability and clustering patterns. The results highlight the challenges in accurately classifying HMTD and TATP based on the measured substances while demonstrating the distinct

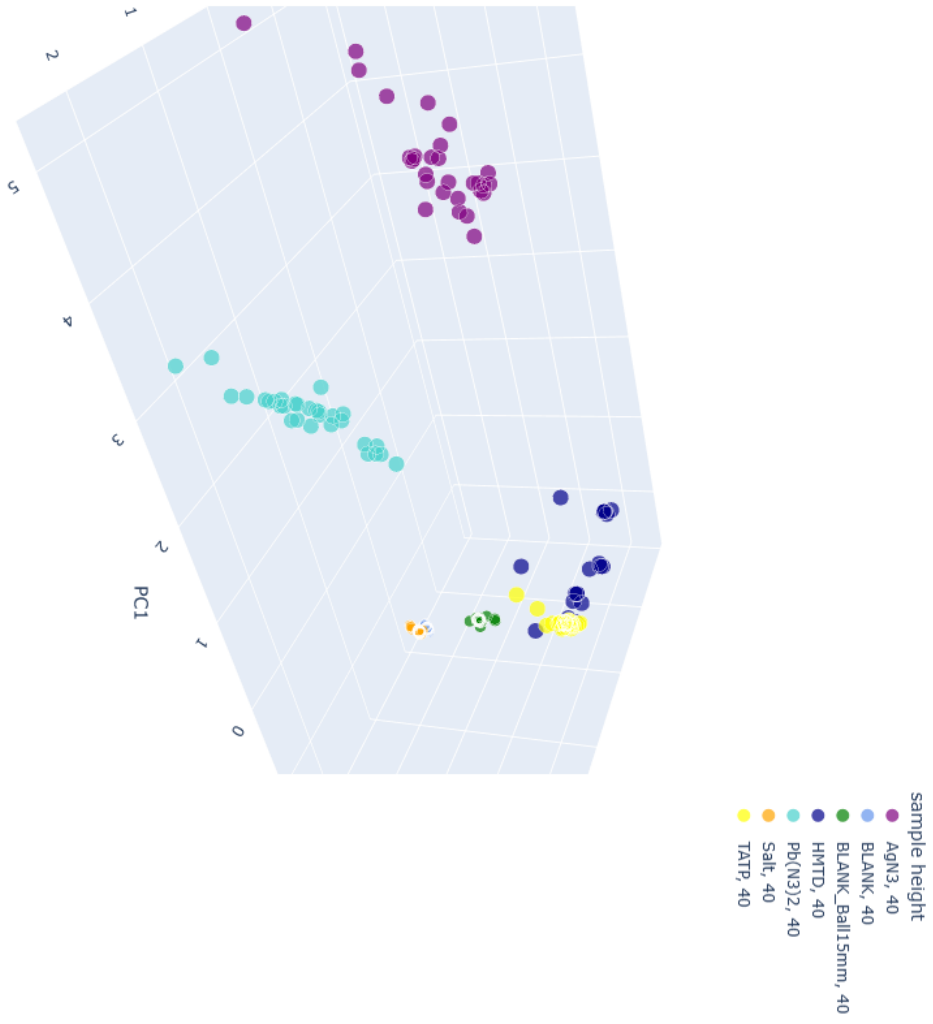

Figure 4.6: PCA-plot of the calculated three components of validation measurements

clustering of blank measurements, those involving salt and azide compounds. These findings align with the observations made regarding the feature analyses.

If we look at the scree plot (Figure 4.7), we can clearly see that the first main component already covers about 60 % of the total variance, the second still provides 15 % and more values, and the third about 8 %.

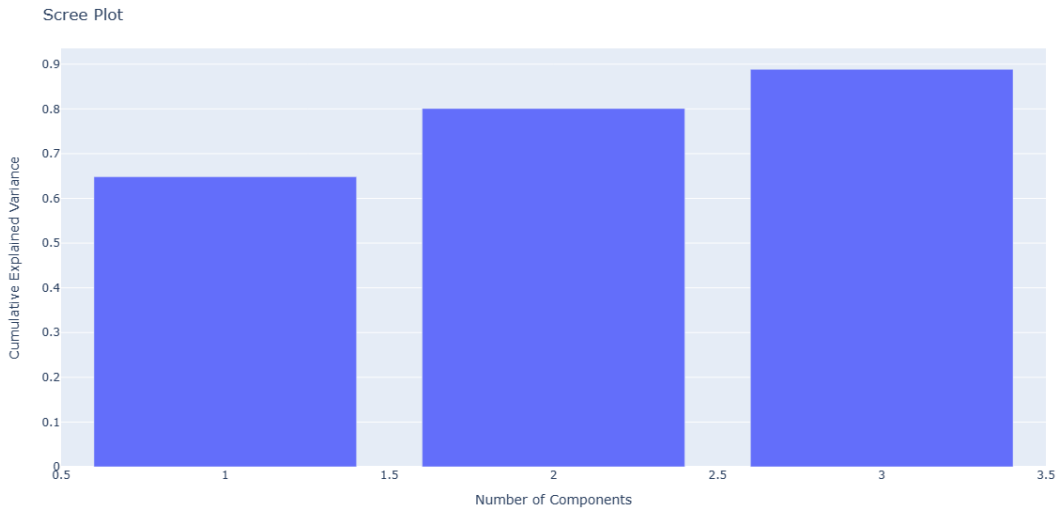

Figure 4.7: Cumulative scree plot of first three PCA components

The LDA is a supervised method, thus characteristics that differentiate the classes from each other are weighted more heavily. Figure 4.8 shows the data reduced by LDA. As in the PCA-reduced data, it is evident that most of the compounds form clusters that are distinct from each other. However, if the peroxides TATP and HMTD are considered, it is evident, as in the raw data and PCA, that the clusters overlap and classification is not possible or only possible to a very limited extent.

To validate the LDA, a leave-one-out cross-validation was performed and a predictor function was created. Iteratively, each measurement was used once as a test measurement and the others as training data. The results of this cross-validation are shown in Figure 4.9 in a heat plot. It can be seen that HMTD was assigned 8 times as TATP and TATP 8 times to HMTD. However, this is sufficient, since a better separation can be expected when differentiating different peroxides by means of LDA without strongly deviating azides.

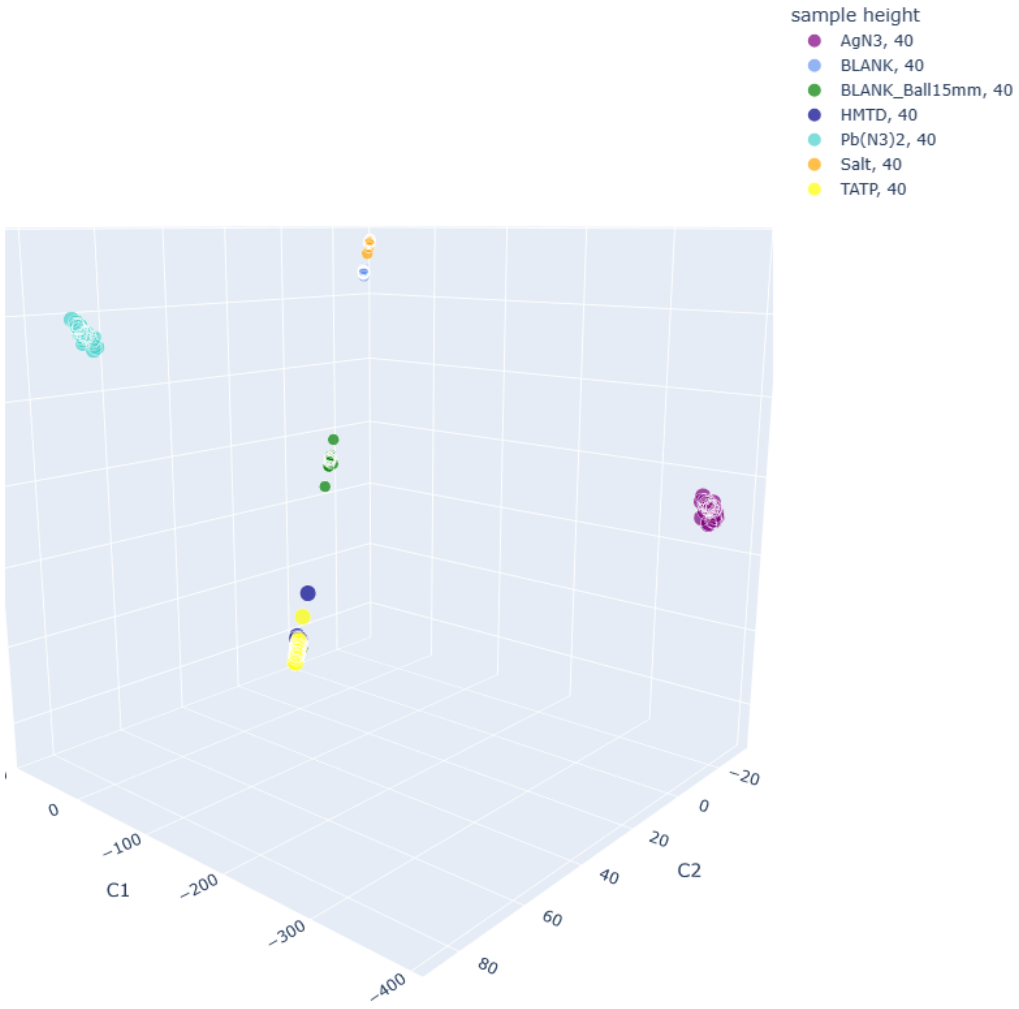

Figure 4.8: LDA-plot of the calculated three components of validation measurements

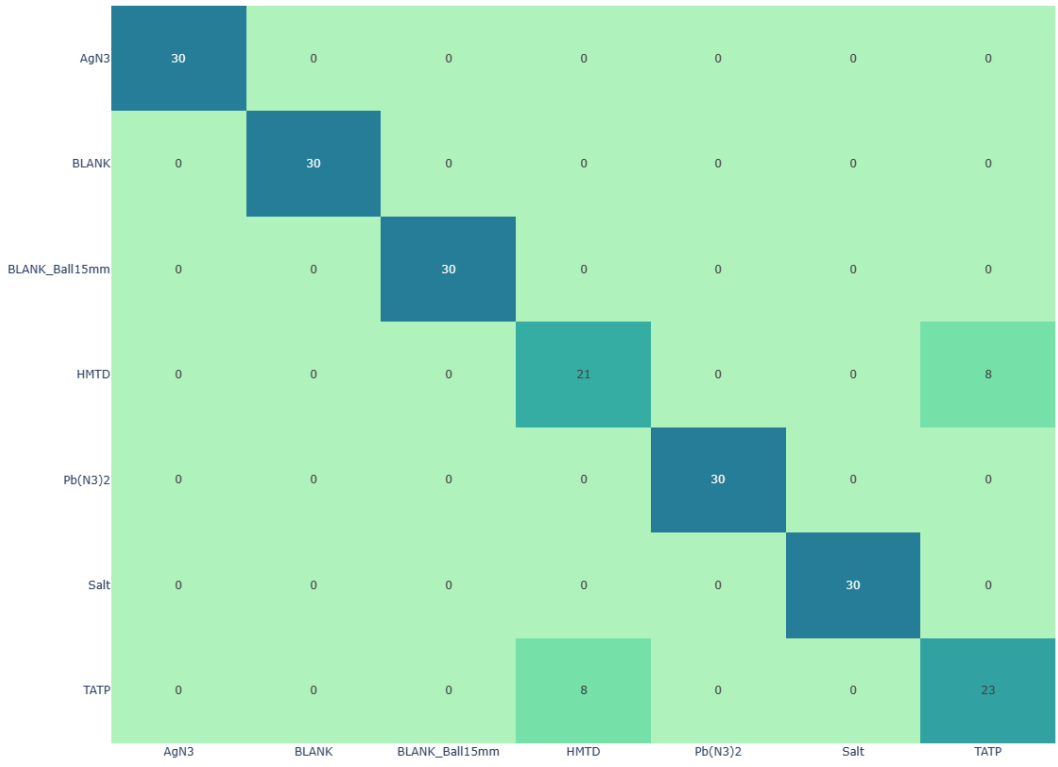

Figure 4.9: Heatplot of the via LDA predicted data from validation measurements

4.3.3 Influence of the ball size

In order to rule out the influence of the ball masses as the sole cause of the observed trends in the sensor signals, blank measurements were performed as part of the experimental protocol. In particular, the microphone and piezo signals were examined during these blank measurements (where no optical emission was expected). Through this analysis, it was confirmed that the intensities of the blank measurements differed from each other. However, it should be noted that the intensities of the blank measurements were significantly lower compared to the signals from the measurements with HMTD and thus do not have a confounding effect on the results. When analysing the results from the comparison measurements, which were performed with different sphere sizes but the same initiation energy, it can be seen that the extracted features show similar behaviour to the validation measurements. To further evaluate the properties of these features, an illustrative example is discussed. In the first example (Figure 4.10), the integral of the piezoelectric sensor response is plotted against the ball size/height. The plot shows that the signal resulting from the responses to the larger sphere is more pronounced compared to the signals from the measurements with a small ball. However, similar to the validation measurements, it can be seen that the values have a high standard deviation. Consequently, a clear distinction between the different measurements is not possible when relying only on this one feature. Other features in this series of measurements also confirm the trend that initiation with the larger ball tends to elicit more violent responses. The reason for this is presumably the larger surface area and ergo a higher attenuation of the sample [11]. This makes fast and complete reaction of the sample more likely. The extracted features of this measurement series were also evaluated using multivariate statistics. Since there are only two parameter sets in this measurement series, an evaluation via LDA is not possible. In Figure 4.11, the features reduced by PCA are plotted. In spite of the fact that PCA is a non-supervised method, it can be seen that clouds of points of the two ball sizes are formed which are separated from each other. It can be seen that the measurements with the large sphere scatter significantly more. This is consistent with the observation that these measurements have a higher standard deviation in many features (Figure 4.10).

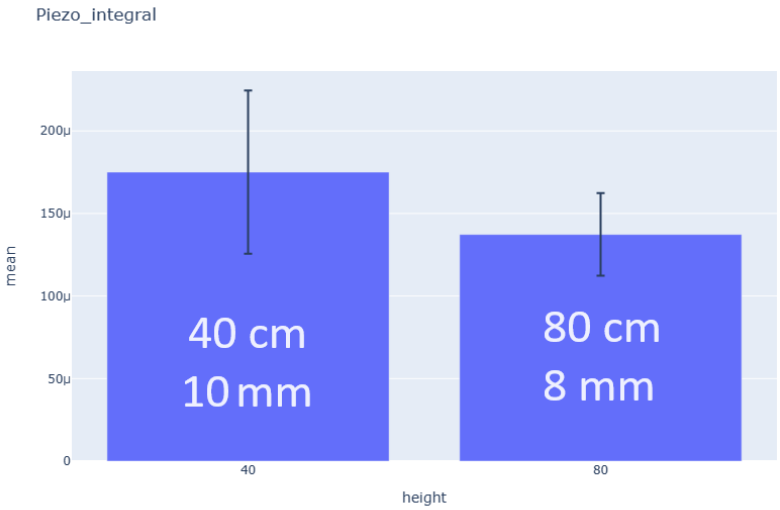

Figure 4.10: Mean of the Piezo integral feature for every sample including standard deviation for ball size measurements

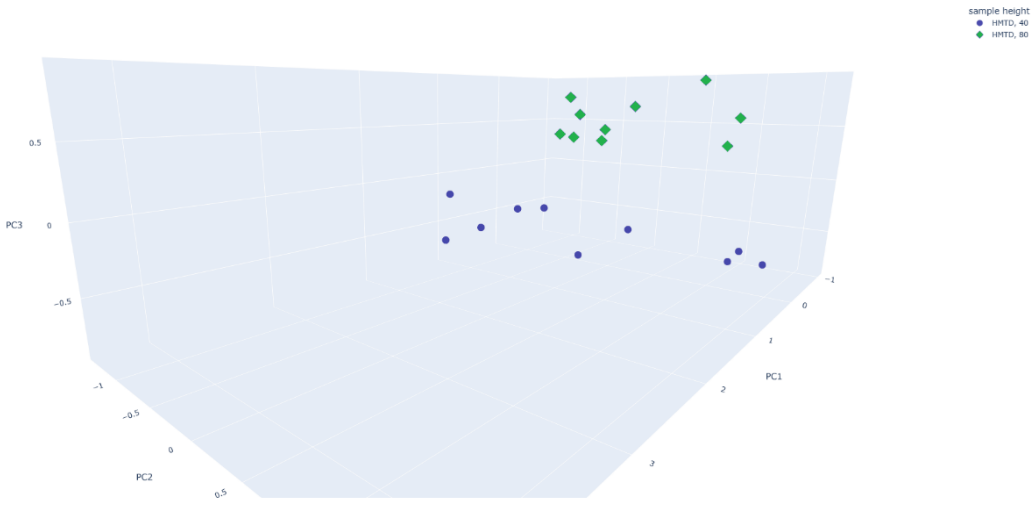

Figure 4.11: PCA-plot of the calculated three components of ball size measurements

Comparison of the ageing stages

The evaluation of this series of measurements is carried out without taking into account the influence of the sphere size, as only one type of sphere was used. In Figure 4.12, the relationship between the frequency of ignitions and impact energy, as well as substance type, is visually represented. The left portion of the figure illustrates the ignition probability per measurement plotted against energy. Notably, at an energy level of 5.19 mJ, all samples, including both the new and old batches, exhibit a 100% ignition rate. The data results in an E_{10} value of around 2.2 J. However, if these results are compared with the existing literature of 6 mJ [11], it is noticeable that the value determined is lower than the value given in the literature. This is remarkable, as ignition due to friction can be ruled out in our setup. The value determined with the BAM drop hammer is also significantly higher than ours at 60 mJ [13]. It should also be noted that these values can fluctuate depending on factors such as crystal modification and water content [11]. Despite the uniform design, synthesis, and handling of the samples, the results presented do not indicate a firm correlation between the course of the reaction and impact sensitivity in connection with the ageing of the substance, but rather show the possibility that a correlation exists.

By examining the ignition probability of the new HMTD, it becomes evident that all samples ignite even at a lower energy level of 3.46 mJ, with the probability decreasing as the energy decreases. In contrast, the behaviour of the old batch HMTD differs. The probability of ignition does not exhibit a consistent decline with increasing energy. For instance, at 3.46 mJ, the ignition probability is only 90%, while at 2.59 mJ, it returns to 100%. At an energy level of 1.73 mJ, no further conversions occur with the old HMTD.

Analysing the frequency of partial conversions for both substances (Figure 4.12, centre), it is evident that no partial reactions are observed at an energy level of 5.19 mJ. The highest likelihood of partial reactions occurs at an energy level of 2.16 mJ, with the old substance demonstrating a tendency towards partial reactions in 50% of the measurements, compared to approximately 30 % for the new substance. Moreover, considering that the old HMTD does not undergo any conversion at an

In the course of this series of measurements, additional information was ex-

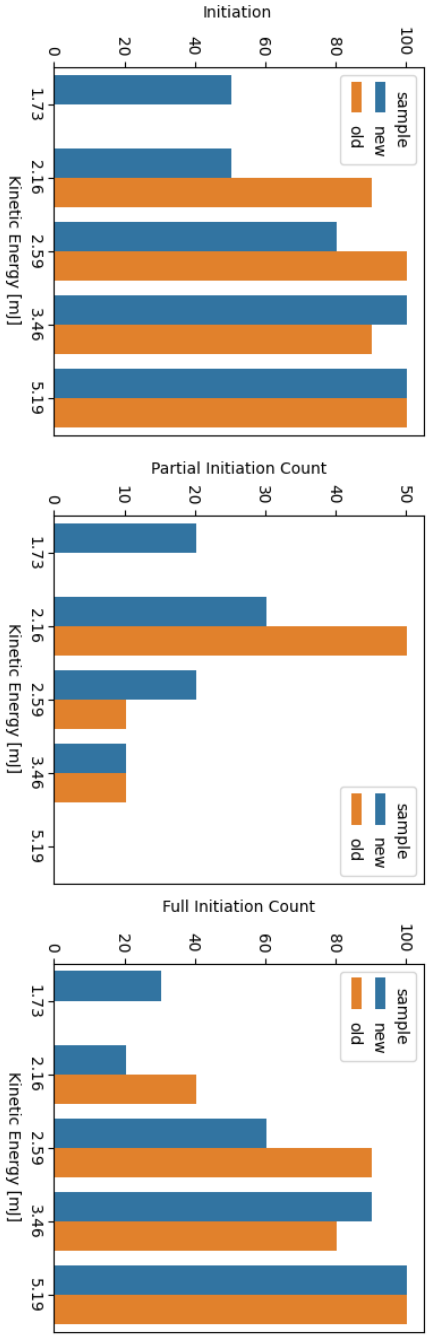

Figure 4.12: Probability of conversion versus impact energy of old and new HMTD. Left: all combustions, middle: only partial combustions, right: only complete combustions

tracted from the collected data and analysed using multivariate statistical methods. To illustrate this process, the feature known as micro_integral (Figure 4.13) was selected as an example. Looking at the data, it is evident throughout all heights and also samples that all measurements, as with those of the validation measurements, show a high standard deviation. For measurements at 20 cm, no ignition occurred for the old HTMD, ergo no signal is seen. Apart from the value for new HMTD at 20 cm, the mean values increase with increasing height, that is, as the energy increases, the violence of the response increases. It is clear to see that the mean values of new HMTD consistently have a higher value, indicating that it responds more violently compared to the old batch. This trend is consistent across almost all of the features extracted. Although differences in the mean values can be seen in almost all features, the substances cannot be discriminated due to the large standard deviation.

The results show that the aged HMTD is more insensitive to impact and shows a milder decomposition reaction compared to the freshly produced product. The reason for this could be that HMTD ages rapidly. In this aging process, the substance decomposes into smaller, non-reactive parts. These are deposited on and in the crystals, which can interrupt the continuation of the reaction front [11]. Other impurities, which can also vary from batch to batch, can have a similar effect. Furthermore, the net explosive amount of the sample decreases, which means that quantitatively less material is present that can react.

Due to the limited number of measurements (10 per parameter set) and the fact that not all measurements resulted in ignition, a comprehensive analysis of class-specific characteristics becomes challenging. Nonetheless, the dataset encompassing all measurements leading to sample conversion, including the validation measurements, underwent a thorough evaluation utilizing multivariate statistical techniques. Out of the 100 measurements conducted in this series, a total of 76 yielded full or partial combustion. These measurements were subjected to Linear Discriminant Analysis (LDA) and subsequently reduced to three dimensions, as depicted in Figure 4.14. Distinct HMTD batches are denoted by various colours, while different symbols represent varying heights. When looking at the plotted points, it is clear that the point clouds of the two samples separate on the axis of the first components, when intersections also occur. Comparing the measurements of the individual heights (marked with different symbols), a

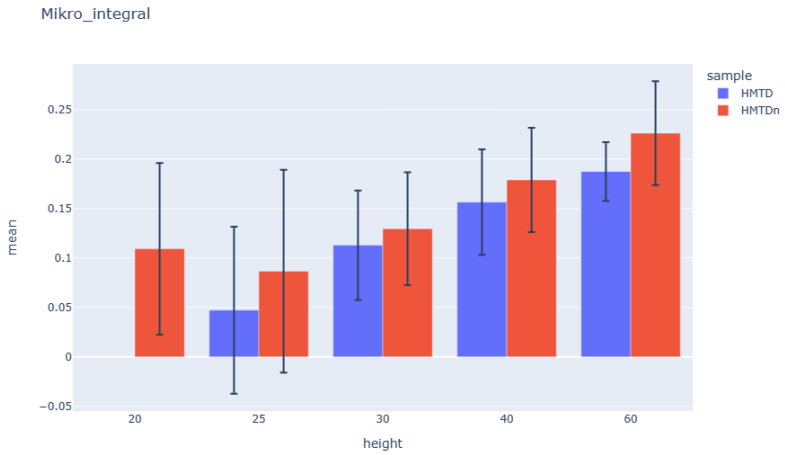

Figure 4.13: Mean of the Mikro integral feature for all combusted samples and heights including standard deviation for impact sensitivity measurements

trend can also be seen. Thus, on average, the values of the points on components 1 and 2 increase with increasing height. Basically, it can be seen that the points of the measurements of the old HMTD show a larger scatter, whereby the height-dependent trend, which can be seen well with the new HMTD, is only weakly developed. The reason for this is presumably the changed morphology and composition of the sample due to aging. Batch to batch variation must also be taken into consideration. In principle, however, it seems possible to discriminate measurements from batches of HMTD of different ages on the basis of the sensor response of the decomposition reaction. In order to validate the possibility of assigning measurements, cross-validation was performed, as was done for the validation measurements (Figure 4.15). In the heat plot shown, the true values of the measurements are plotted on the Y-axis and the predicted values are plotted on the X-axis. All measurements in the red marked area show measurements of the new HMTD, those in the blue those of the old one. Measurements that are not in any of the boxes are incorrectly predicted. Measurements that are within the marked fields are partially predicted to the wrong height, but to the correct substance. It is worth noting that these values can exhibit variations depending on factors such as crystal modification and water content [11]. Despite the uniform design, synthesis and handling of the samples, the results presented do not indicate a firm correlation between the course of the reaction and impact sensitiv-

ity in connection with the ageing of the substance, but rather show the possibility that a correlation exists.

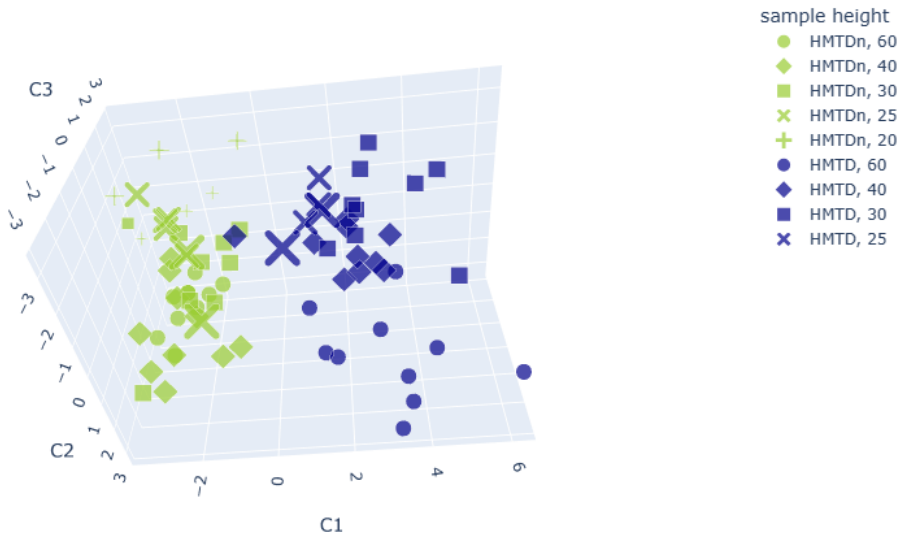

Figure 4.14: LDA-plot of the calculated three components of impact sensitivity measurements

4.4 Conclusion

In conclusion, a drop hammer apparatus resembling the OZM Ball Impact Tester, equipped with optical and acoustic sensors, was utilized for the evaluation of impact sensitivity and response of four distinct initial explosive materials: HTMD, TATP, silver azide and lead azide. The peroxides were synthesized, and two batches of HMTD with different ages were prepared. The substances underwent controlled energy-induced conversions to validate their distinctive characteristics and ensure differentiation capability. Extracting 80 features from each measurement, followed by multivariate statistical analysis and dimensionality reduction, facilitated the differentiation process. Cross-validation yielded a predictor function accuracy of 93 %, confirming the suitability of the setup for distinguishing ignition substances. In the subsequent segment of this research, the reaction behaviour of HTMD was examined at different ball sizes and heights, maintaining a constant energy level as in the initial phase. The objective was to assess the impact of sphere size on the reaction process. Statistical evaluation results indicated that the severity of the reaction increases with larger ball sizes, highlighting the dependency on the impact area rather than the ball velocity. Future experiments will explore this influence with different substances. In the final phase of the study, the impact sensitivities of two differently aged batches of material were determined and the response curves observed. The analytical methods confirmed the ageing phenomena described in the literature [26, 27, 22, 10]. The experiments were performed with energies between 1.73 mJ and 5.19 mJ, and the number of ignitions per height and substance was evaluated as 1 out of 10 [14]. The static evaluation showed that ageing could influence the impact sensitivity. In addition, the statistical analysis revealed that aged materials have a higher tendency to partial combustions. Overall, this study provides insights into the differentiation of igniters, the impact sensitivity of aged materials and the influence of ball size on reaction behaviour. Future studies will include measurements of several batches with different ages in order to exclude batch to batch variations and to obtain more comprehensive and accurate results. It would also be useful to measure the substances at more than just two ageing stages. In future, more comprehensive series of measurements will also have to be carried out for experi-

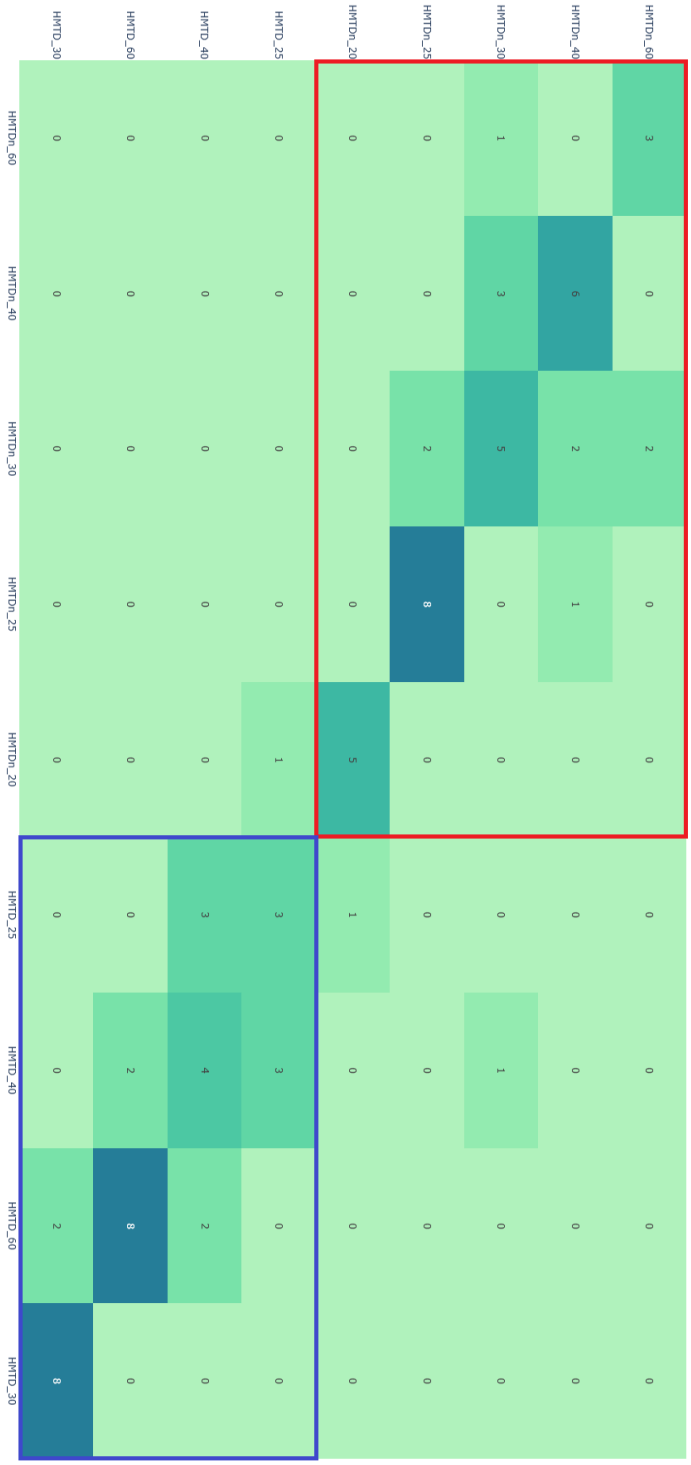

Figure 4.15: Confusion matrix of the cross-validation of the impact sensitivity tests. Z axis true values, x axis predicted values

ments with different sphere sizes. On the one hand, a larger repertoire of spheres and, if necessary, also different substances must be measured.

References

[1] Lindsay McLennan, James L. Smith, and Jimmie C. Oxley. "A new polymorph of HMTD". In: *Journal of Energetic Materials* 39.3 (2021), pp. 361–376. DOI: 10.1080/07370652.2020.1802630.

[2] Kevin Colizza, Alexander Yevdokimov, Lindsay McLennan, James L. Smith, and Jimmie C. Oxley. "Using Gas Phase Reactions of Hexamethylene Triperoxide Diamine (HMTD) to Improve Detection in Mass Spectrometry". In: *Journal of the American Society for Mass Spectrometry* 29.4 (2018), pp. 675–684. DOI: 10.1007/s13361-017-1879-5.

[3] Lauryn E. DeGreeff, Michelle M. Cerreta, and Christopher J. Katilie. "Variation in the headspace of bulk hexamethylene triperoxide diamine (HMTD) with time, environment, and formulation". In: *Forensic Chemistry* 4 (2017), pp. 41–50. DOI: 10.1016/j.forc.2017.03.001.

[4] Zheng Li, Will P. Bassett, Jon R. Askim, and Kenneth S. Suslick. "Differentiation among peroxide explosives with an optoelectronic nose". In: *Chemical Communications* 51.83 (2015), pp. 15312–15315. DOI: 10.1039/c5cc06221g.

[5] Jirí Pachmán, Jakub Selesovský, and Robert Matyás. *New Trends in Research of Energetic Materials (NTREM '14)*. 2014.

[6] M. O. Salles, G. N. Meloni, W. R. de Araujo, and T. R. L. C. Paixão. "Explosive colorimetric discrimination using a smartphone, paper device and chemometrical approach". In: *Anal. Methods* 6.7 (2014), pp. 2047–2052. DOI: 10.1039/C3AY41727A.

[7] Derek F. Laine and I. Francis Cheng. "Electrochemical detection of the explosive, hexamethylene triperoxide diamine (HMTD)". In: *Microchemical Journal* 91.1 (2009), pp. 125–128. DOI: 10.1016/j.microc.2008.08.015.

[8] J.C. Oxley, J.L. Smith, W. Luo, and J. Brady. "Determining the vapor pressures of diacetone diperoxide (DADP) and hexamethylene triperoxide diamine (HMTD)". In: *Propellants, Explosives, Pyrotechnics* 34.6 (2009), pp. 539–543. DOI: 10.1002/prep.200800073.

[9] A.G. Simon and L.E. DeGreeff. "Variation in the headspace of bulk hexamethylene triperoxide diamine (HMTD): Part II. Analysis of non-detonable canine training aids". In: *Forensic Chemistry* 13 (2019), p. 100155. DOI: 10.1016/j.forc.2019.100155.

[10] Jimmie C. Oxley, James L. Smith, Matthew Porter, Lindsay McLennan, Kevin Colizza, Yehuda Zeiri, et al. "Synthesis and Degradation of Hexamethylene Triperoxide Diamine (HMTD)". In: *Propellants, Explosives, Pyrotechnics* 41.2 (2016), pp. 334–350. DOI: 10.1002/prep.201500151.

[11] M. S. Gruhne, M. Lommel, M. H. H. Wurzenberger, N. Szimhardt, T. M. Klapötke, and J. Stierstorfer. "OZM Ball Drop Impact Tester (BIT-132) vs. BAM Standard Method – a Comparative Investigation". In: *Propellants Explos. Pyrotech.* 45 (2020), pp. 147–153. URL: https://doi.org/10.1002/prep.201900286.

[12] C. S. Coffey and V. F. de Vost. "Impact Testing of Explosives and Propellants". In: *Propellants, Explosives, Pyrotechnics* 20.3 (1995), pp. 105–115. DOI: 10.1002/prep.19950200302.

[13] Josef Köhler, Rudolf Meyer, and Axel Homburg. *Explosivstoffe*. 10th revised and expanded edition. Weinheim: Wiley-VCH, 2008.

[14] NATO. *STANAG 4489, 1999 (4489)*. 1999.

[15] David M. Williamson, Sue Gymer, Nicholas E. Taylor, Stephen M. Walley, Andrew P. Jardine, Annette Glauser, et al. "Characterisation of the impact response of energetic materials: observation of a low-level reaction in 2,6-diamino-3,5-dinitropyrazine-1-oxide (LLM-105)". In: *RSC Advances* 6.33 (2016), pp. 27896–27900. DOI: 10.1039/C6RA03096C.

[16] P. J. Rae and P. M. Dickson. "Some Observations About the Drop-weight Explosive Sensitivity Test". In: *Journal of Dynamic Behavior of Materials* 7.3 (2021), pp. 414–424. DOI: 10.1007/s40870-020-00276-2.

[17] Zhiwei Men, Kenneth S. Suslick, and Dana D. Dlott. "Thermal Explosions of Polymer-Bonded Explosives with High Time and Space Resolution". In: *J. Phys. Chem. C* 122.26 (2018), pp. 14289–14295. DOI: 10.1021/acs.jpcc.8b02422.

[18] M. Muhr, T.M. Klapötke, and G. Holl. "Sensory monitoring of drop hammer experiments with multivariate statistics". In: *Propellants, Explosives, Pyrotechnics* 47.11 (2022). DOI: 10.1002/prep.202200025.

[19] S. Maurer, R. Makarow, J. Warmer, and P. Kaul. "Fast testing for explosive properties of mg-scale samples by thermal activation and classification by physical and chemical properties". In: *Sens. Actuators B: Chem.* 215 (2015), pp. 70–76. URL: https://doi.org/10.1016/j.snb.2015.03.045.

[20] William P. Schaefer, John T. Fourkas, and Bruce G. Tiemann. "Structure of hexamethylene triperoxide diamine". In: *Journal of the American Chemical Society* 107.8 (1985), pp. 2461–2463. DOI: 10.1021/ja00294a043.

[21] Andrzej Wierzbicki, E. Alan Salter, Eugene A. Cioffi, and Edwin D. Stevens. "Density Functional Theory and X-ray Investigations of P- and M-Hexamethylene Triperoxide Diamine and Its Dialdehyde Derivative". In: *Journal of Physical Chemistry A* 105.38 (2001), pp. 8763–8768. DOI: 10.1021/jp0123841.

[22] Jimmie C. Oxley, James L. Smith, Matthew Porter, Lindsay McLennan, Kevin Colizza, Yehuda Zeiri, Ronnie Kosloff, and Faina Dubnikov. *Synthesis and Degradation of Hexamethylene Triperoxide Diamine (HMTD)*. 2015. DOI: 10.1002/prep.201500151.

[23] Jimmie C. Oxley, James L. Smith, Patrick R. Bowden, and Ryan C. Rettinger. "Factors Influencing Triacetone Triperoxide (TATP) and Diacetone Diperoxide (DADP) Formation: Part I". In: *Propellants, Explosives, Pyrotechnics* 38.2 (2013), pp. 244–254. DOI: 10.1002/prep.201200116.

[24] M. Muhr. *mattmatt91/Promotion_process*. https://github.com/mattmatt91/Promotion_process. Accessed: 2022-03-25. 2022.

[25] Fabian Pedregosa, Gaël Varoquaux, Alexandre Gramfort, Vincent Michel, Bertrand Thirion, Olivier Grisel, Mathieu Blondel, Peter Prettenhofer, Ron Weiss, Vincent Dubourg, et al. "Scikit-learn: Machine learning in Python". In: *Journal of machine Learning research* 12 (2011), pp. 2825–2830.

[26] R. González-Méndez et al. "Use of rapid reduced electric field switching to enhance compound specificity for proton transfer reaction-mass spectrometry". In: *Analytical Chemistry* 90.9 (2018), pp. 5664–5670. DOI: 10.1021/acs.analchem.7b05211.

[27] R. González-Méndez et al. "Development and use of a thermal desorption unit and proton transfer reaction mass spectrometry for trace explosive detection: Determination of the instrumental limits of detection and an investigation of memory effects". In: *International Journal of Mass Spectrometry* 385 (2015), pp. 13–18. DOI: 10.1016/j.ijms.2015.05.003.

Part IV

Results and Discussion: Laser Initiation

Sensory Monitoring and Analytical Study of Laser Initiated Graphite-Coated TATP Using PTR-ToF-MS and Microphone

by

Emre Ünal, Matthias Muhr, Jennifer Braun, Thomas M. Klapötke, Peter Kaul

Accepted for publication in
Journal of Energetic Materials, Taylor & Francis, Open Select

The work described in this publication was conducted in collaboration with Mr. Matthias Muhr, with my personal contribution amounting to approximately 50 %. My primary focus was on preparing the explosives and samples for the measurements, as well as conducting the analytical work. Additionally, I contributed to the work on the laser system, which involved adjusting the laser parameters, performing coating tests, and optimizing both the experimental setup and procedures. The central emphasis was on enhancing sensory monitoring during the laser irradiation process.

Abstract: Triacetone triperoxide (TATP) is a significant threat due to its use in improvised explosive devices (IED), attributed to its simple synthesis and readily available precursors. TATP exhibits high sensitivity to impact, friction, and heat. This study investigates detection methodologies focusing on the effects of various laser beam parameters on TATP. By applying coatings with known absorption coefficients, energy can be coupled in a controlled manner without prior knowledge of the substance. This allows for controlled local initiation, preventing mass detonation. In our setup, graphite-coated TATP is irradiated with laser radiation, analysed and controlled using PTR-ToF-MS and a sensitive microphone.

5.1 Introduction

Triacetone triperoxide (TATP) is a highly unstable and sensitive explosive, known for its hazardous nature. Even in small quantities, TATP is prone to detonation from minimal stimuli, such as friction, impact, or changes in temperature. This sensitivity makes it extremely dangerous to handle and transport. TATP's volatility and unpredictability have made it one of the most challenging explosives to manage safely, highlighting the significant risks associated with its presence. The simplicity of its synthesis, coupled with the ready availability of its reactants, makes TATP a popular yet dangerous explosive among terrorist circles, presenting considerable challenges to civil security pattern [1, 2, 3, 4]. Unlike many explosives, TATP contains neither metallic elements nor nitro groups, complicating detection with traditional spectroscopic methods [5, 6, 7, 8, 9, 10, 11, 12]. The significance of this research lies in the fact that TATP represents a major threat to public safety due to its extreme instability and susceptibility to detonation. Developing reliable and safe detection methods for TATP is crucial to preventing its use and mitigating its dangers. In particular, non-destructive detection methods that do not require mechanical sampling are of utmost importance, as traditional approaches are often unreliable or pose safety risks. This research contributes to the exploration of new laser-based detection methods that address the specific challenges posed by TATP and offers a valuable contribution to enhancing civilian security measures. Due to TATP's high sensitivity and the dangerous nature of substance transformation, non-destructive detection meth-

ods and those without mechanical sampling are clearly advantageous in identifying the material. Laser supported techniques such as Raman spectroscopy have been employed, with notable successes [13, 14]. In fact, several commercialized systems now utilize Raman spectroscopy for TATP detection, developed by companies like Pendar Technologies, Thermo Fisher Scientific, and Detectachem [15, 16]. Pendar's X10 handheld Raman spectrometer is capable of identifying hazardous materials, including highly sensitive explosives like TATP, at standoff distances up to six feet, offering enhanced safety and efficiency in field operations. Similarly, Thermo Fisher's FirstDefender and TruNarc systems are widely used by law enforcement and military agencies for rapid identification of explosives, leveraging both Raman and FTIR technologies to detect TATP and other hazardous substances. These systems exemplify the successful transition from research to practical, deployable solutions in enhancing security. In addition to commercial systems, several academic studies have validated the effectiveness of Raman spectroscopy in detecting TATP. For example, Fan et al. demonstrated that Raman spectroscopy could be successfully employed to identify TATP, even at trace levels, making it a robust technique for explosive detection [7]. Bulatov et al. further explored the advantages of Raman spectroscopy in distinguishing between different peroxide-based explosives, highlighting its selectivity and sensitivity [5]. The use of portable Raman systems in real-world environments has also been discussed by Zapata et al., emphasizing their utility in explosive detection [17]. These studies support the view that Raman spectroscopy, particularly in its commercialized handheld forms, is both effective and reliable for TATP detection. For instance, Pendar X10 has been recognized for its ability to detect dangerous materials, including black powders and dark explosives, while minimizing the risk of ignition, thanks to its innovative design that disperses laser heat over a larger area [15]. Thermo Fisher's FirstDefender RM and TruDefender also offer non-contact chemical identification, crucial for safe and efficient handling of explosives like TATP in real-time scenarios [16]. Additionally, the potential for laser initiation of explosive substances has been explored, where a short ignition time is typically the goal [18, 19, 20, 21, 22]. In the field of analysing TATP using MS methods, especially with PTR-ToF-MS, a number of results have been achieved. This technique has been particularly successful in the detection of very low concentrations [12, 23, 24]. A major advantage of this is the extremely short

analysis time of the device, which can be regarded as real time analysis. This makes the measuring method very suitable for live monitoring of processes and reactions [25, 26, 27]. However, the local and controlled initiation of energetic materials using laser radiation comes with a range of problems, particularly for primary explosives. For these, the ignition thresholds are comparatively low, and complete conversion of the sample is likely [18, 20, 28]. The use of coatings in the context of laser processing was investigated [18, 29]. The results show that the energy required to achieve the desired effects can be significantly reduced by using coatings. In this context, the controlled coupling of energy through laser radiation, using coatings, into the materials under investigation is of great interest for the monitoring of the reaction, especially without knowledge of their specific absorption coefficients. One approach is the coating of substances with materials that have a known and significantly higher absorption coefficient than that of the explosive. The desired effect of the coating is to determine laser parameters and conditions at which no conversion of the entire explosive mass occurs, particularly with highly sensitive substances, and at which non-critical quantities (e.g. individual crystals) are initiated simultaneously. For this publication, TATP was synthesized and subjected to photonic radiation. The samples were exposed to power levels ranging from 25 mW to 100 mW, and a set of the samples was coated with graphite to investigate the influence on the processing and decomposition of the substance. The purity of TATP was initially assessed using PTR-ToF-MS and Raman spectroscopy. PTR-ToF-MS was used to analyse the reaction gases. In addition, measurements were taken using a microphone. As a sensor, this can provide a certain amount of information about the degree and intensity of decomposition and, if necessary, about partial decomposition. [30, 31, 32]. The objective of this study is to investigate the relationship between the behaviour of TATP under photonic irradiation and the applied power levels. Furthermore, the influence of highly absorptive coatings on the decomposition of the substance will be examined, as well as the extent to which these coatings promote partial reactions at lower power levels.

5.2 Experimental Section

5.2.1 Synthesis of TATP

A 30% aqueous solution of hydrogen peroxide was carefully dispensed into a reaction vessel using a slender mixing rod for stirring. The vessel was securely sealed with parafilm to prevent any contamination or evaporation and then placed within an ice bath to maintain a low reaction temperature. Afterward, an aliquot of anhydrous acetone was added to the vessel already containing the hydrogen peroxide solution. The two reagents were mixed for at least 15 minutes to ensure uniform distribution. Concentrated sulfuric acid was then slowly introduced to the homogenous solution. The obtained mixture was left to stand undisturbed at a low temperature for a full 24- hour period. Following this incubation period, the reaction mixture was subjected to a purification process to separate Diacetone diperoxide (DADP), using heated methanol as the purification agent. The final product was further cleansed with distilled H2O to eliminate residual contaminants as reported by Oxley et al. [33]. Verification of TATP and DADP within the sample was performed employing Raman spectroscopic techniques, as outlined in Analytical Methods. The synthesis of TATP involves the reaction of hydrogen peroxide with acetone under acidic conditions, with concentrated sulfuric acid acting as the catalyst, as described in the method adapted from Oxley et al. One of the key aspects of this reaction is the formation of various peroxide species, including diacetone diperoxide (DADP), which necessitates further purification to isolate TATP. Acetone is tracked and measured as a critical decomposition product of TATP, as its formation is indicative of the breakdown of the peroxide bond structure within TATP molecules. The identification and monitoring of DADP, along with acetone, are crucial for confirming the purity of the synthesized TATP, since the presence of DADP may complicate the decomposition behavior of TATP in subsequent experiments. This provides a more thorough validation of the experimental data and ensures that the TATP used is not contaminated by significant amounts of other peroxides.

5.2.2 Sample Preparation

Ahead of conducting the experimental measurements, the prepared samples were placed in a climatic chamber and left undisturbed for a minimum duration of 48 hours at a controlled relative humidity of 20 % and a temperature of 18 °C. For the experimental analysis, each sample was transferred into cylindrical metallic tubes of 2 mm diameter and gently pressed by hand. The fill level was set at 5 mm, yielding an average sample mass of 10 mg. For the coated samples, a layer of graphite was applied. The graphite coating was administered using an aerosol technique, employing an airbrush at a consistent distance of 10 cm and a spray duration of 500 ms. Figure 5.1 shows a prepared coated and an uncoated sample as an example.

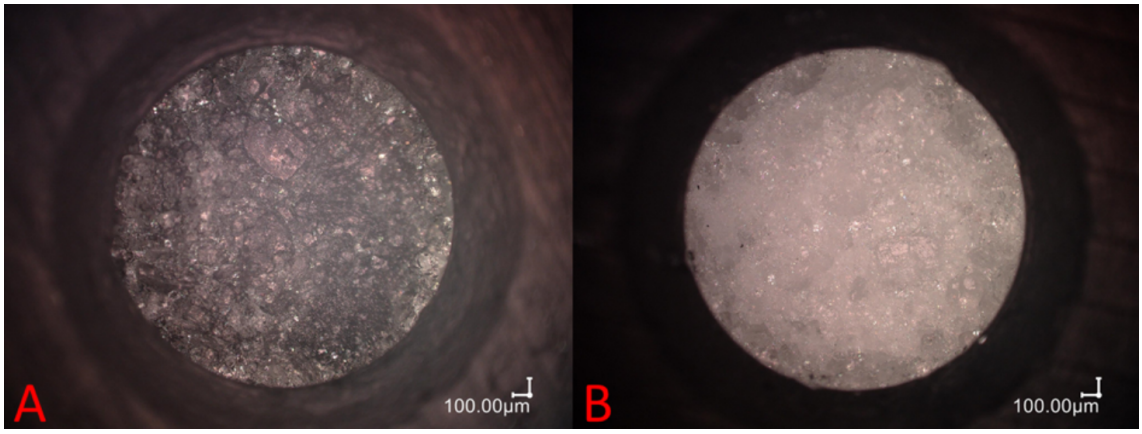

Figure 5.1: Image of the prepared TATP samples, coated on the left (a), uncoated on the right (b)

5.2.3 Analytical Methods

Microphone

A MEMS microphone (ELV MEMS1) was used for acoustic monitoring of the experiments under laser processing. The data was recorded using a DAQ card (Meilhaus Redlad FS 1208) with a sampling rate of 10 kHz.

Raman

The synthesized sample was subjected to analytical scrutiny to confirm the predominance of TATP and its anticipated by-products within the product mix. This was achieved through Raman spectroscopic analysis utilizing a First Defender R device. Instrumental readings were conducted following the standard operating parameters of the device. The resulting spectral data were then cross-referenced and assessed against the device's built-in chemical substance library for verification.

PTR-ToF-MS

A Proton Transfer Reaction Time-of-Flight Mass Spectrometer (PTR-ToF-MS), particularly the Ionicon 2000 model, was utilized for the characterization of synthesized triacetone triperoxide (TATP). This included confirming its identity and detecting prevalent by-products and decomposition compounds. The PTR-ToF-MS comprises an ion source, reaction chamber, drift tube, and a time-of-flight mass spectrometer. For analysis, a 5 mg sample of TATP was placed in a sample vessel and left undisturbed for 60 minutes to facilitate the accumulation of volatile compounds in the gas phase. Subsequently, the PTR-ToF-MS's suction tube was introduced into the vessel to collect the gas sample, using an ionization voltage of 80 Townsend. The same protocol was adhered to during laser experiment measurements [34, 35].

Laser

The samples were irradiated using a laser system developed by Laser Zentrum Hannover e.V. This system is based on a pulsed neodymium-doped yttrium aluminum garnet (NdYAG) laser, with its output wavelength shifted to 532 nm via a frequency conversion crystal. The laser operates at a maximum power of 5 W and a pulse repetition rate of 2000 Hz. Each burst delivers exactly 10 pulses, with each pulse providing 2.5 mJ of energy and lasting for 10 nanoseconds. A 250 mm focal length converging lens is integrated to focus and enhance the optical power. Additionally, a polarization filter is utilized for fine-tuning the laser output. The laser power was measured using a power meter, revealing fluctuations of approx-

imately ±1 mW during adjustments. Measurements of optical power and stability were taken in 1-minute intervals. A shutter was used to precisely control the timing and duration of irradiation.

Setup

For the experiments, the samples were irradiated with laser. The irradiation was controlled with a shutter, which was opened for 15 s per measurement. The microphone and the hose for aspirating the sample for the PRT-ToF-MS are located in front of the sample. A schematic sketch of the setup is shown in Figure 5.2.

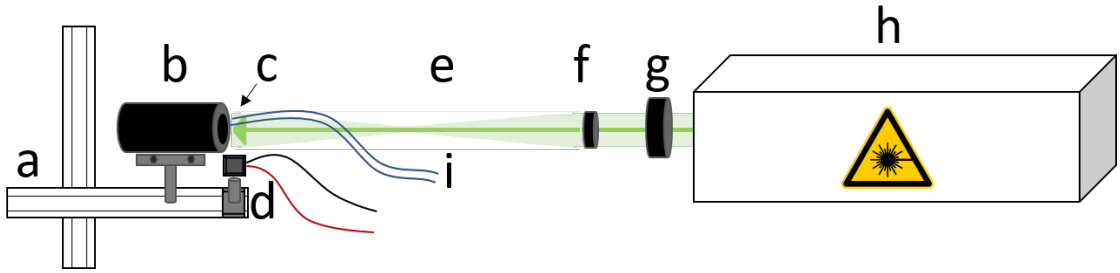

Figure 5.2: Experimental setup: a: yz-stage, b: sample holder, c: sample surface, d: microphone, e: laser beam, f: lens, g: shutter, h: laser system, i: PTR-ToF-MS

Experiments

The experiments were organised as follows: 3 sets without coating (25 mW, 50 mW, 100 mW), one with coating (25 mW) and in total 10 measurements per set were carried out. The shutter opened for 15 seconds. During the each experiment the spot of the beam was defocused on the surface of the sample, to a ratio of 500 µm. Here 5 measurements per parameter set were carried out. Various power levels with and without coating were tested in preliminary trials. Power levels of up to 100 mW proved to be useful for uncoated samples. Power levels above this have led to ignitions in many cases. As conversion inevitably leads to oversaturation of the PTR-ToF and this is undesirable, measurements with higher power were not carried out. In measurements with coating, ignitions frequently occur above 25 mW. Here too, measurements with higher power were not carried out.

5.3 Results and Discussion

Raman

Figure 5.3 shows the Raman measurement of the TATP, the spectra were corrected with the internal software of the measuring device and plotted against a reference spectrum (here in red). The analysis shows that the substance is TATP and that the proportion of DADP (diacetone diperoxide) is negligible.

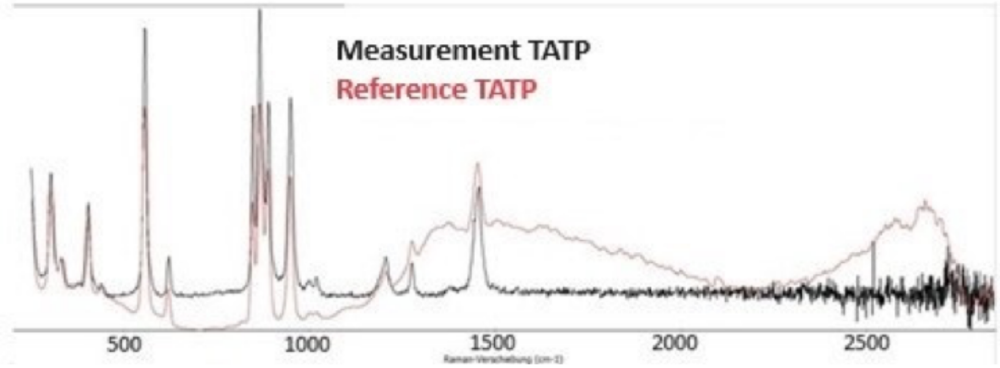

Figure 5.3: Raman spectrum of TATP highlighting the characteristic peaks

Data PTR-ToF-MS

Figure 5.4 shows the mass peaks relevant for the identification of TATP. Due to the protonation of the fragments with a proton, the mass is always 1 g/mol higher than the expected fragment. The peak at 59.049 can be assigned to acetone and the peak at 223.240 to TATP. Mass peaks that are visible in our measurement such as m/z 59.049, 74.000, 75.000, 91.000 are also described in the literature and are typical for TATP [36].

The masses given below for TATP and acetone each contain the additional mass of a proton due to ionisation in the PTR-ToF-MS. The following section presents representative measurements for each class and the investigated mass traces of acetone (59 g/Mol) and TATP (223 g/Mol), as a comprehensive discussion of all data would exceed the scope of this paper. Figure 5.5 illustrates mea-

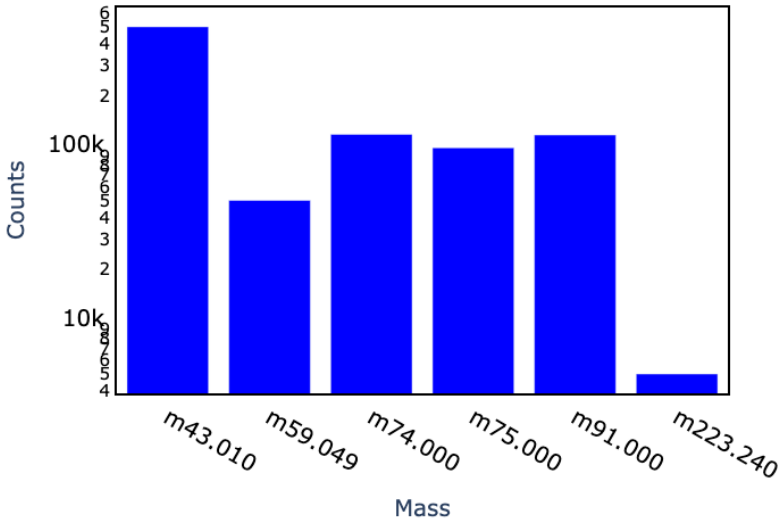

Figure 5.4: Relevant mass peaks of the PTR-ToF-MS measurement of TATP

surements for the mass of acetone. The shutter opens at 10 seconds and remains open for a duration of 15 seconds. Observing the representative measurement of the uncoated sample at 25 mW (oG 25 mW), it is evident that the concentration of acetone slightly increases at around 25 seconds, which can be attributed to a gradual heating of the sample. The power is insufficient to significantly convert TATP into acetone, or to evaporate existing acetone. The measurement at 50 mW (oG 50 mW) exhibits a comparatively stronger increase, with the peak reaching about 75k counts. Here, too, there is a noticeable delay between the opening of the shutter and the detection of acetone, suggesting that the sample is likely being heated slowly rather than being instantaneously vaporized or decomposed. The highest peaks are observed in the 100 mW uncoated class (oG 100 mW), with top values just under 300k counts. It is notable that the signal begins to rise at approximately 12 seconds. Taking into account the offset sampling time of the PTR-ToF-MS, it can be deduced that acetone is immediately transferred to the gas phase upon laser impact. Additionally, the concentration continues to rise after about 20 seconds, which may also be a result of the comparatively slow heating of the sample. When analysing the signal from the coated sample at 25 mW (mG 25 mW), an initial increase is also visible at around 12 seconds. The presence of graphite at this energy level is apparently sufficient to cause immediate decomposition and va-

porisation of the sample. Similar to the 100 mW measurements, the concentration starts to increase more significantly after 20 s. In our experimental setup, acetone is closely monitored because it is one of the primary decomposition products of TATP, formed during its thermal decomposition or photodecomposition. The mass peak at m/z 59.049 corresponds to acetone, while m/z 223.240 corresponds to TATP, both of which are crucial in confirming the decomposition dynamics. The measurement and tracking of these mass peaks provide valuable insight into the integrity of TATP during heating processes. As shown in figure 5.5, the gradual increase in acetone concentration across the power classes suggests that TATP is undergoing slow decomposition at lower power levels, with more rapid breakdown at higher power levels. This correlation between acetone formation and TATP degradation is further supported by figure 5.6, which tracks the behavior of TATP fragments at different power levels. Notably, the delayed signal rise of TATP compared to acetone indicates that TATP decomposes in a more staggered manner, releasing acetone as a primary byproduct. The presence of acetone and the corresponding decrease in TATP signals provide strong evidence of TATP decomposition, with the acetone concentration serving as a marker for the extent of the reaction.

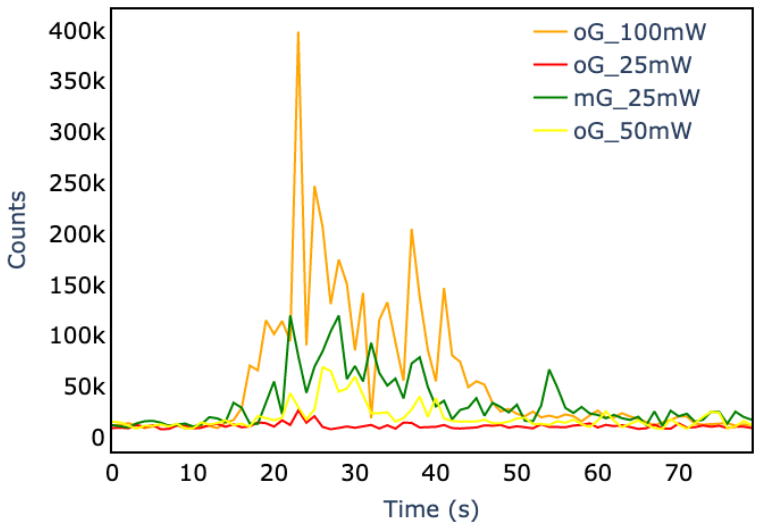

Figure 5.5: Exemplary measurements, one per class, of the acetone (59 g/mol) traces in the PTR-ToF-MS

Figure 5.6 showcases representative traces of TATP from the PTR-ToF-MS measurements. For each class, a single measurement is depicted. Initially, it is evident that the counts for TATP are significantly lower than those for acetone, and the signal-to-noise ratio is also poorer. Examining the measurement from the uncoated series at 25 mW (oG 25 mW), no discernible increase in TATP concentration is observed in relation to the opening of the shutter. The class oG 50 mW exhibits an increase to just over 50 counts around 25 seconds. Here, the delay between the shutter opening and the signal rise is greater than that observed for acetone (the reason for this discrepancy remains to be explored). The signals are difficult to distinguish from noise. Looking at the oG 100 mW class measurement, a clear TATP signal is detectable, peaking at around 65 counts. As with acetone, the delay between the signal and the shutter opening is shorter, yet longer than that for acetone (approximately at 22 seconds). The class with the strongest signals is mG 25 mW. Similar to the oG 100 mW, a clear signal is noticeable, with a timing that mirrors the 100 mW measurements. In the measurement shown, the signal rises to over 75 counts. In both the oG 100 mW and mG 25 mW cases, an energy threshold appears to have been reached where vaporization occurs suddenly, not through comparatively slow heating. Additionally, the throw out of TATP from the borehole by minor partial decompositions could have locally increased the concentration.

For the subsequent analysis of acetone and TATP traces, the measurements were integrated and the average value per class was determined. Figure 5.7 presents the average values of the integrated data per class for acetone. Consistent with the integrated microphone data, it is apparent that the class oG 25mW shows the smallest value (1 M counts). This is followed by class oG 50 mW with approximately 1.7 M counts. The class oG 100 mW yields the highest value at 4.5 M counts. The class mG 25 10 mW is around 3 M counts. This trend is in line with the results from the microphone data evaluation. However, the average value of the integrals per class for the TATP trace exhibits a different pattern (figure 5.8). Here, the value for class mG 25 mW, at just about 2500 counts, is higher than that for the oG 100 mW series (approximately 2200 counts). The reason for this behaviour is presumably that although continuous decomposition and evaporation of TATP takes place in the oG 100 mW class, partial decomposition tends to occur sporadically. In the mG 25 mW class, hotspots are formed

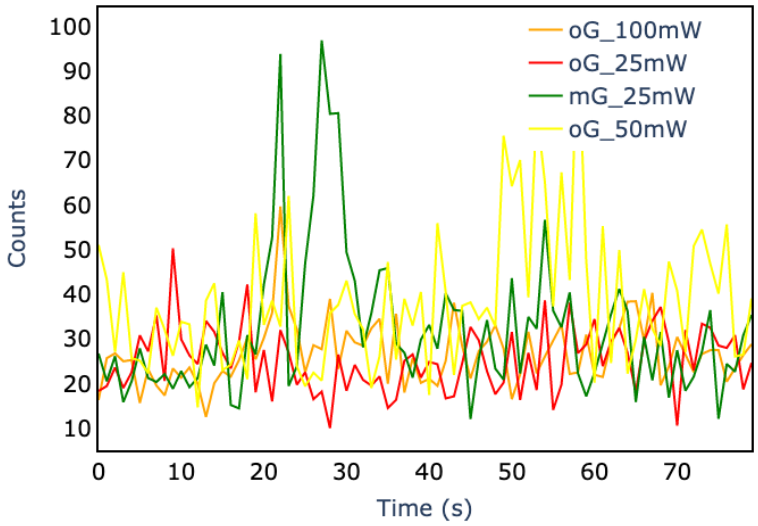

Figure 5.6: Exemplary measurements, one per class, of the TATP (223 g/mol) traces in the PTR-ToF-MS

by the graphite, which lead to partial decompositions. These eject TATP particles from the sample into the air, increasing the concentration. The value for class oG 25 mW is the smallest, with the value for oG 50 mW being slightly higher.

Data Microphone

The raw microphone data is discussed here first. Figure 5.9 shows an example measurement of the microphone data for each category (as the amplitudes of the signals are very different, different y axes are used). Absolute values were used and corrected for their offset. Looking at the measurements without graphite at 25 mW (red), the shutter opening at about 0.75 V is clearly visible. The values do not indicate that significant partial reactions take place. At a power of 50 mW (oG 50 mW, yellow) it can be seen that the signals are significantly stronger than at 25 mW. Here, a signal usually does not exceed 0.4 V. This trend continues at 100 mW (oG 100 mW, orange), where signals of up to 2 V are observed, some even higher. Such peaks could indicate small partial reactions in the TATP, as short and strong pressure increases are typical for explosives. However, the data suggest regular processing without many irregularities. Examination of the signal from the coated sample shows that the signal is more uneven. Most peaks are

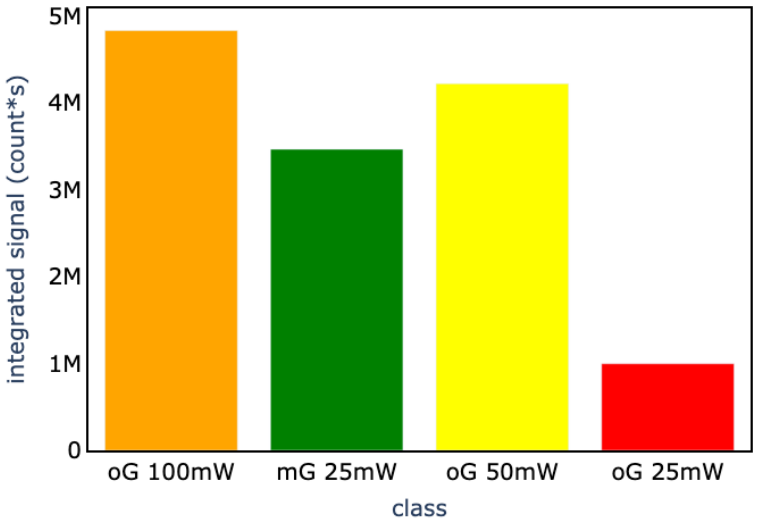

Figure 5.7: Mean value of the integral of the mass traces of acetone (59 counts) per class

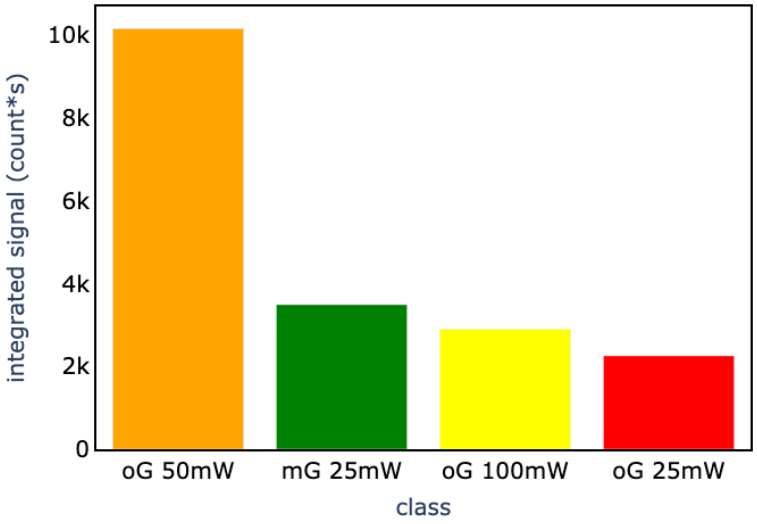

Figure 5.8: Mean value of the integral of the mass traces of TATP (223 counts) per class

around 0.5 V, some are over 1 V. The signals indicate that smaller partial reactions could also take place here. It can be seen that the course of the data at the beginning of the measurement is more irregular and has more large peaks. This could indicate that at the beginning of the measurement there is a stronger interaction with the graphite, which erodes over time and is carried into the sample. Many irregularities are also recognisable during the measurement, which indicate partial conversions. Upon closer examination of the data (figure 5.10), the laser pulse packet is discernible within the measurements. For the oG 25 mW measurement, the peaks caused by the laser are barely distinguishable from noise. At 50 mW, these become clearer, and at 100 mW, they are distinctly visible. The interaction of the radiation with the sample is also clearly visible in the mG 25 mW measurement. Looking at the shape of the peaks, it is generally observed that there is an initial "main peak" caused by the laser, followed by further reactions from the sample, especially at oG 100 mW and mG 25 mW, resulting in small shoulders or subsequent peaks. These are significantly more intense in the 100 mW measurement compared to the coated 25 mW sample. The measurements from all categories were integrated between the opening and closing of the shutter. To account for slight variations in the opening times, the integrated values were then normalized by the duration of the shutter being open. An overview of the maximum values of the respective measurements shown can be seen in table 5.1.

Sample Class	**Signal Amplitude Range (V)**
oG 25 mW	up to 0.75 V
oG 50 mW	up to 0.4 V
oG 100 mW	up to 2 V
mG 25 mW	0.5 V (some over 1 V)

Table 5.1: Summary of Signal Amplitude Range for Each Category

Subsequently, the average values for each category were calculated and are displayed in figure 5.11. Upon examining the data, it is noticeable that the measurements from the uncoated 25 mW (oG 25 mW) samples exhibit the lowest value, approximately 0.4 V. This is followed by the uncoated 50 mW (oG 50 mW) samples showing around 0.45 V. The uncoated 100 mW (oG 100 mW) measurements reach a value of about 1.15 V. The coated 25 mW (mG 25 mW) measurements are positioned between these values, aligning with observations made

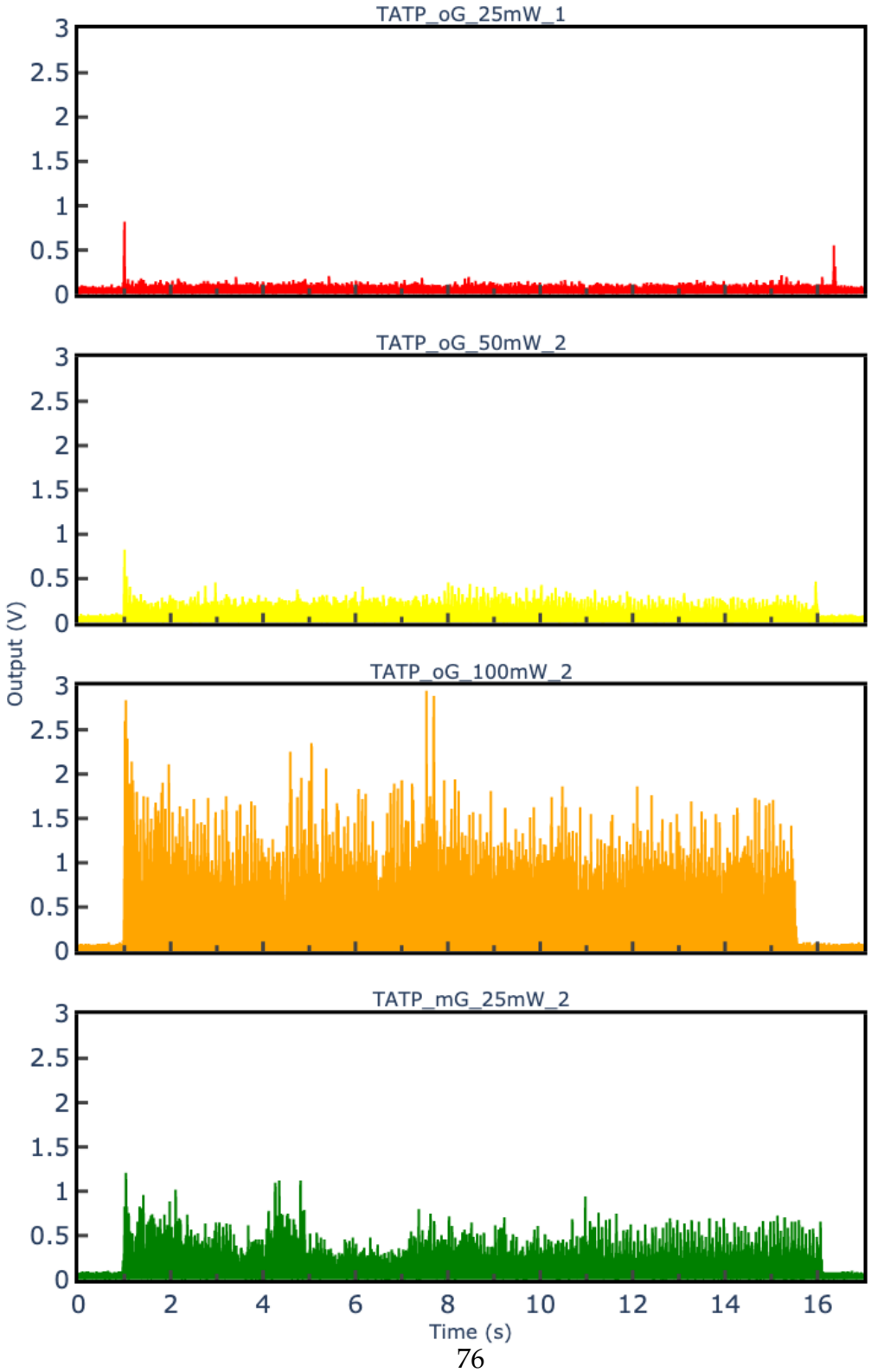

Figure 5.9: Raw data from one measurement per class of microphone

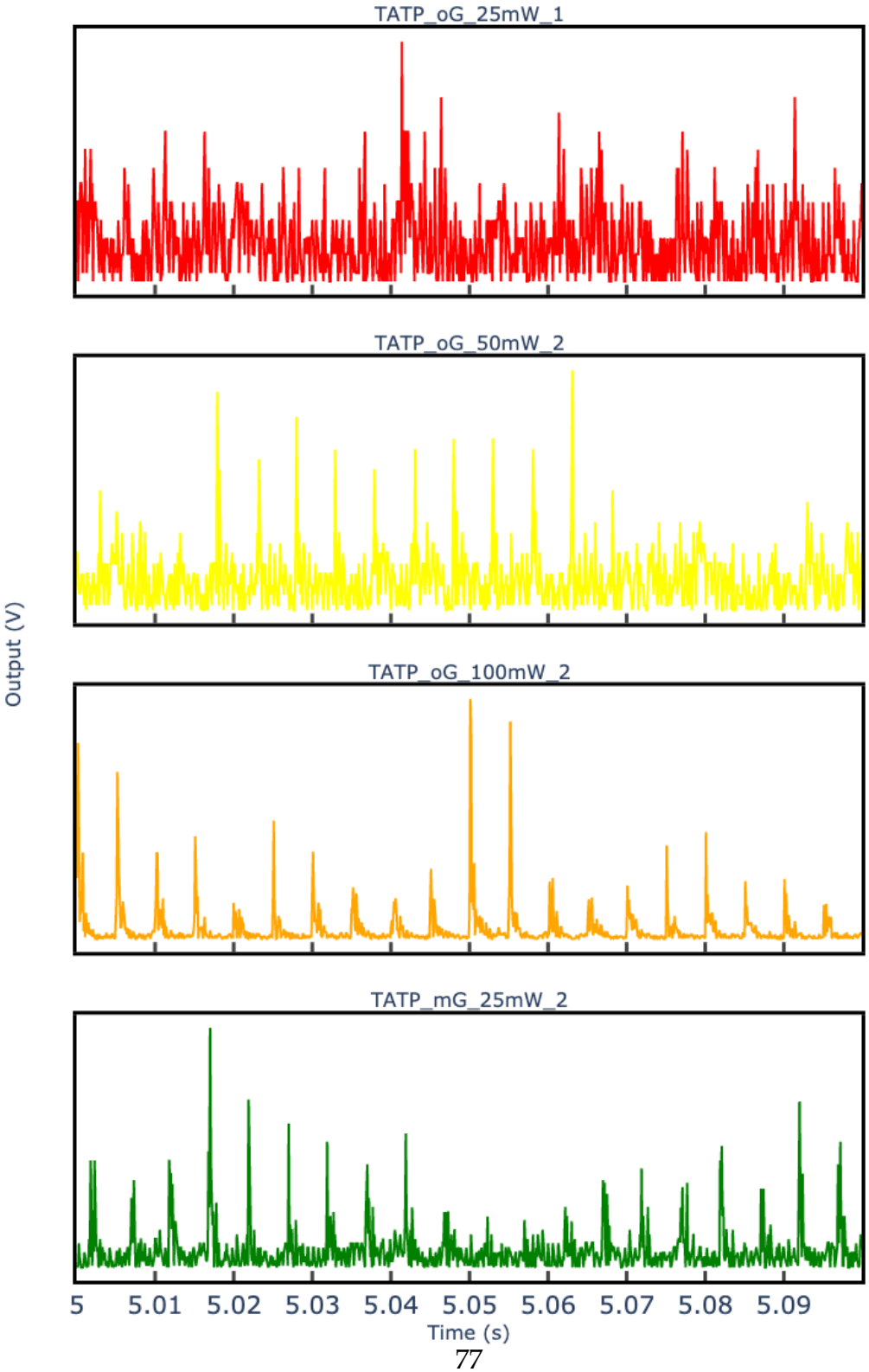

Figure 5.10: Raw data from one measurement per class of microphone, zoomed in

from the raw data. The relationship between the emitted acoustic signal and the power appears to be exponential for uncoated samples, given the available data. In order to obtain more accurate and statistically relevant results, larger measurement volumes will be used in future work.

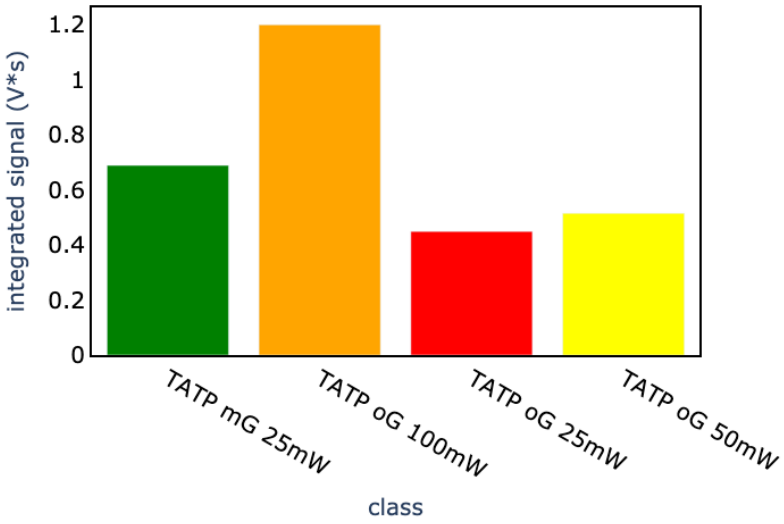

Figure 5.11: Mean values of the integral of all measurements per class of microphone data divided by the shutter opening time

5.4 Conclusion and Outlook

This investigation has demonstrated the successful initiation of triacetone triperoxide (TATP), both graphite-coated and uncoated, using laser irradiation, with analytical emphasis placed on proton-transfer-reaction time-of-flight mass spectrometry (PTR-ToF-MS). The results highlight PTR-ToF-MS as the superior analytical technique, offering highly sensitive and precise quantification of reaction intermediates and products. This method provided critical insights into the reactivity and energetic thresholds of TATP under varying laser parameters, particularly concerning the influence of the graphite coating.

The application of the graphite coating was found to significantly modulate the energetic response of TATP, increasing reproducibility and enhancing control over partial initiation events. These findings suggest that the coating facilitates

localized energy absorption, likely leading to the formation of hot spots that induce crystal reorganization and reaction without full detonation. The graphite layer, by virtue of its high absorption coefficient, appears to play a critical role in mediating the energy transfer dynamics, enabling partial initiation at lower, non-hazardous laser powers—conditions conducive to controlled analytical study.

In contrast, acoustic monitoring via microphone, while capturing sound phenomena during laser initiation, does not offer the same level of precision or direct analytical value as PTR-ToF-MS. Although the microphone provided supplementary data on initiation events, it does not meet the stringent criteria required for robust analytical metrics in energetic material studies. Thus, its utility in this context is limited to secondary, qualitative observations rather than quantitative analysis.

In conclusion, PTR-ToF-MS has proven to be an indispensable tool for the precise monitoring and analysis of laser-induced initiation in sensitive energetic materials like TATP, offering clear advantages over acoustic monitoring in terms of specificity and analytical rigor. Future research will focus on further characterizing the role of various coatings in modulating initiation behavior and enhancing detection sensitivity, as well as optimizing the interplay between laser parameters and material response. Further measurements with different explosives are also planned, so that a basis for a broader data and thus stronger scientific statement on the methods and initiation mechanism can be made.

5.5 Declarations

Data will be made available on a reasonable request.

References

[1] DER STANDARD. *Moscheenanschlag in hernals: Selber sprengstoff wie in london verwendet*. Available at: `https://www.derstandard.at/story/2637639/moscheenanschlag-in-hernals-selber-sprengstoff-wie-in-london-verwendet`. Accessed: 13-11-2023. 2007.

[2] G.M. Segell. "Terrorism on london public transport". In: *Defense & Security Analysis* 22.1 (2006), pp. 45–59. DOI: 10.1080/14751790600577132.

[3] Merkur. *Sprengstoff-Brief an Gauck abgefangen*. Available at: https://www.merkur.de/politik/sprengstoffverdaechtiger-brief-bundespraesidialamt-zr-2861520.html. Accessed: 13-11-2023. 2023.

[4] C. A. Mayhew, P. Sulzer, F. Petersson, S. Haidacher, A. Jordan, P. Watts L. Märk, and T. D. Märk. "Applications of proton transfer reaction time-of-flight mass spectrometry for the sensitive and rapid real-time detection of solid high explosives". In: *International Journal of Mass Spectrometry* 289.1 (2010), pp. 58–63. DOI: 10.1016/j.ijms.2009.09.006.

[5] V. Bulatov, O. Reany, R. Grinko, I. Schechter, and E. Keinan. "Time-resolved, laser initiated detonation of TATP supports the previously predicted non-redox mechanism". In: *Physical Chemistry Chemical Physics* 15.16 (2013), pp. 6041–6048. DOI: 10.1039/C3CP44662J.

[6] F. Dubnikova, R. Kosloff, Y. Zeiri, and Z. Karpas. "Novel approach to the detection of triacetone triperoxide (TATP): Its structure and its complexes with ions". In: *The Journal of Physical Chemistry A* 106.19 (2002), pp. 4951–4956. DOI: 10.1021/jp014189s.

[7] W. Fan, M. Young, J. Caninoan, J. Smith, J. Oxley, and J. R. Almirall. In: *Analytical and Bioanalytical Chemistry* 403.2 (2012), pp. 401–408. DOI: 10.1007/s00216-012-5878-x.

[8] S. Fan, J. Lai, P. L. Burn, and P. E. Shaw. "Solid-state fluorescence-based sensing of TATP via hydrogen peroxide detection". In: *ACS Sensors* 4.1 (2019), pp. 134–142. DOI: 10.1021/acssensors.8b01029.

[9] C. Fischer et al. "TATP stand-off detection with open path: FTIR techniques". In: *Optics and Photonics for Counterterrorism, Crime Fighting, and Defence VIII*. Ed. by C. Lewis and D. Burgess. Vol. 8546. Proceedings of SPIE. SPIE. Edinburgh, United Kingdom, 2012, p. 85460. DOI: 10.1117/12.974592.

[10] Y. Li et al. "Rapid and selective on-site detection of triacetone triperoxide based on visual colorimetric method". In: *Journal of Chemical Research* 46.4 (2022), p. 174751982211174. DOI: 10.1177/17475198221117409.

[11] D. Nascimento Correa et al. “Direct detection of triacetone triperoxide (TATP) in real banknotes from ATM explosion by EASI–MS”. In: *Propellants, Explosives, Pyrotechnics* 42.4 (2017), pp. 370–375. DOI: 10.1002/prep.201600046.

[12] C. Shen et al. “Triacetone triperoxide detection using low reduced-field proton transfer reaction mass spectrometer”. In: *International Journal of Mass Spectrometry* 285.1-2 (2009), pp. 100–103. DOI: 10.1016/j.ijms.2009.04.007.

[13] X. Fang and S.R. Ahmad. “Detection of explosive vapour using surface-enhanced Raman spectroscopy”. In: *Applied Physics B* 97.3 (2009), pp. 723–726. DOI: 10.1007/s00340-009-3644-3.

[14] F. Zapata, M. López-López, and C. García-Ruiz. “Detection and identification of explosives by surface enhanced Raman scattering”. In: *Applied Spectroscopy Reviews* 51.3 (2016), pp. 227–262. DOI: 10.1080/05704928.2015.1118637.

[15] Pendar Technologies. *Pendar X10 Handheld Raman Spectrometer*. https://www.pendar.com/introducing-pendar-x10/. Accessed: 2024-09-05. 2024.

[16] Thermo Fisher Scientific. *FirstDefender RM and TruDefender Handheld Raman Systems*. https://www.thermofisher.com/us/en/home/industrial/spectroscopy-elemental-isotope-analysis/portable-analysis-material-id/raman-spectrometers.html. Accessed: 2024-09-05. 2024.

[17] F. Zapata et al. “Portable Raman spectroscopy for explosive detection: Field testing and applications”. In: *Sensors* 16.3 (2016), p. 352. DOI: 10.3390/s16030352.

[18] N.K. Bourne. “On the laser ignition and initiation of explosives”. In: *Proceedings of the Royal Society of London. Series A: Mathematical, Physical and Engineering Sciences* 457.2010 (2001), pp. 1401–1426. DOI: 10.1098/rspa.2000.0721.

[19] M.D Bowden. “Laser initiation of energetic materials: a historical overview”. In: *Optical Technologies for Arming, Safing, Fuzing, and Firing III*. Ed. by J.W.J. Thomes and F.M. Dickey. SPIE Proceedings. SPIE. 2007, p. 666208. DOI: 10.1117/12.734225.

[20] J.G. Du, H.H. Ma, and Z.W. Shen. "Laser initiation of non–primary explosive detonators". In: *Propellants, Explosives, Pyrotechnics* 38.4 (2013), pp. 502–504. DOI: 10.1002/prep.201200132.

[21] X. Fang and W.G. McLuckie. "Laser ignitibility of insensitive secondary explosive 1,1-diamino-2,2-dinitroethene (FOX-7)". In: *Journal of Hazardous Materials* 285 (2015), pp. 375–382. DOI: 10.1016/j.jhazmat.2014.12.006.

[22] Y. Wang et al. "Laser ignition of energetic complexes: impact of metal ion on laser initiation ability". In: *New Journal of Chemistry* 45.28 (2021), pp. 12705–12710. DOI: 10.1039/d1nj02345d.

[23] P. Sulzer et al. "Designer drugs and trace explosives detection with the help of very recent advancements in proton-transfer-reaction mass spectrometry (PTR-MS)". In: *Future Security*. Ed. by N. Aschenbruck et al. Vol. 318. Communications in Computer and Information Science. Springer Berlin Heidelberg. Berlin, Heidelberg, 2012, pp. 366–375.

[24] Q. Zhang et al. "Ammonia-assisted proton transfer reaction mass spectrometry for detecting triacetone triperoxide (TATP) explosive". In: *Journal of the American Society for Mass Spectrometry* 30.3 (2019), pp. 501–508. DOI: 10.1007/s13361-018-2108-6.

[25] I. Khomenko et al. "Non-invasive real time monitoring of yeast volatilome by PTR-TOF-MS". In: *Metabolomics* 13.10 (2017), p. 118. DOI: 10.1007/s11306-017-1259-y.

[26] F. Wieland et al. "Online monitoring of coffee roasting by proton transfer reaction time-of-flight mass spectrometry (PTR-TOF-MS): towards a real-time process control for a consistent roast profile". In: *Analytical and Bioanalytical Chemistry* 402.8 (2012), pp. 2531–2543. DOI: 10.1007/s00216-011-5401-9.

[27] L. Zhu et al. "Real-time monitoring of emissions from monoethanolamine-based industrial scale carbon capture facilities". In: *Environmental science & technology* 47.24 (2013), pp. 14306–14314. DOI: 10.1021/es4035045.

[28] R. Akhmetshin et al. "Effect of laser radiation wavelength on explosives initiation thresholds". In: *Journal of Physics: Conference Series* 552 (2014), p. 012015. DOI: 10.1088/1742-6596/552/1/012015.

[29] F. Dausinger et al. “Energy coupling in surface treatment processes”. In: *Journal of Laser Applications* 2.3 (1990), pp. 17–21. DOI: 10.2351/1.4745263.

[30] X. Chen et al. “Standoff photoacoustic detection of explosives using quantum cascade laser and an ultrasensitive microphone”. In: *Applied optics* 52.12 (2013), pp. 2626–2632. DOI: 10.1364/AO.52.002626.

[31] T.M. Klapötke and C.M. Rienäcker. “Drophammer test investigations on some inorganic and organic azides”. In: *Propellants, Explosives, Pyrotechnics* 26.1 (2001), pp. 43–47. DOI: 10.1002/prep.200100073.

[32] M. Muhr, T.M. Klapötke, and G. Holl. “Sensory monitoring of drop hammer experiments with multivariate statistics”. In: *Propellants, Explosives, Pyrotechnics* 47.11 (2022). DOI: 10.1002/prep.202200025.

[33] Jimmie C. Oxley, James L. Smith, and H. Chen. “Decomposition of a Multi-Peroxidic Compound: Triacetone Triperoxide (TATP)”. In: *Propellants, Explosives, Pyrotechnics* 27.4 (2002), pp. 209–216. DOI: 10.1002/prep.200290019.

[34] R. González-Méndez et al. “Development and use of a thermal desorption unit and proton transfer reaction mass spectrometry for trace explosive detection: Determination of the instrumental limits of detection and an investigation of memory effects”. In: *International Journal of Mass Spectrometry* 385 (2015), pp. 13–18. DOI: 10.1016/j.ijms.2015.05.003.

[35] R. González-Méndez et al. “Use of rapid reduced electric field switching to enhance compound specificity for proton transfer reaction-mass spectrometry”. In: *Analytical Chemistry* 90.9 (2018), pp. 5664–5670. DOI: 10.1021/acs.analchem.7b05211.

[36] Jimmie C. Oxley, James L. Smith, Patrick R. Bowden, and Ryan C. Rettinger. “Factors Influencing Triacetone Triperoxide (TATP) and Diacetone Diperoxide (DADP) Formation: Part I”. In: *Propellants, Explosives, Pyrotechnics* 38.2 (2013), pp. 244–254. DOI: 10.1002/prep.201200116.

Investigation of laser initiation of graphite-coated TATP and HMTD with regard to the influence of coating thickness accompanied by sensor-safe surveillance using a microphone

by

Emre Ünal, Matthias Muhr, Thomas M. Klapötke*, Peter Kaul

Publication in Propellants, Explosives, Pyrotechnics
DOI: 10.1002/prep.202400188

This publication reports work carried out in collaboration with Mr. Matthias Muhr, with my contribution accounting for approximately 50 %. My main responsibilities included the synthesis and preparation of the substances, along with the development of the sensor technology. I also contributed to the work on the laser system, optimizing both the samples and sensors, as well as determining and fine-tuning the laser parameters. Furthermore, I was actively involved in the analysis and interpretation of the resulting data.

Abstract: Triacetone triperoxide (TATP) and Hexamethylene triperoxide diamine (HMTD), known for their propensity towards use in improvised explosive devices due to facile synthesis from readily accessible precursors, present a considerable security challenge. Their sensitivity to mechanical stimuli, such as impact and friction, as well as to thermal input, necessitates the development of advanced detection methodologies. This study is dedicated to evaluate the influence of varied laser beam parameters during radiation on these peroxide-based energetic materials. A novel approach for the controlled energy delivery to substances under investigation involves the application of coatings with predefined absorption coefficients. This technique, coupled with the careful selection of laser parameters, enables the controlled local initiation of reaction in the energetic material without reaching the threshold for mass combustion, thereby avoiding detonation or deflagration. The experimental setup involves the laser irradiation of defined quantities of graphite-coated TATP and HMTD, with the subsequent laser processing being monitored using a sensitive microphone. This set-up enables a detailed investigation of the physical phenomena that manifest themselves during the interaction and thus contributes to the state of knowledge about the safe handling and detection of these energetic materials.

6.1 Introduction

Triacetone triperoxide (TATP) and Hexamethylene triperoxide diamine (HMTD) are highly dangerous explosives due to their extreme sensitivity to accidental ignition and propensity for spontaneous detonation [1, 2]. Their acute sensitivity to accidental ignition and likelihood of spontaneous detonation make them especially challenging to handle and detect safely [3, 4, 5, 6, 7]. The simplicity of their synthesis and the accessibility of their reactants have made them explosives of choice among terrorist groups, posing significant challenges to civil security [8, 9, 10, 11]. Unlike many explosives, TATP and HMTD lack metallic elements and nitro groups, which complicates their detection through traditional spectroscopic techniques [12]. Consequently, non-destructive detection methods, especially those that do not require mechanical sampling, are preferred for identifying these materials. Techniques such as Raman spectroscopy, supported by

laser technology, have achieved notable success in this area [13, 14]. Furthermore, approaches from the combination of microphone and the detection of explosives and vapours by means of acoustical spectroscopy have been tested and have produced promising results [15, 16]. Furthermore, the exploration of laser initiation of these explosives, aiming for a brief ignition time, has been a focus of research [17]. However, the use of laser radiation for the local and controlled initiation of energetic materials presents challenges, especially with primary explosives that have relatively low ignition thresholds and are likely to undergo complete combustion [15]. The application of coatings in laser processing has been studied to reduce the energy required for desired effects [18]. This approach involves coating substances with materials that possess a significantly higher absorption coefficient than the explosives themselves. The goal is to identify laser parameters and conditions that prevent the combustion of the entire explosive mass, especially with highly sensitive substances, while simultaneously initiating non-critical quantities, such as individual crystals. In this study, TATP and HMTD were synthesized and exposed to photonic radiation at power levels from 12.5 mW to 100 mW. The effect of graphite coatings of varying thicknesses on the processing and decomposition of these substances was investigated. Raman spectroscopy assessed the purity of the substances, while a microphone served as a reliable sensor for detecting partial conversions. This research aims to explore the behavior of TATP and HMTD under photonic irradiation, the impact of graphite coating on their decomposition, and how these coatings facilitate partial reactions at lower power levels.

6.2 Experimental

6.2.1 Synthesis of TATP

Caution. TATP is a strong explosive compound and requires experienced personnel. The synthesis was carried out according to Oxley et al. [19]. Hydrogen peroxide at a concentration of 30 % was carefully added to a reaction vessel. The vessel was then sealed with parafilm to prevent any contamination or evaporation and placed in an ice bath to keep the reaction temperature low. Anhydrous acetone was then added to the vessel containing the hydrogen peroxide solution.

The components were stirred for at least 15 minutes to ensure good mixing. Concentrated sulphuric acid was then gradually added to the homogeneous solution. The mixture was left undisturbed for 24 hours at a reduced temperature. The reaction mixture was purified with methanol to remove DADP. The final product was then rinsed with distilled water to remove any remaining impurities.

6.2.2 Synthesis of HMTD

Caution. HMTD is a strong explosive compound and requires experienced personnel. For the synthesis, hexamine was added to an aqueous solution of formaldehyde in an ice bath. Subsequently, a hydrogen peroxide solution was gradually added. The reaction mixture was further treated by addition of citric acid. Precipitation of HMTD was observed within two hours, a significant reduction from the 5-6 hours normally required in the absence of formaldehyde. The reaction was allowed to run overnight while the temperature of the ice bath gradually increased to room temperature. The crude HMTD product was isolated by vacuum filtration, washed with distilled water to remove residual acid and then washed methanol to facilitate drying. The product was dried at room temperature [2, 20].

6.2.3 Sample Preparation

Ahead of conducting the experimental measurements, the prepared samples were placed in a climate chamber and left undisturbed for a minimum duration of 48 hours at a controlled relative humidity of 20 % and a temperature of 18 °C. In the experimental setup, each specimen was placed into cylindrical metallic tubes with a diameter of 2 mm. The tubes were filled to a height of 5 mm and gently pressed manually with a suitable metal rod, which corresponds to an approximate sample mass of 10 mg. This type of sample preparation creates a surface that is not microscopically planar, which can increase the variability of the results. After filling, the samples were carefully sealed. For the preparation of coated samples, a mono or bilayer graphite deposition was executed, ensuring the complete drying of the initial layer prior to the application of the subsequent one. The graphite layers were administered using an aerosolised delivery method, facili-

tated by an airbrush apparatus positioned at a fixed distance of 10 cm from the target, with a spray exposure time precisely controlled at 500 ms. The particle size of the graphot was between 1 and 10 µm. Figure 6.1 shows specimens that have been prepared exemplary. A is an uncoated sample, B is a single-coated sample and C is a double-coated sample. In the following, samples are mostly labelled with abbreviations. oG stands for uncoated, mG for single-coated and 2mG for double-coated. The power and the consecutive number of the parameter set are given below. For example, TATP_mg_50mW_2 is the second measurement of single-coated TATP and a power of 50 mW.

6.2.4 Analytical methods

RAMAN

Samples were analysed for purity and the presence of by-products by Raman spectroscopy using a First Defender R by Thermo Fischer. The measurements were performed according to the standard operating procedures of the instrument. The spectral data subsequently obtained were compared to the instrument's inbuilt chemical library and analysed for confirmation.

Microphone

During laser processing experiments, acoustic monitoring was carried out using a MEMS microphone (ELV MEMS1). Output voltage was captured via a DAQ card (Meilhaus Redlab FS 1208) set to a sampling 10 kHz.

Laser

For the experiments, the samples were irradiated with a laser contructed by Laser Zentrum Hannover e.V.. The laser used is a pulsed neodymium-doped yttrium aluminium doped laser (NdYAG). Its output wavelength is converted to 532 nm using a conversion crystal. The system has a maximum output power of 5 W and a pulse frequency of 2000 Hz. Each burst consists of exactly 10 pulses with a single-pulse energy of 2.5 mJ, with each pulse having a duration of 10 nanoseconds. A converging lens with a focal length of 250 mm is integrated into the system to refine and concentrate the optical power. A polarisation filter is

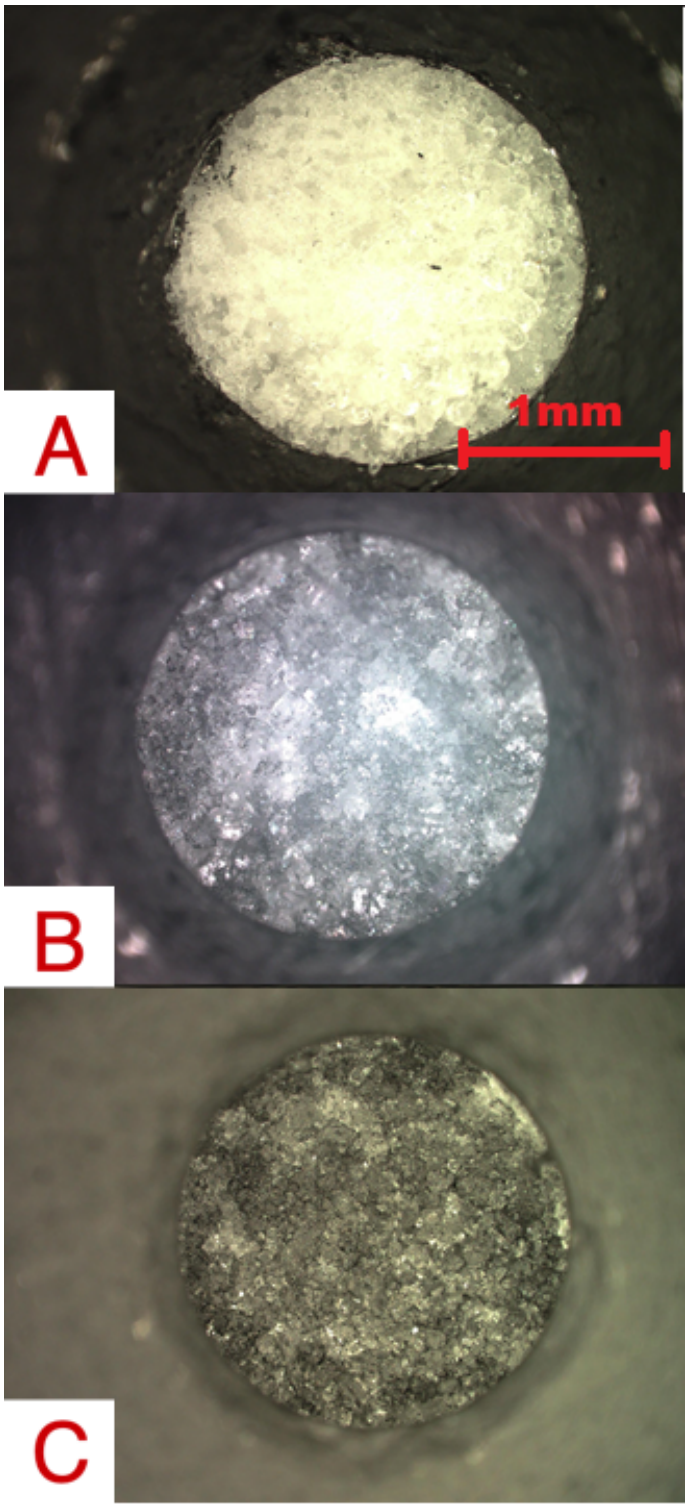

Figure 6.1: Preparation and coating of TATP samples (magnification: 100x): A: uncoated, B: single-coated, C: double-coated

used to precisely adjust the laser power. The power was checked using a power meter. The power fluctuations during adjustment are around ± 1 mW. The optical power and fluctuations were checked using a power meter in a time interval of about 1 min. The regulation of the irradiation was precisely controlled with the aid of a shutter programmed for an exposure time of 15 seconds per measurement cycle.

6.2.5 Experiments

TATP and HMTD samples were investigated. These were each coated with graphite a different number of times and irradiated with the laser at different laser power and constant irradiation time. The basic influence of the graphite coating was analysed in order to be able to make a comparison with inert and explosive materials. As an organic reference material, sugar, also coated and uncoated, was analysed in the same structure and with the same parameters. All samples were irradiated with 12.5, 25, 50 and 100 mW for 15 s each at a distance of about 20 mm from the focus. The focus was located behind the sample so that the laser spot was defocused on the surface to a ratio of 500 µm. With the exception of HMTD, all tests were repeated three times. A schematic sketch of the structure is shown in Figure 6.2. Measurements with HMTD with two graphite layers and power >= 50mW and TATP with power of 100 mW were omitted, as this always led to complete combustion of the sample. Data acquisition was performed using a DAQ card with a sampling 10 kHz, followed by moving average and envelope smoothing which is explained in detail in 6.2.6.

6.2.6 Preprocessing

The preprocessing script for analogue microphone data involves cleaning the data by subtracting the mean of the first 1000 points to remove baseline drift and taking the absolute value to ensure all positive values [21]. An upper envelope is created by applying a rolling maximum over 1000 points, which highlights the data peaks and smooths short-term fluctuations. Subsequently, a rolling mean is calculated over 100 points to further smooth the data, followed by downsampling to reduce data size and emphasize overall trends. These steps ensure the

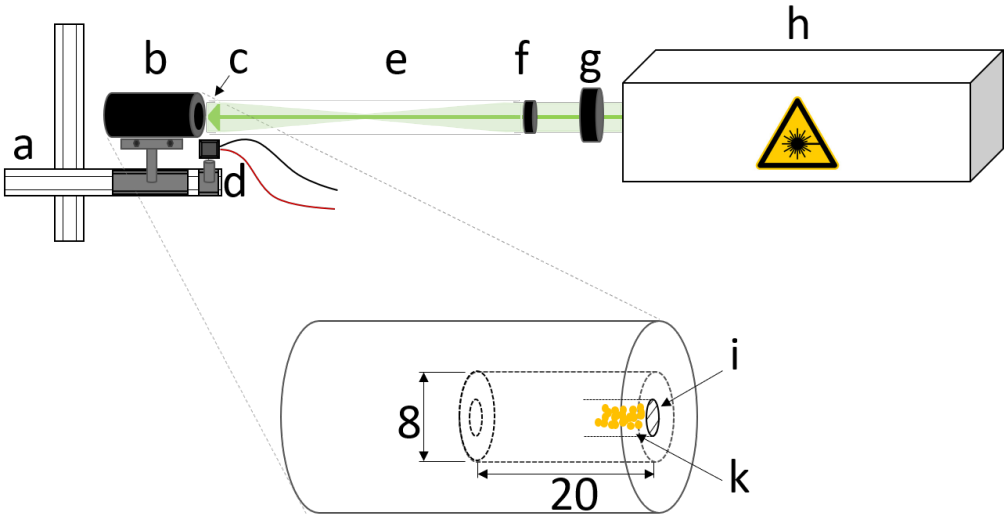

Figure 6.2: Schematic sketch of the set-up - a: x-y stage, b: sample container, c: sample container; sample, d: microphone, e: laser beam, f: converging lens, g: shutter, h: laser system, i: sample container; coating (enlarged), k: sample (enlarged)

data are clean, smooth, and ready for accurate analysis by reducing noise and highlighting key features.

6.3 Results and Discussion

6.3.1 Raman Measurements

The spectra were acquired using the integrated software of the employed device and plotted against existing reference spectra. The spectra confirm that the substances used are indeed TATP and HMTD, with no significant impurities or competing products detected.

6.3.2 Microphone Measurements

The data recorded by the microphone are discussed below. The presented plots are representative and illustrate the trends observed for each substance. The voltage output from the microphone was captured, and the following plots display

measurements for each substance at a specific power level with all coating variations. To facilitate data analysis, pre-processing was conducted. Specifically, the absolute values of the signals were utilized, as a significant signal can be identified at the start of each plot.

Data discussion

The following section presents and discusses the preprocessing voltage output of the microphone from measurements with varying coating and power. Measurements with HMTD with two graphite layers and power >= 50 mW and TATP with power of 100 mW were omitted, as this always led to complete combustion of the sample.

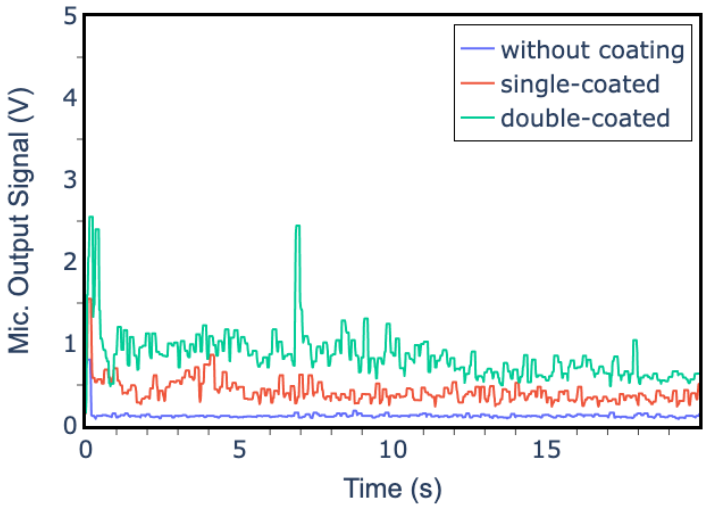

Figure 6.3: Exemplary preprocessed microphone data of HMTD - 25 mW - all coatings

Figure 6.3 shows the test results for a laser power of 25 mW and all three coatings as examples of HMTD measurements. At the beginning of each graph, a strong high signal can be seen, caused by the first impact of the laserbeam on the sample. This can be observed in all measurements and is generally stronger the higher the laser power. For the measurement without graphite coating, the microphone signal is around 0.8 V (Figure 6.3). Subsequently, a low, noisy signal can be recognised, which indicates a low level of processing (interaction of

the laserbeam and the investigated material). There is no significant variation in intensity over time. The signal does not exceed 0.2 V after the laser has been applied for the first time. The exemplary measurement of the single coated HMTD sample shows a significantly stronger signal. The opening of the shutter can also be recognised here, whereby the signal is around 1.5 V. The signal then shows some irregularities, with smaller peaks of up to 0.7 V. The peaks that occur are presumably caused by smaller partial combustions in the sample, which do not lead to complete combustion of the sample. It can be seen that the occurrence of these peaks decreases with time. This can be caused by the removal of the graphite layer or the pushing of the graphite particles into the depth of the explosive sample. This trend continues in the measurements with a double graphite layer. The first impact of the laser on the sample is also clearly visible here. This is higher than in the other two measurements and is around 2.5 V. Here too, the signal tends to be rather irregular, which indicates a partial decomposition of the sample. One peak directly after opening the shutter and another at around 7 seconds are particularly noticeable. It can also be seen here that the occurrence and intensity of these peaks decrease with time.

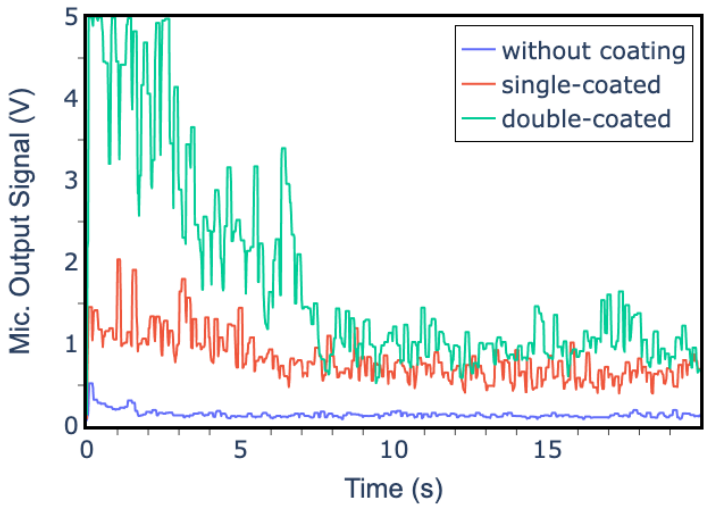

Figure 6.4: Exemplary preprocessed microphone data of TATP - 50 mW - all coatings

Figure 6.4 shows exemplary measurements with all three coatings at 50 mW

for TATP. The measurement without graphite shows, with the exception of the first impact of the laser, similar to HMTD, only very weak signals whose intensity remains constant over time and does not exceed 0.2 V. At the first impact of the laser, the signal is about 0.5 V high. The data show that the sample is processed without coating, but no significant partial conversion takes place. The measurement shown with a graphite coating shows more irregular peaks, which could be caused by partial conversions. The signals reach levels of up to 2 V. It can be seen that the intensity decreases with time, which is presumably caused by removing or pressing the graphite particles into the sample. If this is compared with the double-coated sample, it is noticeable that the latter has very strong peaks in the signal. The first impact of the laser is comparatively small in this measurement, but this is not the rule for these parameters. The signals sometimes exceed the microphone's dynamic range of 5 V. It is noticeable that the signal decreases sharply and almost falls to the level of the single-coated sample. This is also due to the removal of the graphite particles or the introduction of the graphite particles into the sample, which increases the absorption.

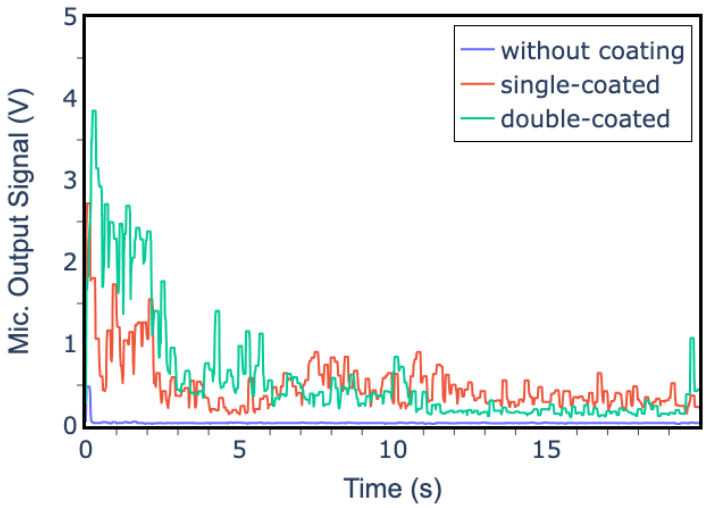

Figure 6.5: Exemplary preprocessed mikrophone data of combusted samples - 50 mW - double coated

Exemplary measurements for sugar with 50 mW with all coating variations are shown in Figure 6.5. Looking at the measurement without graphite coating,

the first impact of the laser on the sample with an amplitude of approximately 0.3 V is clearly recognisable. Otherwise, this measurement shows little deflection, which indicates that the sample is not or only very slightly processed. The signal does not exceed 0.1 V. If one compares the measurements with the simple graphite layer, significantly stronger signals can be seen. When the laser hits the sample for the first time, the signal reaches over 2.5 V. The subsequent signal curve shows many smaller peaks, which indicate processing. The peaks are smaller than with the explosives, which is due to the fact that the decomposition is not self-propagating and only small amounts of the sugar are decomposed. It is also noticeable that the signal intensities decrease with time, which indicates that the graphite particles are being driven into the sample or removed. Compared to the single-coated measurement, however, the signals are higher. When the laser strikes the graphite layer, a signal of just under 4 V is generated.

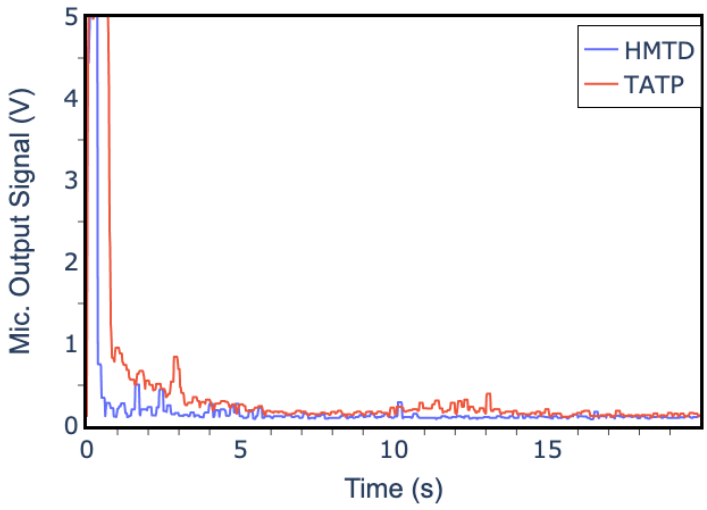

Figure 6.6: Exemplary preprocessed mikrophone data of combusted samples - 50 mW - double coated

Figure 6.6 also shows some examples of data from samples where processing via laser led to complete combustion of the sample. As these would falsify the statistical analysis, these data were not taken into account. It is noticeable that when a sample is combusted, this happens in most cases directly after opening the shutter. This is probably due to the initially high amount of graphite which

increases the formation of hot spots.

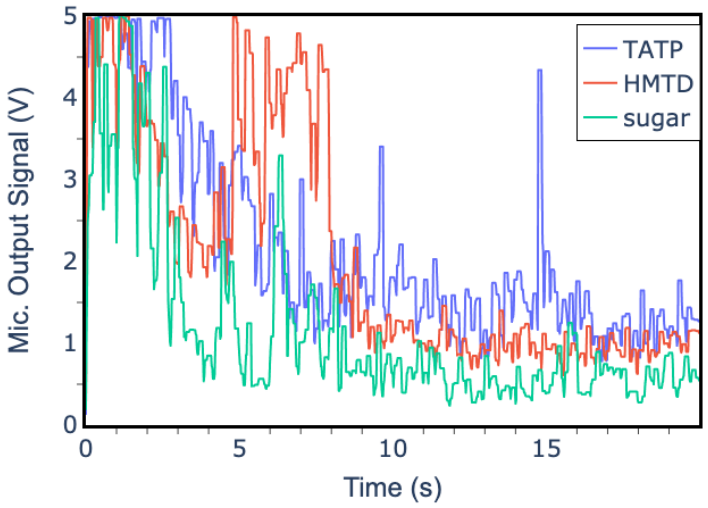

Figure 6.7: Exemplary measurement for TATP, HMTD and sugar with single graphite coating at 100 mW

If one compares the exemplary measurements of all three substances in Figure 6.7, you can see that all substances show a clear signal. It can be seen that all samples also generate signals that exceed the dynamic range of the 5 V microphone. Over time, it is noticeable that the signal decreases for all samples. Compared to the other samples shown in this plot, the measurement of sugar shows fewer and also smaller peaks above the signal, which are caused by the decomposition of the sugar. The measurement with TATP shows high, narrow peaks over the entire measurement, whereby their frequency decreases over time. This is characteristic for measurements with TATP. It is also noticeable that a high basic low level of the signals can be recognised at the beginning of the measurement. This is due to partial redistribution of the material and a high availability of graphite at the beginning of the measurement. The observable partial combustion of the sample, as well as the general mechanism of decomposition, are probably triggered by hotspots, in which a graphite particle is heated by the strong absorption of the laser radiation and initiates the decomposition [22, 23, 24]. If this behaviour is compared with that of the HMTD sample, a high baseline of the signal can be seen here, particularly at the start of processing. This decreases

in the course of the measurement. In contrast to TATP, HMTD shows a stronger accumulation of peaks during the measurement. It appears that the partial reactions are more intense here at the same laser power. This is also consistent with the observations that HMTD tends to react faster in the double-coated samples. In general, the microphone signal of the measurements with HMTD is not significantly higher than that of TATP, which may indicate that HMTD tends to react more strongly once a hotspot is created.

Statistical Evaluation

In order to quantitatively analyze the data of the measurements, the data of all measurements with the same parameters (i.e. sample, reading and coating) were integrated and averaged over the groups. In the following, the data are shown in bar plots. Each plot represents the data of a substance at all powers and different coatings. The standard deviation is shown as an error bar.

Figure 6.8 shows the extracted integrals of the microphone data of all HMTD measurements. Looking at the mean values of the integrals over the different powers (Figure 6.8), it is clear to see that the amount of noise emissions generated by processing and partial decomposition increases with number of graphite layers applied. The uncoated sample shows a slight increase in the integral, with values increasing from 0.12 Vs at 12.5 mW to 0.31 Vs at 100 mW. It can be assumed that the values observed are dependent on the laser power. This is also shown by the HMTD measurements with a graphite layer. Here the values increase from 0.17 Vs at 12.5 mW to 1.42 Vs at 100 mW, too. Such an increase can also be seen in the measurements with two layers of graphite. The values here are approximately 0.19 Vs at 12.5 mW to 0.60 Vs at 25 mW. For future investigations, it could be determined whether there is an acoustic threshold above which a sample tends towards complete combustion.

Looking at the data situation for TATP (Figure 6.9), the picture is similar. Here, too, it is clear that the noise emissions increase with increasing power. The values 0.09 Vs at 12.5 mW rise to 0.35 Vs at 100 mW. It is noticeable that the values for TATP in the section are more power-dependent than those of the HMTD. This trend is also confirmed in the measurements with a single graphite layer. These range from 0.24 Vs at 12.5 mW to 2.04 Vs at 100 mW, which is higher than the

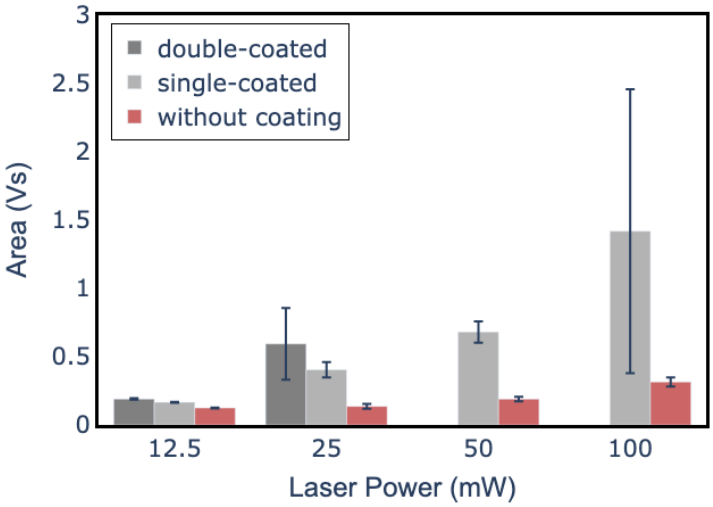

Figure 6.8: Integral of the microphone signal of the HMTD measurements averaged over all measurements with all coating types

value for HTMD. Looking at the plots for double coated samples, it can be seen that these are at 0.19 Vs at 12.5 mW and increase to 1.66 Vs at 50 mW. Again, this confirms the trend that the dependence of noise emissions on conductivity increases with increasing coating thickness. It is striking that the values of the single-coated samples at 12.5 and 25 mW are higher than those of the double-coated samples.

Looking at the statistically analysed data for sugar (Figure 6.10), there are differences to those for explosives. Basically, it can also be recognised here that the noise emissions increase with increasing laser power, but this is not as clear as with the explosives. For example, the emission of uncoated samples increases from 0.023 Vs at 12.5 mW to 0.045 Vs at 25 mW, but no further increase can be observed thereafter. However, both the single-coated sample and the double-coated sample with graphite show an increase. The values for single-coated samples and 12.5 mW range from 0.17 Vs to 1.4 Vs at 100 mW. What is striking about this substance is that the integrals of the signals for the single-coated sample are higher than those of the double-coated sample for three out of four lines. However, the differences are small compared to the differences between the single and double coated samples for the explosives, as can be seen from the standard deviations in

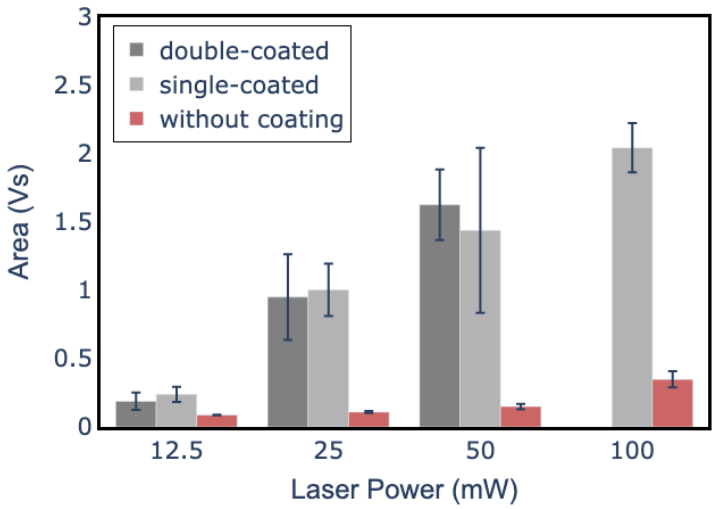

Figure 6.9: Integral of the microphone signal of the TATP measurements averaged over all measurements with all coating types

the plots (TATP in Figure 6.9 and HMTD in Figure 6.8). The reason for this could be that the amount of graphite is relatively large and is not thrown out of the hole by smaller amounts, as could be the case with the explosives.

Optical Evaluation

igure 6.11 shows a single-coated TATP sample after treatment with 50 mW. The focus point of the laser is marked with a red cross. It can be seen that the processing has created a cavity. This has a diameter of about 600 µm. This is significantly larger than the beam diameter in the area where the laser hits the sample. The reason for this is that gas is produced during the processing of the sample, which flows out through the drill hole. This effect is intensified by the occurrence of small partial reactions that take place in explosives under laser irradiation. This observation is consistent with the fact that the intensity of the treatment decreases over time and that graphite is lost due to the partial over-expansion of the sample.

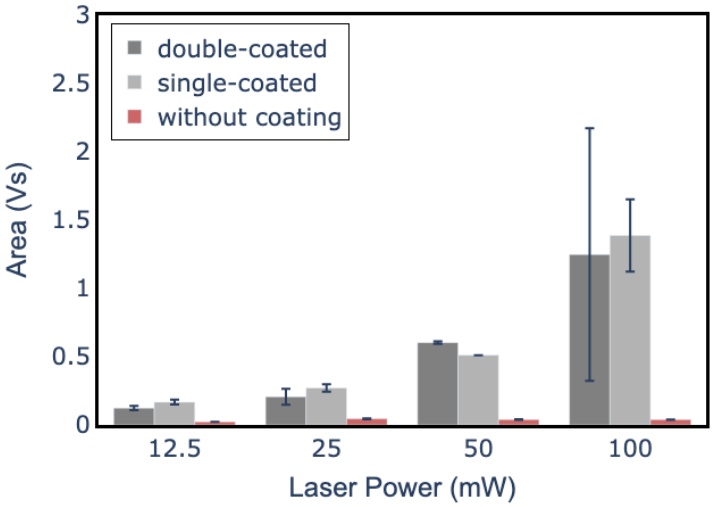

Figure 6.10: Integral of the microphone signal of the sugar measurements averaged over all measurements with all coating types

6.4 Conclusion and Outlook

In this work we have analysed the behaviour of energetic materials under photonic irradiation. In experiments, HMTD, TATP and sugar with one, two and no graphite coatings were processed with a pulsed laser system at different power levels. The resulting acoustic signals were recorded and analysed using a MEMS microphone. On the one hand, the data show that the processing noise increases as expected with increasing power; this is basically independent of the material. It is noticeable that the increase in noise emissions as a function of power is dependent on the coating, particularly in the case of explosives. The processing noise per power increases the least without coating and the most with two coatings. The results suggest that the graphite particles increase the absorption of light and thus the energy absorption of the particles. This leads to an increase in the formation of hotspots [22, 23]. This in turn leads to partial conversion, which does not result in complete combustion of the sample, at least up to a certain value. The final threshold for HMTD is lower than that for TATP, which may indicate that HMTD, once initiated, is more likely to result in complete combustion than TATP. One reason for this could be the higher total specific energy release of

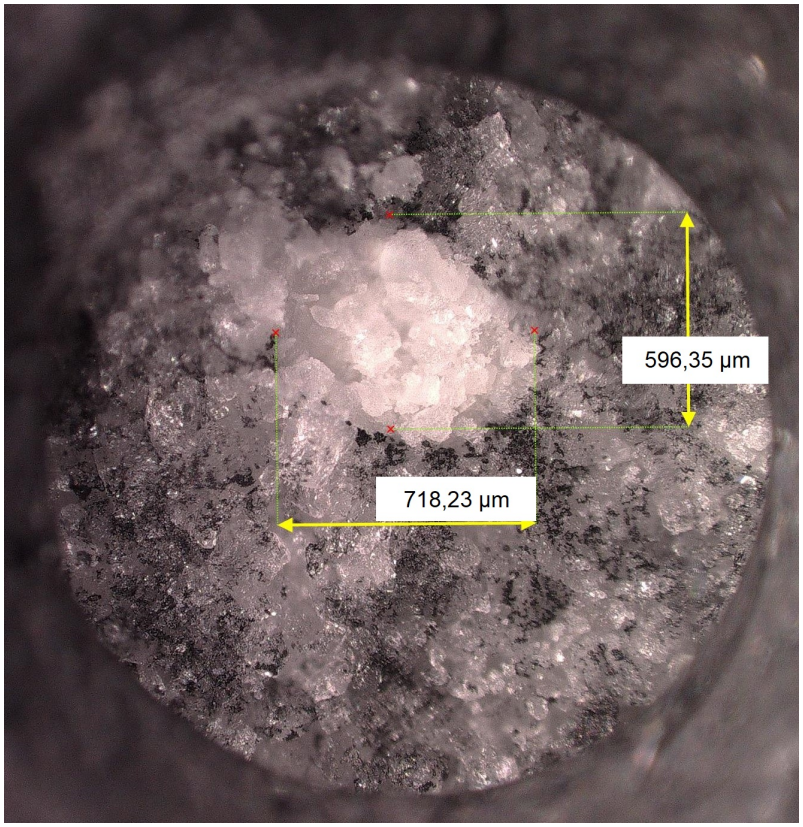

Figure 6.11: Processed single-coated TATP sample ,the focus point of the laser is marked with a red cross

HMTD, which favours a continuation of the reaction. This is 2.80 kJ/g for TATP and 5.08 kJ/g for HMTD [25].

Another reason for this could be that different non-graphitized substances absorb light of different wavelengths to different degrees. In experiments with other wavelengths, the values could vary. The nature of the sample also plays a role. The reaction behaviour can vary due to grain sizes and geometries [23]. In the case of sugar, the influence of the graphite layer is significantly less. In particular, there is hardly any difference between single and double coating. It is also noticeable that the graphite is removed or particles are pushed into the sample over time. Another possibility is that the graphite is oxidised by the high energy input. This reduces the absorption of light over time and the colouration decreases. In particular, there is hardly any difference between single and double coating, the reason for this could be that with a layer of graphite there is already a kind of saturated layer. This means that the particles do not react so violently and also do not self-propagate, which means that fewer particles are transported away from the reaction zone, although some particles are still driven into the sample. One factor that can significantly influence the results is the quality of the layers. For the series of measurements carried out, the quality of the layers was checked under a microscope, and the results can vary due to irregularities and defects, as the surface of the samples is not completely flat despite pressing.

To summarize, the coating of samples combined with laser processing offers a method for decomposing or partially converting explosives in a more controlled manner and at lower power levels. Possibilities include both the targeted decomposition of substances and the transfer of decomposition products into the gas phase, as well as individual particles of the substance, and subsequent sampling for rapid identification of the substances. For future measurements, the substances should first be better characterised regarding particle size. A further step is to visualise the absolute optical sensitivities of the substances.

6.5 Data Availability Statement

The data that support the findings of this study are available from the corresponding author upon reasonable request.

References

[1] J.C. Oxley, J.L. Smith, W. Luo, and J. Brady. "Determining the vapor pressures of diacetone diperoxide (DADP) and hexamethylene triperoxide diamine (HMTD)". In: *Propellants, Explosives, Pyrotechnics* 34.6 (2009), pp. 539–543. DOI: 10.1002/prep.200800073.

[2] Jimmie C. Oxley, James L. Smith, Matthew Porter, Lindsay McLennan, Kevin Colizza, Yehuda Zeiri, Ronnie Kosloff, and Faina Dubnikov. *Synthesis and Degradation of Hexamethylene Triperoxide Diamine (HMTD)*. 2015. DOI: 10.1002/prep.201500151.

[3] A.G. Simon and L.E. DeGreeff. "Variation in the headspace of bulk hexamethylene triperoxide diamine (HMTD): Part II. Analysis of non-detonable canine training aids". In: *Forensic Chemistry* 13 (2019), p. 100155. DOI: 10.1016/j.forc.2019.100155.

[4] V. Bulatov, O. Reany, R. Grinko, I. Schechter, and E. Keinan. "Time-resolved, laser initiated detonation of TATP supports the previously predicted non-redox mechanism". In: *Physical Chemistry Chemical Physics* 15.16 (2013), pp. 6041–6048. DOI: 10.1039/C3CP44662J.

[5] F. Dubnikova, R. Kosloff, Y. Zeiri, and Z. Karpas. "Novel approach to the detection of triacetone triperoxide (TATP): Its structure and its complexes with ions". In: *The Journal of Physical Chemistry A* 106.19 (2002), pp. 4951–4956. DOI: 10.1021/jp014189s.

[6] W. Fan, M. Young, J. Caninoan, J. Smith, J. Oxley, and J. R. Almirall. In: *Analytical and Bioanalytical Chemistry* 403.2 (2012), pp. 401–408. DOI: 10.1007/s00216-012-5878-x.

[7] S. Fan, J. Lai, P. L. Burn, and P. E. Shaw. "Solid-state fluorescence-based sensing of TATP via hydrogen peroxide detection". In: *ACS Sensors* 4.1 (2019), pp. 134–142. DOI: 10.1021/acssensors.8b01029.

[8] DER STANDARD. *Moscheenanschlag in hernals: Selber sprengstoff wie in london verwendet*. Available at: https://www.derstandard.at/story/2637639/moscheenanschlag-in-hernals-selber-sprengstoff-wie-in-london-verwendet. Accessed: 13-11-2023. 2007.

[9] G.M. Segell. "Terrorism on london public transport". In: *Defense & Security Analysis* 22.1 (2006), pp. 45–59. DOI: 10.1080/14751790600577132.

[10] Merkur. *Sprengstoff-Brief an Gauck abgefangen*. Available at: https://www.merkur.de/politik/sprengstoffverdaechtiger-brief-bundespraesidialamt-zr-2861520.html. Accessed: 13-11-2023. 2023.

[11] Ilya Dunayevskiy, Alexei Tsekoun, Manu Prasanna, Rowel Go, and C. Kumar N. Patel. "High-sensitivity detection of triacetone triperoxide (TATP) and its precursor acetone". In: *Applied Optics* 46.25 (2007), pp. 6397–6404. DOI: 80372.

[12] Matin Amani, Yun Chu, Kellie L. Waterman, Caitlin M. Hurley, Michael J. Platek, and Otto J. Gregory. "Detection of triacetone triperoxide (TATP) using a thermodynamic based gas sensor". In: *Sensors and Actuators B: Chemical* 162.1 (2012), pp. 7–13. DOI: 10.1016/j.snb.2011.11.019. URL: https://doi.org/10.1016/j.snb.2011.11.019.

[13] X. Fang and S.R. Ahmad. "Detection of explosive vapour using surface-enhanced Raman spectroscopy". In: *Applied Physics B* 97.3 (2009), pp. 723–726. DOI: 10.1007/s00340-009-3644-3.

[14] F. Zapata, M. López-López, and C. García-Ruiz. "Detection and identification of explosives by surface enhanced Raman scattering". In: *Applied Spectroscopy Reviews* 51.3 (2016), pp. 227–262. DOI: 10.1080/05704928.2015.1118637.

[15] Aleksej M. Rodin, Jonas Sarlauskas, Jelena Tamuliene, and Augustinas Petrulėnas. "Detection of Explosives by Ultrasonic Spectrum upon Pulsed Laser Initiation". In: *Proceedings of SPIE Security + Defence, 2020, Counterterrorism, Crime Fighting, Forensics, and Surveillance Technologies IV*. Vol. 11542. SPIE. 2020, 115420E. DOI: 10.1117/12.2573678. URL: https://doi.org/10.1117/12.2573678.

[16] Sara Wallin, Anna Pettersson, Henric Östmark, and Alison Hobro. "Laser-based standoff detection of explosives: a critical review". In: *Analytical and Bioanalytical Chemistry* 395 (2009), pp. 259–274. DOI: 10.1007/s00216-009-2844-3. URL: https://doi.org/10.1007/s00216-009-2844-3.

[17] M.D Bowden. “Laser initiation of energetic materials: a historical overview”. In: *Optical Technologies for Arming, Safing, Fuzing, and Firing III*. Ed. by J.W.J. Thomes and F.M. Dickey. SPIE Proceedings. SPIE. 2007, p. 666208. DOI: 10.1117/12.734225.

[18] Maria Isabel Sierra-Trillo, Ralf Thomann, Ingo Krossing, Ralf Hanselmann, Rolf Mülhaupt, and Yi Thomann. “Laser Ablation on Isostatic Graphite—A New Way to Create Exfoliated Graphite”. In: (2023).

[19] Jimmie C. Oxley, James L. Smith, Patrick R. Bowden, and Ryan C. Rettinger. “Factors Influencing Triacetone Triperoxide (TATP) and Diacetone Diperoxide (DADP) Formation: Part I”. In: *Propellants, Explosives, Pyrotechnics* 38.2 (2013), pp. 244–254. DOI: 10.1002/prep.201200116.

[20] Andrzej Wierzbicki, E. Alan Salter, Eugene A. Cioffi, and Edwin D. Stevens. “Density Functional Theory and X-ray Investigations of P- and M-Hexamethylene Triperoxide Diamine and Its Dialdehyde Derivative”. In: *Journal of Physical Chemistry A* 105.38 (2001), pp. 8763–8768. DOI: 10.1021/jp0123841.

[21] M. Muhr, T.M. Klapötke, and G. Holl. “Sensory monitoring of drop hammer experiments with multivariate statistics”. In: *Propellants, Explosives, Pyrotechnics* 47.11 (2022). DOI: 10.1002/prep.202200025.

[22] Thomas M. Klapötke. *High Energy Materials*. Berlin, New York: Walter de Gruyter, 2009. ISBN: 9783110207453.

[23] Josef Köhler, Rudolf Meyer, and Axel Homburg. *Explosivstoffe*. 10th revised and expanded edition. Weinheim: Wiley-VCH, 2008.

[24] Will P. Bassett, Belinda P. Johnson, Nitin K. Neelakantan, and Dana D. Dlott. “Shock initiation of explosives: High temperature hot spots explained”. In: *Applied Physics Letters* 111.6 (2017), p. 061902. DOI: 10.1063/1.4985593.

[25] Ashot Nazarian and Cary Presser. “Thermochemical analysis of improvised energetic materials by laser-heating calorimetry”. In: *Thermochimica Acta* 707 (2022), p. 178971. DOI: 10.1016/j.tca.2022.178971.

Sensory Monitoring for Breakthrough Detection in Mobile Laser Cutting of Various Materials in the Context of IED Disposal

by

Emre Ünal, Matthias Muhr, Dominik Wild*, Cathrin Theiss, Moritz Schumacher, Gerhard Holl, Peter Kaul

University Bonn-Rhein-Sieg, Institute for Safety and Security Research, Von-Liebig-Straße 20, 53359 Rheinbach, Germany

*German Aerospace Center (DLR), Institute for the Protection of Terrestrial Infrastructures, 53757 Sankt Augustin, Germany

Submitted for publication in IEEE Open Journal of Instrumentation and Measurement

The work reported on in this publication was carried out together with several colleagues from the list of authors. The main focus of my work was on carrying out and optimising the experiments with the laser cutting system. Work was also carried out on optimising the cutting tests and the sensor technology. I was also involved in presenting the results and analysing the collected data.

Abstract: Unattended luggage or containers in public areas such as railway stations and buildings, like airports, may trigger bomb disposal operations. While these instances frequently involve harmless forgotten bags, they can also signal the presence of unconventional explosive and incendiary devices, which may include chemical, biological, radiological, nuclear, and explosive (CBRNe) elements. Research aspects of this work include the development of a mobile laser cutting system (LCS) to enhance the capabilities of police bomb disposal units in neutralising improvised explosive devices (IEDs) and forensic evidence collection, thereby improving the safety of the public and defusing experts. This paper presents the results of the development of a breakthrough detection system using an appropriate sensor technology. Parameters are determined by means of sensory monitoring to cut through various materials without interacting with the layer behind them. The investigation includes real cutting tests with the mobile laser cutting system (LCS) on various materials. The results show that sensor-based breakthrough detection is feasible for the laser cutting of IED-relevant objects.

7.1 Introduction

Objects with suspected hazardous substances, often concealed in everyday objects such as luggage or boxes in public places, pose a significant security threat. At best, these items are simply misplaced personal effects; however, in more serious cases, they may contain sophisticated explosive mechanisms, potentially enriched with CBRNe elements. These represent a particular challenge as they are often stored in opaque and containers difficult to penetrate such as backpacks, suitcases and parcels. Traditional methods of assessing and neutralising these threats often require direct physical contact, which carries risks. To mitigate these risks, remote handling technologies are favoured that prioritise security while attempting to preserve forensic evidence. Many systems have already been developed to capture images of the shape and content of suspicious objects, such as X-ray based technologies [1, 2, 3, 4, 5, 6, 7].

One of the most common techniques currently used to open suspicious items is manual opening by Explosive Ordnance Disposal (EOD) technicians protected

by bomb disposal suits. [8, 9, 10]. Instead of suspicious objects being opened manually by an EOD technician, mechanical devices are used. Water jet systems are used for bomb disposal, where pressurised liquids are used to cut materials suitable for cutting large-calibre unexploded ordnance. The disadvantage of this technology can be the destruction of evidence inside the package or even a release of CBRNe substances due to the high forces at work [11, 12, 13, 14].

Laser processing methods for EOD applications have also been reported [15, 16]. These methods were developed to neutralize unexploded ordnance, but are not suitable for safely opening an improvised explosive device (IED), especially for complex objects made of different materials to access their contents. In general, no laser cutting methods have been found in research that have extracted substances from laser processing. However, the device to develop is important for opening objects with an IED to prevent laser energy coupling in the next layer.

Laser machining is an advanced and highly precise material processing technique that utilizes focused laser beams to remove material through melting, vaporization, or ablation. This method is favored in industries requiring intricate detailing and minimal thermal impact on the surrounding material. Pulsed lasers, such as Nd:YAG and CO_2 lasers, are particularly advantageous due to their ability to deliver high peak power in short bursts, which reduces the heat-affected zone and minimizes thermal damage [17, 18, 19]. These properties make pulsed lasers suitable for micro-machining, drilling, and cutting complex profiles in materials like ceramics, metals, and polymers. For example, in the laser drilling process described in [20], a pulsed laser is used to create high-precision boreholes, where the short pulse duration allows for controlled energy input and efficient material removal. Additionally, innovations such as the use of a jet nozzle to remove molten material during the laser drilling process further enhance the quality of machining by preventing recasting and ensuring clean cuts [21]. These advantages have led to the widespread adoption of pulsed laser machining in various high-precision applications, including aerospace and medical device manufacturing [22, 21, 23].

In laser machining, real-time process monitoring is essential for maintaining quality and precision, especially in applications where tolerances are tight and material integrity is crucial. Sensory monitoring systems are integrated into laser machining setups to track key parameters such as laser power, focus position,

and material removal rates. For instance, the use of acoustic sensors to monitor the noise generated during laser ablation provides critical feedback that can be used to adjust the process in real-time, ensuring consistent quality and preventing defects. In the study detailed in the investigation on acoustic monitoring, it was found that analyzing the acoustic signals produced during laser ablation can effectively differentiate between different material layers, such as distinguishing between necrotic and vital tissue in medical applications [21]. Moreover, the integration of advanced sensor systems, as outlined in [22], allows for precise control over the laser machining process, improving safety and efficiency by enabling automated adjustments to the cutting parameters based on real-time feedback. These developments underscore the importance of sensory monitoring in enhancing the capabilities of laser machining systems, ensuring high precision and safety across various industrial and medical applications [20, 24, 25].

This work addresses these challenges by developing a laser cutting system capable of remotely opening IED-containing containers without destroying a potential explosive charge or similar. The cutting scenario is to be understood as follows. In the first step, an X-ray image of the suspected object (e.g. suitcase) would be taken to identify the dangerous load in the object. The LCS is then placed on the object and a test cut is made at a non-hazardous location to feed process data to the system preparing the aimed cutting. After this test cut and checking all the necessary parameters, the LCS is placed in the correct position and the outer material (here: suitcase) is cut. Once the material has been removed, the IED can be treated appropriately using the LCS (defusing or sampling) or other equipment. The required system must integrate advanced sensor technology that monitors and controls the cutting process in real time. This technology must ensure precise thermal management to minimize the risk of accidental ignition or detonation of the explosives inside. The laser system must be designed so that it can be mounted to robotic manipulators or modular positioning systems. This will allow defusing teams to work from a safe distance and minimize the risk to personnel. This paper presents the development of the sensory monitoring of laser cutting.

7.2 Experimental

7.2.1 Setup

At the beginning of the research work, an attempt was made to carry out initial cutting tests in order to generate specifications for the laser system. Initial tests were also carried out on enclosed and open samples containing explosives. Figure 7.1 shows the setup used for the first series of measurements (in the following **LS I**).

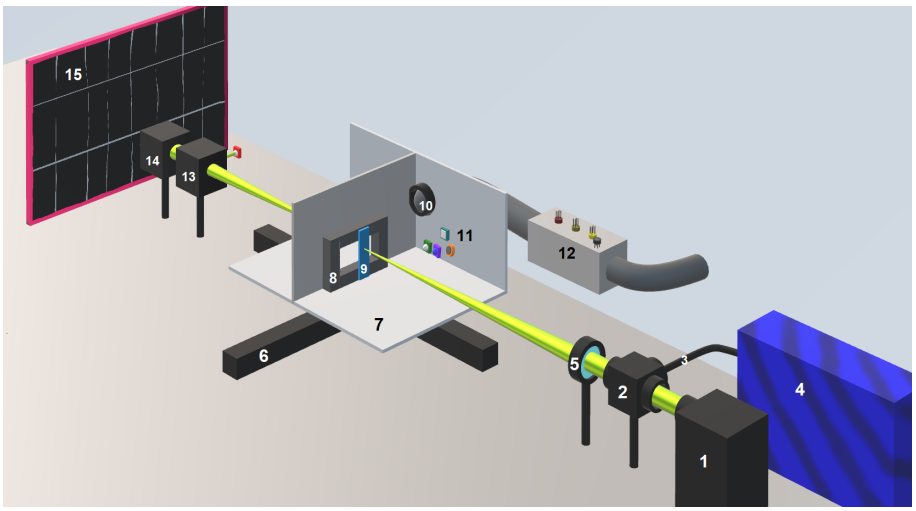

Figure 7.1: Schematic setup of the laser system used for preliminary experiments: 1. laser, 2. parabolic mirror, 3. optical fiber, 4. spectrometer, 5. lens, 6. xy table (z manual), 7. sample chamber, 8. sample holder, 9. sample, 10. exhaust air, 11. physical sensors, 12. chemical sensors, 13. beam splitter with breakthrough diode, 14. power meter, 15. solar cell

The pulsed neodymium-doped yttrium aluminium garnet (Nd:YAG) laser was initially used for the investigations into laser cutting and performance parameters. This laser emits nanosecond pulses at three different wavelengths (1064 nm, 532 nm, 355 nm) and offers the possibility of infinitely variable regulation of individual pulse energies. The Nd:YAG-laser has a maximum output power of 3 W at 532 nm and a pulse frequency of 2000 Hz. Each burst consists of exactly 10 pulses with a single-pulse energy of 1.5 mJ, with each pulse having a duration of 10 ns.

To refine and concentrate the optical power, a converging lens with a focal length of 250 mm is integrated into the system. Additionally, a polarization filter is used to precisely adjust the laser power. The power was monitored using a power meter, and power fluctuations during adjustment were around ± 1 mW. These meticulous adjustments ensured the precision and safety necessary for processing the relevant explosive materials.

The experimental series included investigations into the influence of laser fluence on the machinability and penetration duration when cutting various predefined, practically relevant materials. The cutting process was realised by repeatedly moving the sample being hit by the laser beam on a defined linear trajectory (figure 7.2).

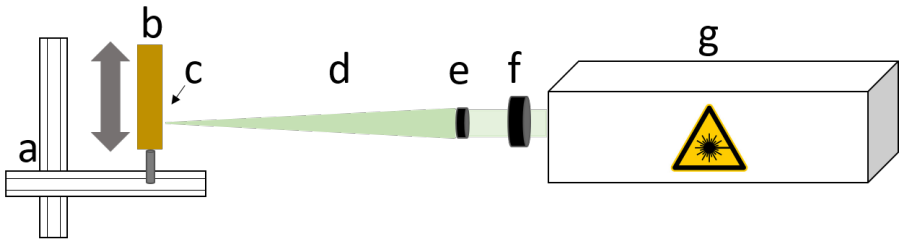

Figure 7.2: Stationary laser system (**LS I**); a: xy-table, b. Sample, c. Focus point, d. Laser beam, e. focusing lens, f. shutter, g. laser system

After determining the relevant parameters, a new laser cutting system was used (in the following **LS II**). After merging it with the sensors and integrating it into the overall system. The structure looked as showed in figure 7.3.

This system allowed a flexible positioning of the laser beam via a galvanometer scanner as well as precise focus tracking and focusing to change the laser spot area using a motorized focus control. The system had a maximum pulse energy of 5 mJ for a wavelength of 515 nm. Additionally, it was possible to use the wavelength of 1030 nm after replacing wavelength-dependent optical elements.

At this stage, the adjustment of the laser pulse energy and the position of the focal plane was still done manually or with the help of preliminary operator software. The integration of a spectrometer to capture radiation in the UV and visible wavelength ranges was achieved by coupling it via an optical fiber with the optical setup and beam path of **LS II**. This setup allowed for the detection of reflected and emitted light from the processing zone. Figure 7.4 shows the interior of the

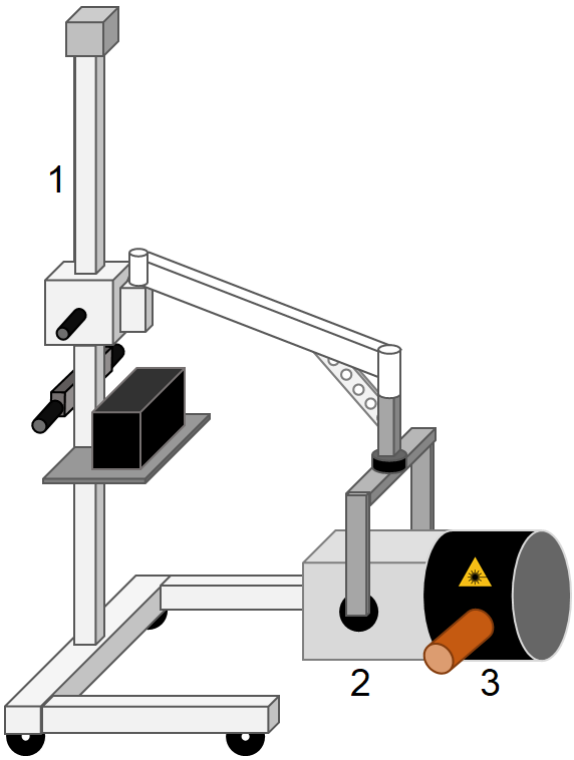

Figure 7.3: Sketch of the final mobile laser cutting system; 1. support and positioning system in the form of a mobile stand with swivelling spring arm device, 2. laser system, 3. sensor tube

laser head, featuring a motorised power adjustment (1), motorised focus tracking (2), a laser switch/shutter (3), a fibre connection to the spectrometer (4), a camera with a filter for topography scanning and positioning aid (5), an f-theta lens (6), a galvanoscanner (7), and a laser diode (laser class 2) (8). Throughout the project, and in preparation for hardware integration, additional components were added or replaced to facilitate easier handling and control of **LS II**.

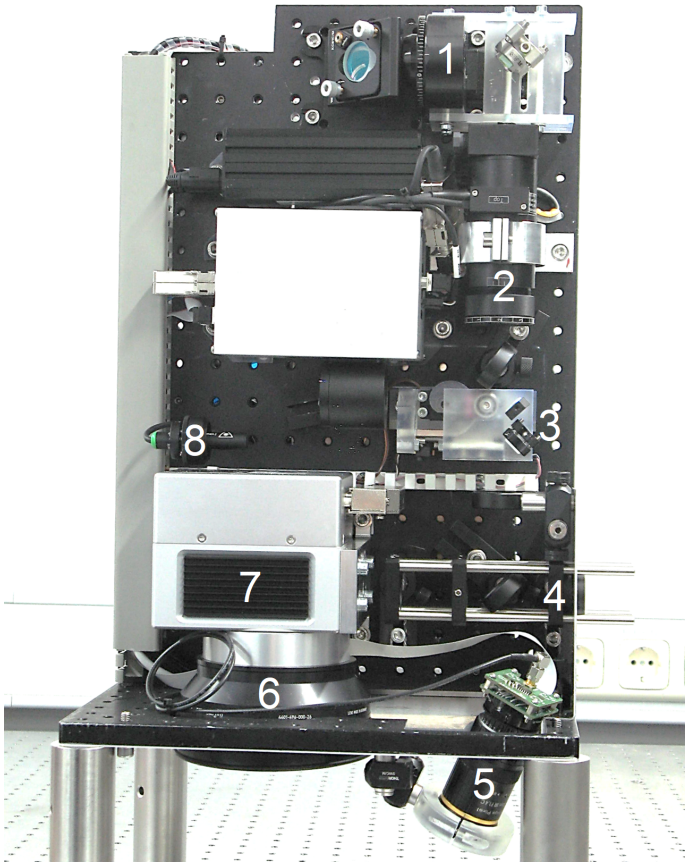

Figure 7.4: Interior of the laser system: 1. motorised power adjustment, 2. motorised focus tracking, 3. Laser switch / shutter, 4. fibre connection to spectrometer, 5. camera + filter for topography scan and positioning aid, 6. f-theta lens, 7. galvanoscanner, 8. laser diode (laser class 2)

Topography Scan

The new LCS was also equipped with a topography scan unit. This system operates by projecting a lase r (safe for the human eye) onto the object's surface, while the reflected light is captured. By analyzing the distortions in the projected pattern, the system calculates the precise 3D geometry of the surface, creating a detailed topographical map. The focus point can then be adjusted automatically to follow the surface contour based on the acquired data.

Explosives

A specially designed sample holder was used for measurements with explosives. The explosive, in this test series triacetone triperoxide (TATP), was fixed in a cylindrical plastic container, which was placed inside a metal cylinder. The reason for selecting TATP was to test an explosive that was as sensitive as possible and hazardous (typical terrorist explosive) in order to identify critical parameters for processing. The sample holder was covered with a plastic plate (5) to simulate packaging of an IED. The material to be processed was placed so that it was directly exposed to the laser beam (figure 7.5). The Figure shows shows a schematic representation of the sample holder used for measurements on explosives, consisting of a bracket (1), a sleeve (2), the explosive (3), a PU hose (4), a polystyrene (PS) cover (5), and cardboard (6).

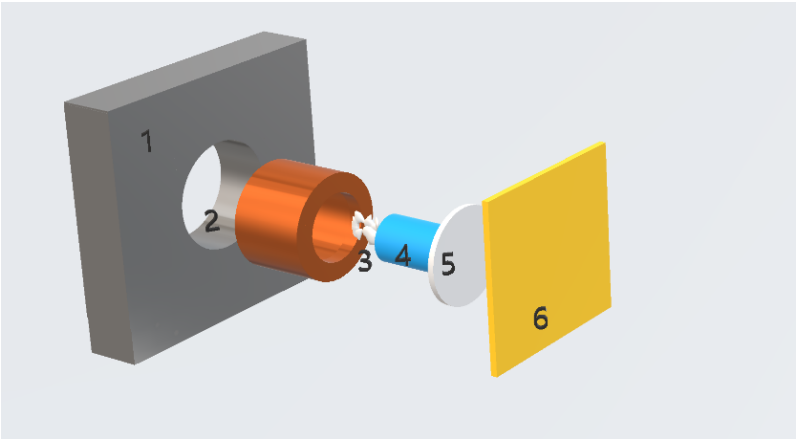

Figure 7.5: Schematic representation of the sample holder for measurements on explosives; 1. bracket, 2. sleeve, 3. explosive, 4. PU hose, 5. Polystyrene (PS) cover, 6. cardboard

7.2.2 Sensors

Sensory processing monitoring in laser cutting involves various sensors and the integration of a laser sensing system to assist operators in aligning with objects, visualizing the cutting process and overall operation. Our work has focused on integrating the laser system into the sensor setup, aiming to monitor and optimize the laser cutting process.

To achieve this, different sensor techniques were investigated and evaluated for monitoring critical process parameters. We developed a sensor system designed as a tube equipped with various sensors to shield against scattered radiation from the laser interaction zone and to extract harmful gases and particles. This sensor system includes (figure 7.6). Microphones, UV- and VIS-diodes are mounted are arranged several times to get a good all-round view, but are not all labelled:

- **Two microphones (4)** for sound evaluation. During laser processing experiments, acoustic monitoring was carried out using two MEMS microphones (ELV MEMS1).

- **Broadband and UV photodiodes (2)** for detecting generated and scattered radiation. The diodes were positioned differently to the spectrometer (section monitoring) and had a higher sampling rate and were purchased from the manufacturer Roithner LaserTechnik GmbH. Some were used for the UV range (330-445 nm), the laser wavelength (515 nm) and the visible wavelength range.

- **Various metal oxide gas sensors (not displayed)** for assessing changes in gas composition. Semiconductor gas sensors from the manufacturer UST Umweltsensortechnik GmbH (1000 and 3000 series) were used to monitor the environmental (as reference) and process gases.

- **A spectrometer (not displayed)** from Ocean Optics (HR series) for analyzing emitted radiation within the UV/VIS spectral range. In-line measurements were carried out and the backscattered light was decoupled via a beam splitter (figure 7.4).

- **An infrared camera (1)** to assess heat development in the cutting zone, which is critical due to the material's thermal conductivity. The IR camera (optris Xi-series) was used to monitor temperature development on the cutting trajectory taking especially the hottest spot (of the laser machining process) into account. This allowed the cutting process to be followed live. In addition, the data and information obtained could be subsequently assigned to the process.

This comprehensive sensor system enhances the monitoring and control of the laser cutting process, ensuring efficiency and safety.

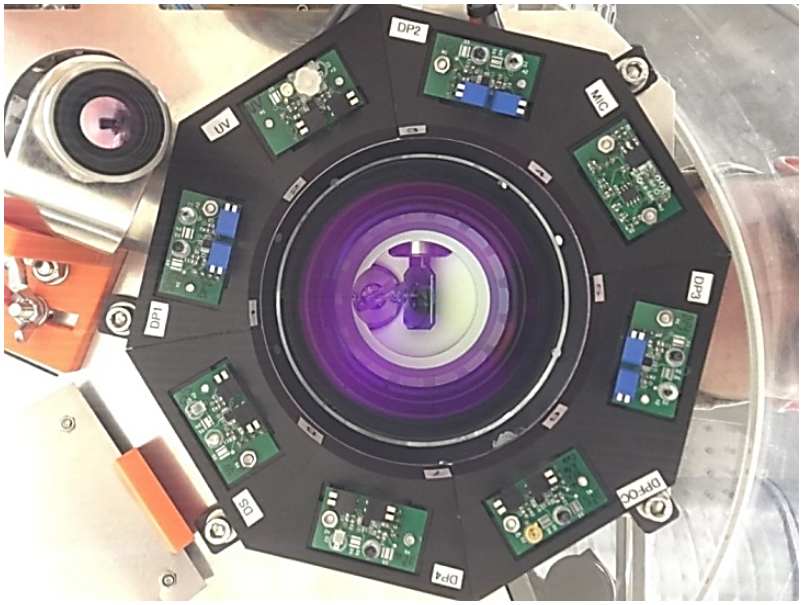

Figure 7.6: Interior view of the tube with a view of the sensor ring, the mentioned sensors are selected as examples: 1. IR camera, 2. UV-diode, 3. f-theta lens of the LCS, 4. microphone

7.3 Results

The experiments and results obtained are presented below. At this point it is important to consider possible laser cutting systems and sensors as well as the necessary interfaces for realisation in a mobile laser cutting system, taking into account the current state of science and technology as well as laser safety regulations.

7.3.1 Objective

The overall aim of the work is to optimise and control the laser cutting process with suitable parameters and to equip the LCS with relevant sensor technology in such a way that the cutting of different materials and stopping of the cutting process at a suitable point (avoiding initiation of the explosive charge) is achieved.

In this chapter the focus will be on the presentation of the results of the experiments to generate suitable cutting parameters to enable cutting of relevant materials / objects and identification of relevant sensors and process monitoring / cutting detection. Relevant materials and containers were selected with the involvement of the end user.

7.3.2 Determination of the Laser Parameters for the Laser System

The aim of these experiments was to determine the required performance characteristics of a laser cutting system concerning laser parameters, beam guidance, cutting system, process gas guidance, and material extraction for processing explosives. These determinations were made through investigations using **LS I**.

It was observed that many materials could already be processed with the existing laser system, although limitations were reached, particularly with poorly absorbing materials and thicker metals. Experiments to determine material-specific plasma thresholds identified the laser fluence at which plasma emissions could be detected at the process site. Exceeding this threshold resulted in initial material removal, indicating the commencement of the cutting process. It was found that for processing relevant materials in an adequate time, especially those poorly absorbing ones, higher fluences around $40\,J/cm^2$ were necessary (figure 7.7). This value was considered the minimum necessary fluence, which, however, did not achieve sufficient material removal for the given scenario.

Measurements with explosives indicated that the safe laser parameters for drilling processes in packaging containing explosives, as determined in previous projects. The LAGEF project could not be transferred to laser cutting processes due to insufficient fluence, which leads to a too long procedure [26]. TATP was used as the energetic material in the experiments with explosives.

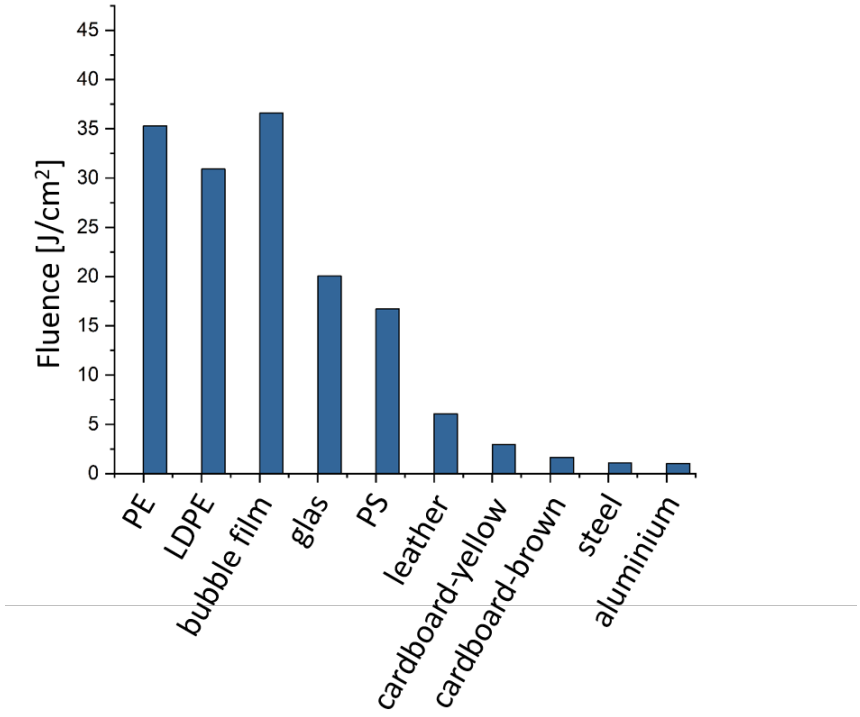

Figure 7.7: Energy thresholds beyond which the listed materials undergo processing

Explosives specifically mixed with highly light-absorbing particles posed an a additional challenge. This necessitated defining a limited time window for the laser cutting process, within which the process should be terminated after penetrating the material thickness, without affecting the next material layer.

Requirements of the System

The results of the measurements led to the following requirements and properties of the new laser system for the LCS (**LS II**): The laser system should be a fibre-pumped solid-state laser with pulse durations in the nanosecond range (3-10 ns). The wavelength should be in the green spectral range (515 to 532 nm) with an optional switchable mode to the NIR range (1030 to 1064 nm), achievable, for example, via a folding mirror in the system. The individual pulse energy should be at least 5-10 mJ in the green spectral range and 10-20 mJ in the NIR range, with continuous attenuation possible down to a minimum of 0.05 mJ. The attenuation and radiation emission (on/off) must be controllable via a corresponding interface. The repetition rate must also be variably controllable, with a minimum of 500 Hz and a preference for 2 kHz. The beam quality must have an M^2 value of less than 3. The fluence required for processing a variety of materials should be greater than 80 J/cm². The laser system should be operable with a standard 230 V AC connection, whilst being designed in a compact way and capable of being integrated in the whole system.

7.3.3 Development of the Laser System

Essential for the future use of the LCS is the monitoring of the cutting process through online evaluation of sensor data, enabling feedback on the process progress. Initial investigations on a test stand using an existing laser system examined various sensor principles (optical, spectroscopic, acoustic, chemical) to monitor relevant materials, including those with explosives.

These studies provided insights into evaluating reflected laser radiation, emitted radiation during processing, sound development, and resulting reaction products. The aim was to determine their suitability and develop potential evaluation algorithms for intelligent control and automation of the cutting process. This enabled the acquisition of information regarding material classification, ma-

terial breakthroughs, cutting progress, and material changes, which in turn allows for the selection and adjustment of power parameters and selective processing.

In addition to evaluating different sensor concepts, a programme for data recording, storage, and analysis was developed. As a result, a sensor system for the LCS was developed, designed as a tube equipped with various sensors. In addition to the other existing sensors an infrared camera was installed to assess heat development in the cutting zone, as the material's thermal conductivity significantly impacts cutting efficiency. Given the planned direct coupling of the tube with the LCS, the optimal placement of the sensors (see figure 7.8) and the camera was developed.

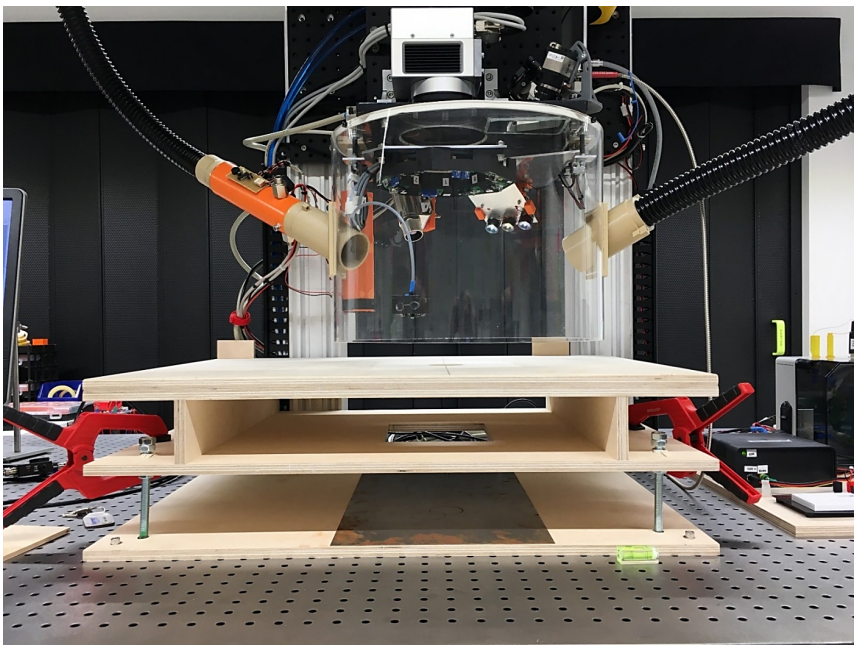

Figure 7.8: Implemented sensor tube with air extraction

System Tests - Laser Cuts in Test Surfaces and Objects

This section provides information on the actual cutting of various test materials.

Due to the fact that different cutting geometries and sizes may be required, the standard test cut (polystyrene, 4 W, 40 mm/s) was converted and cut to other and larger cutting geometries. The values for larger diameters were calculated

using the test cuts of 2 cm circular geometries with standard parameters. The first breakthroughs occurred in the test cut after 60 s and the cut sample fell off after 70 s. This results in breakthrough times of 150 s for a 5 cm circle and the average should occur after 175 s.

Figure 7.9 presents an example of sensor data during the laser cutting of suitcase material (**LS II**). In this case only microphone data is shown and the solar cell data as reference. The plot on the left shows the microphone and solar cell data of a 2 cm cut of polystyrene (one cycle : 1,57 s) and the plot on the right shows a 5 cm circular cut of the same material at an offset position (one cycle: 3,93 s). The two microphones capture signal curves that represent the laser cutting process and the material's circular cut-out over time. The signal curve from microphone 2 reveals three phases: initial laser entry into the surface, the cutting phase within the material and the final penetration phase. The solar cell, functioning as the reference sensor, detects laser light passing through the material. Although all other sensors produce similar patterns, they vary in their temporal resolutions.

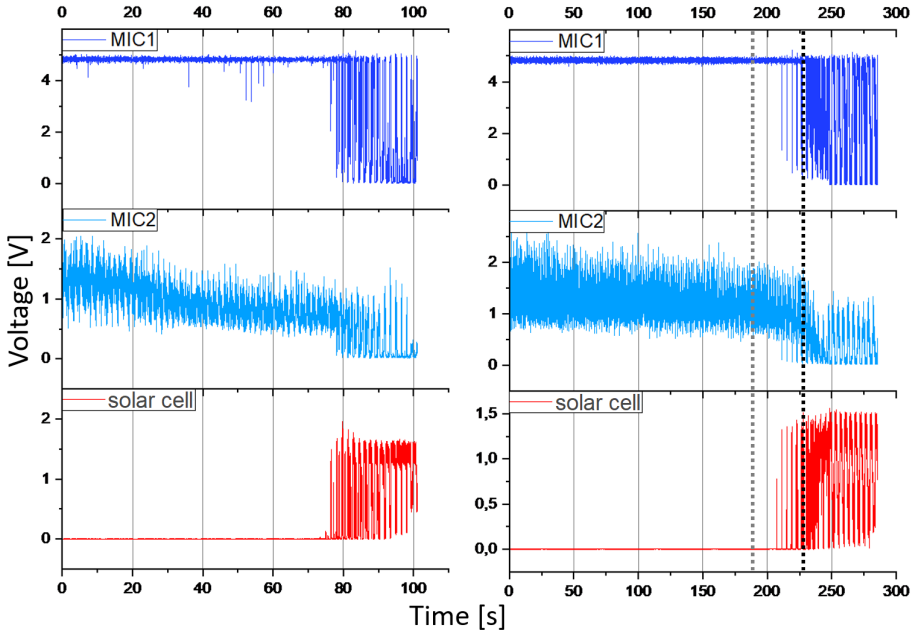

Figure 7.9: Microphone and solar cell data of exemplary 2 cm and 5 cm cuts of PS; Mic1: Microphone is placed inside the sensor tube, Mic2: is placed outside the sensor tube, the solar cell is located below the sample to be cut

In the left-hand plot, the solar cell data show that the first breakthrough through the material occurs after about 75 s (increase in the solar cell signal). In addition, the actual cut through (material is cut by the interaction with the laser beam, the laser beam hits the solar cell permanently) of the material takes place after 91 s, which can be read from the bending of the microphone signal in combination with the solar cell data. Assuming a linearly transferable cut, the events of the cut on the larger circle should occur 188 s (grey line) and 228 s (black line). However, the data shows that the first breakthrough is around 210 s and the cut through is at almost 250 s.

Because repeating experiments showed similar results, investigations were carried out with regard to laser power and laser beam profile. The beam profile image showed the following profile at different z-axis shifts (0 cm and 2.5 cm) (7.10).

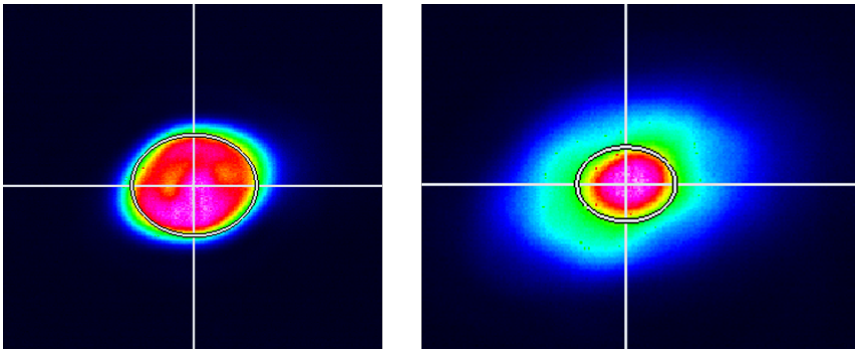

Figure 7.10: Beam profile measurement of the laser beam of the LCS; shift in focus: left: 0 cm, right: 2.5 cm

The images show an oval-shaped profile with a further widening when the focal position is shifted, mainly caused by the profile shape in combination with the selected cutting parameters. The laser spot geometry caused one axis to irradiate more than the other. As a pulsed laser system was used, the individual pulses overlapped more frequently on one side, which resulted in a stronger treatment of individual areas (figure 7.11).

As already mentioned, sensors such as photodiodes, microphones and others were used to develop and control the cutting process. The following illustration (figure 7.12) shows the sensor data development of an exemplary cut. Plotted are recorded data using photodiodes and solar cells (reference sensor) against

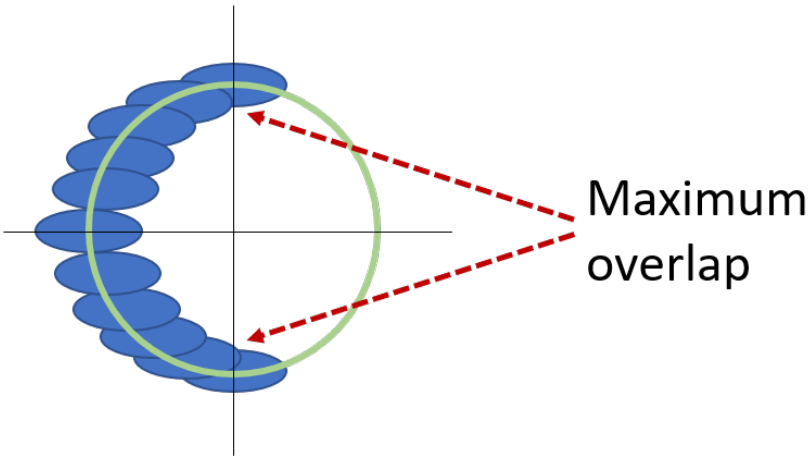

Figure 7.11: Schematic representation of the overlapping of individual laser pulses; the green circle represents the scan trajectory and the blue shapes the laser pulses

time, around 25 s corresponding to one scan. The first breakthroughs can be seen after 30 s (grey line; 2nd scan). It can be observed that after an increase in breakthroughs, the material is cut after about 50 s (black line). The cut sample falls off after approx. 78 s (green line). The sensor data of the diodes DPFOC, DP2 and DP3 show an increase contrary to the periodicity of the previous course (DPFOC and the DP series are abbreviations for photodiodes). The drop in the intensity of the solar cell (between the red dotted lines) can be explained by the fact that at this point the laser beam hits again on the sample, which has already fallen off but is in the beam path (under the clamped cut sample; above the solar cell). This interrupts the contact of the laser beam with the solar cell in this area.

The IR camera and the spectrometer were used intensively in the development of early breakthrough detection. The spectrum shown in Figure 7.13 is from a laser cutting test on black PS. The sample was cut with a laser power of 5 W and the spectra were integrated over 100 ms. It can be clearly seen that the light backscattered from the sample has a relatively high intensity. The recorded intensity at 515 nm originates from the laser beam and is not completely filtered out. Approximately 5-10 nm is missing to the right and left of the laser signal. This is due to the fact that a 515 nm-notch filter was used to prevent too much light from entering the spectrometer directly.

Figure 7.14 shows an example of data acquisition with an IR camera. This is

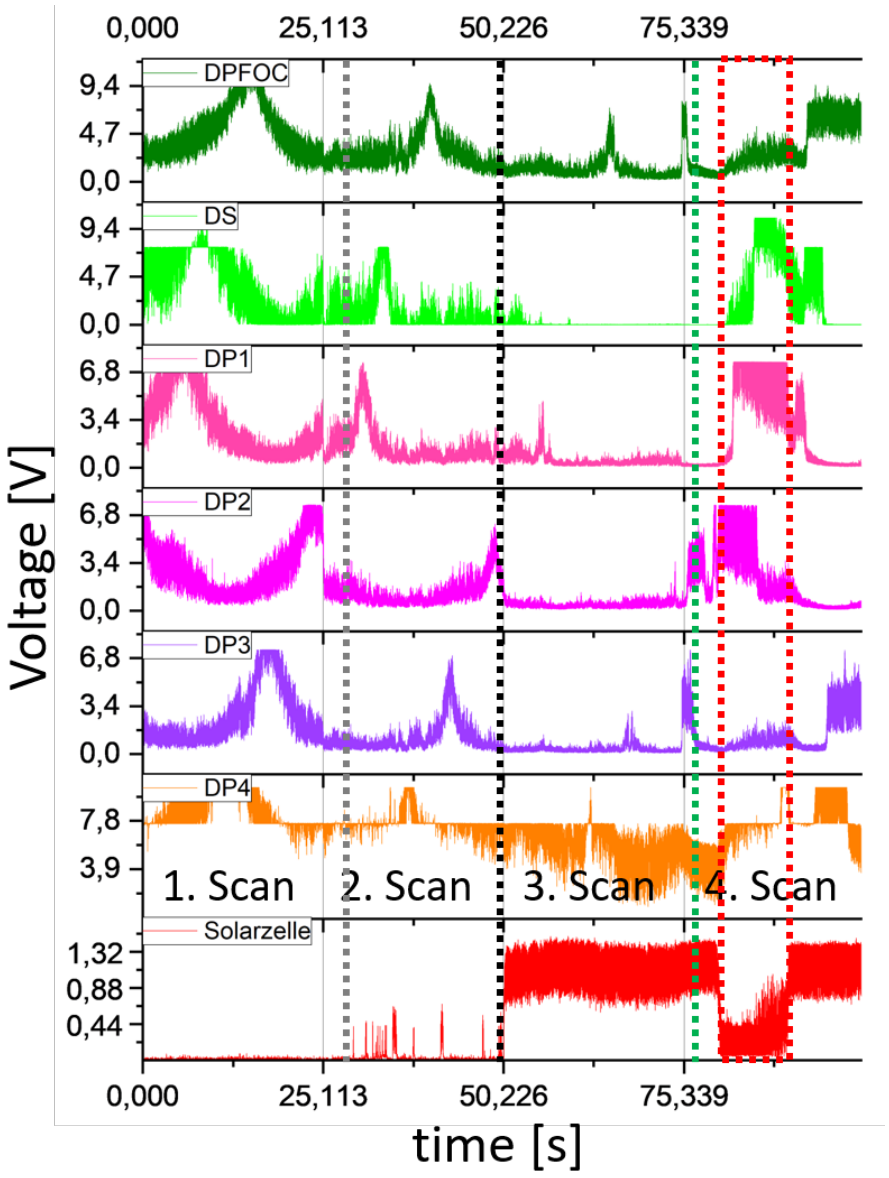

Figure 7.12: Sensor data development (photodiodes and solar cell) based on an exemplary section; grey line: first breakthroughs, black line: cut through, green line: material falls off

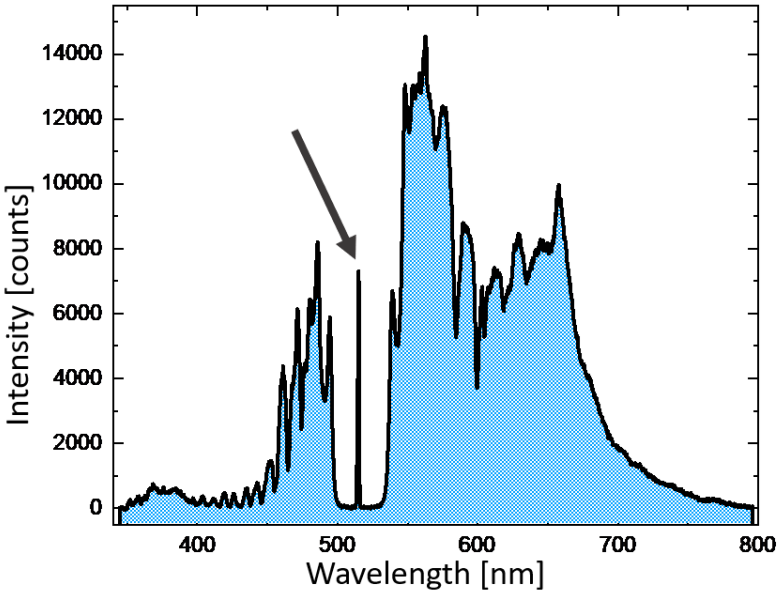

Figure 7.13: Spectrum of black PS during a cutting test; the grey arrow shows the wavelength of the laser; laser power: 5W, integration time: 100 ms

also a circular section of 2 cm on PS. The highest temperature in the measurement field (hotspot temperature) was plotted and the data from the solar cell was used as a reference sensor (the blue line displays the moving average of the data). The data show that the temperature in the material rises with increasing processing until it firstly stagnates. The hotspot temperature begins to scatter from around 20 s onwards. This can be explained by the higher energy input and the higher sum after a certain time in the material. Another reason could be the further penetration into the material and the uneven distribution of energy. The first breakthroughs through the material are difficult to recognise with the IR camera alone. In the range of 70 to 78 s, the material buckles (the hotspot temperature drops). After approx. 78 s, the material collapses. The increase in the hotspot temperature is also due to the laser beam hitting the collapsed material again.

Figure 7.15 shows a stacked plot of the sensor data from a cutting test on real suitcase material. A laser power of 4 W and a cutting speed of 40 mm/s was used. This figure shows the sensor responses of the two microphones, the hotspot temperature, the integral of the recorded spectra over the measurement time, the solar cell voltage and the intensitiy of the wavelength of 515 nm (indicator for the

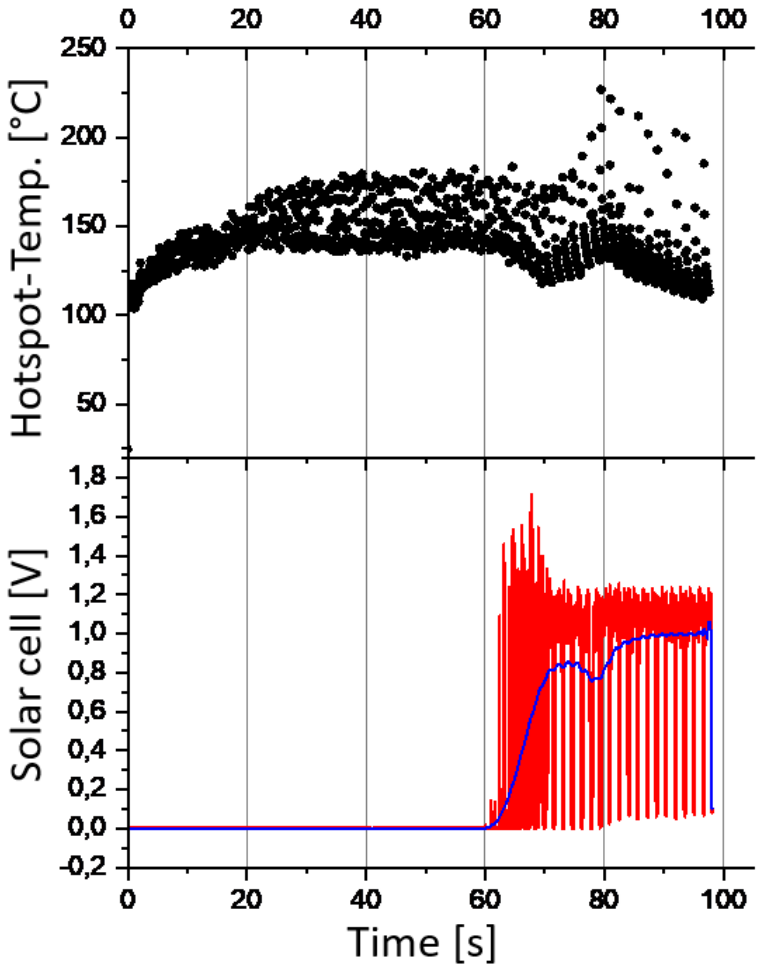

Figure 7.14: Viewing the hottest pixel in the IR cam's field of view and correlating solar cell data

laser power). At this point, an attempt was made to use a threshold value (red line in the figure on the microphone data) to identify the termination point of the cutting process before processing of the materials/objects behind can take place. It can therefore be recommended that the cutting process should be terminated if the measured voltage falls below the specified value. As shown in the figure, the relevant microphone level falls below after around 65 s. A detailed analysis of the data progression shows that the first breakthroughs occur from this point onwards (area marked in green in the figure). In the further course, the material is cut through (yellow area in the figure). The laser power was also measured in order to be able to trace and guarantee power-specific events and a uniform progression.

With the aim of developing a complete breakthrough detection system, a LabView programme was written for live monitoring of the cutting process. The programme provides a visual representation of the cutting process based on the sensor responses. In this way, the cutting process can be monitored. Figure 7.16 shows an example of the programme output. In the software-generated illustration, the breakthroughs are visible as green points on a circular trajectory. Nearly identical breakthroughs can be seen on the real sample (right hand side - light behind sample demonstrates cut through parts) in comparison to the breakthrough detection programme output. The breakthrough detection measures the heating and the processing intensity of the points on the cutting trajectory. on the one hand, the data from the spectrometer is used, which is well suited for breakthrough detection due to its high spatial resolution. In addition, the microphone data of the inner microphone is used and the spatial resolution is calculated using the spectrometer. This data can be used to calculate the extent to which a point has been affected on the trajectory. Furthermore, if one of the signals breaks away at a certain point, it can be determined whether material is no longer being processed, as the laser does not hit material in the focus.

Various materials such as plastic sheets, metal plates, glass, and an aluminum can contaminated with trace amounts of explosive residue were processed, along with combinations of these materials. The topography scan was tested on angled plastic samples to evaluate its functionality. The majority of tested materials were successfully cut using the LCS, with the cut material being removable. Organic and non-transparent materials, such as black polystyrene, were particularly effec-

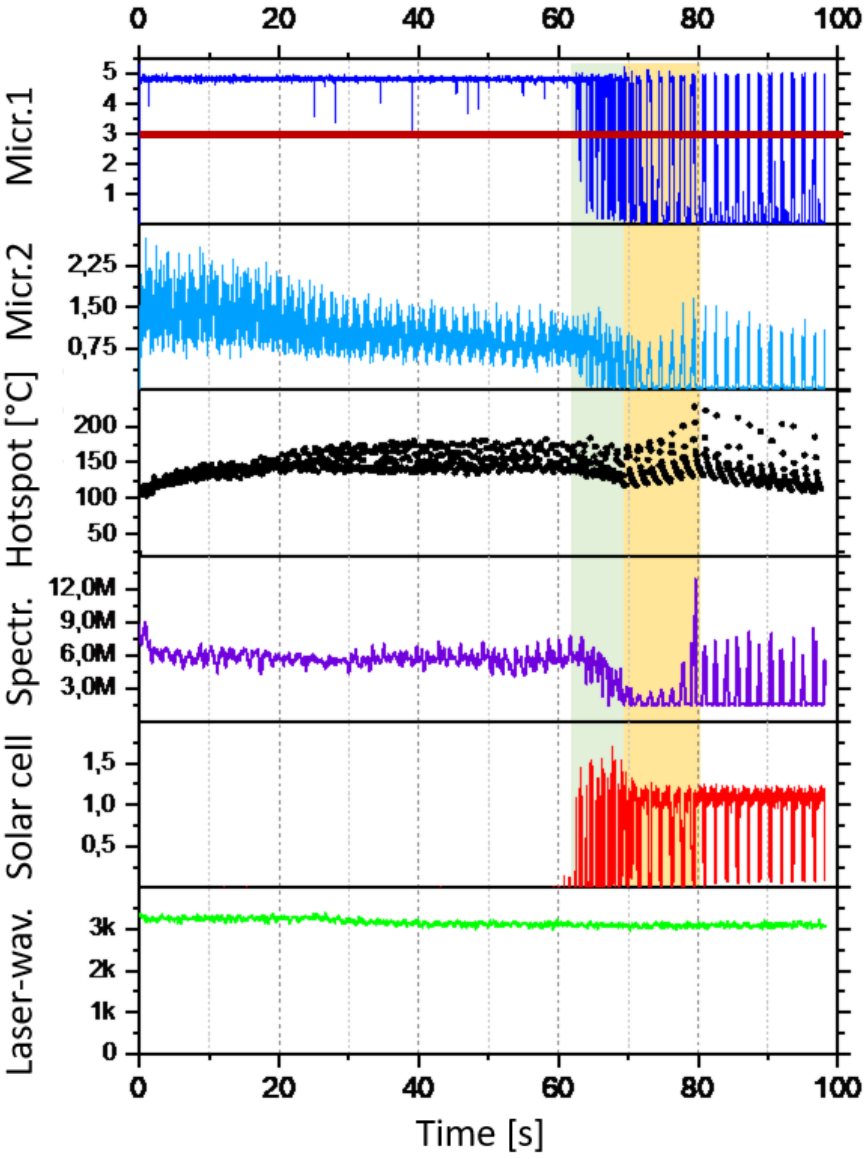

Figure 7.15: Cutting test on a plastic case; diameter of the circle: 2 cm, traversing speed of the laser: 40 mm/s, laser power: 4 W

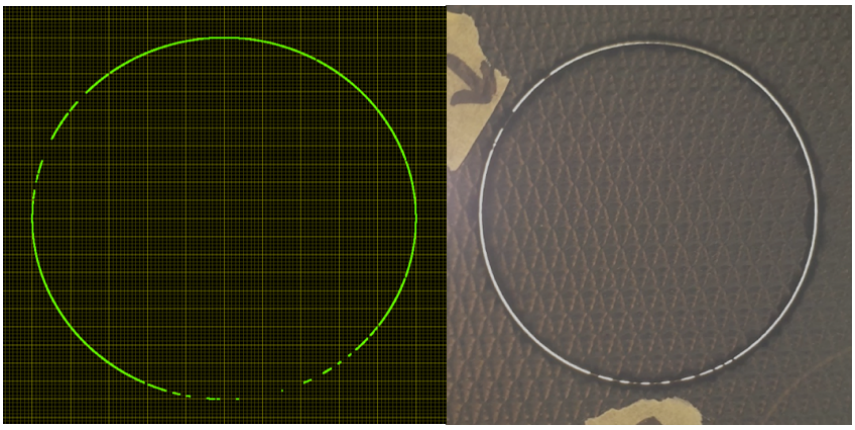

Figure 7.16: Software-generated view of a cutting process (left) and a real cutting sample (right)

tively cut in a controlled manner (sensor-monitored with laser breakthrough detection). Thinner aluminum plates were also cuttable after prolonged, consistent laser exposure. However, cutting thicker metals (>1 mm) had to be discontinued due to insufficient ablation. This was attributed to both the low fluence (inadequate focusing) and the high thermal conductivity and melting behavior of the metals (re-melting of the processed areas). Unfortunately, a detailed investigation could not be performed. Nonetheless, it can be concluded that the cutting quality for a range of materials was good and comparable across the experimental series (see figure 7.17).

To automate this process, topography measurement and focus plane tracking are necessary. In this procedure, the surface of the sample to be processed is illuminated with a laser diode before the actual cutting attempt, while a camera captures the reflected laser radiation. The surface information is then computed using software developed by a project partner and subsequently combined with the predetermined cutting trajectory. Consequently, the laser focus was adjusted to the sample's topography during the cutting process, automatically fine-tuning the focus. An example of this functionality is shown in figure 7.18.

Furthermore, experiments were conducted to detect explosives on surfaces post-laser cutting. The surface of the sample (plastic, aluminum) to be cut was contaminated with a defined amount of explosive (1,3,5-Trinitroperhydro-1,3,5-triazine - RDX). The RDX contained in the solvent was dripped onto the object to

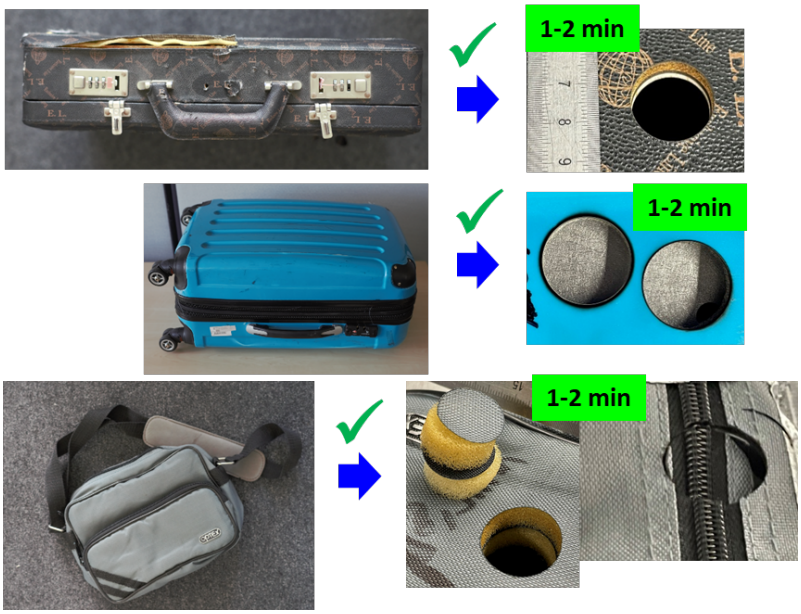

Figure 7.17: Cut samples with respective breakthrough times; from top to bottom: leather case, plastic case, textile bag with zip fastener

be cut and waited until the solvent had evaporated. For this purpose, the sample containing the explosive was clamped in the beam path of the laser beam. The cut was performed with the known parameters. After completing the cutting process, a sampling strip for a mobile ion mobility spectrometer (IMS) was used to wipe the object's surface, and the detectability of the explosive was assessed. The IMS was able to detect explosive amounts greater than 10 ng.

7.4 Summary and Conclusion

This work aimed to develop and test a mobile laser cutting system with sensor-based control for use on explosive objects. The project spanned several phases, each addressing specific components and goals necessary for the realization of this system. In the initial phase, system specifications and conditions were defined. This involved comprehensive state-of-the-art analyses and the identification of system requirements, possible laser and cutting systems, necessary sensors, overall system architecture, and adherence to laser safety regulations. Subsequently, the project focused on determining the laser parameters and ac-

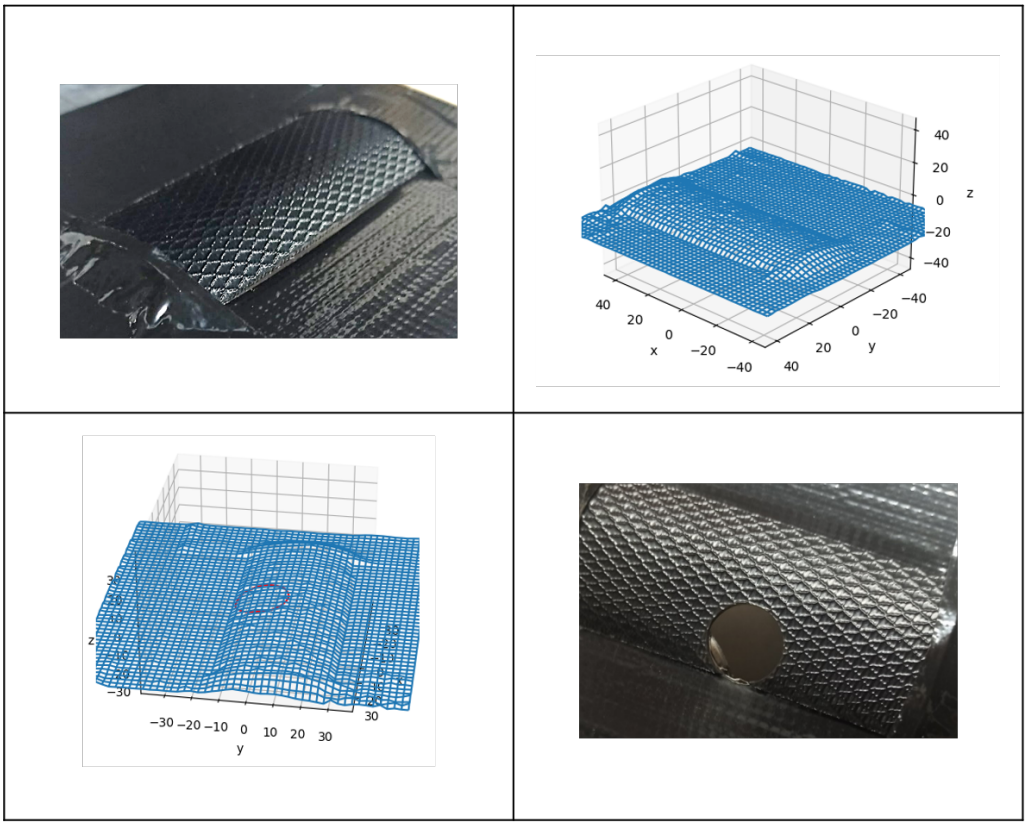

Figure 7.18: Scan of the surface of a curved plastic sample; curved sample (top left), scanned sample (top right), projected circular cut on the sample (bottom left), processed sample (bottom right)

quiring and installing the system. Various laser parameters were tested using a frequency-converted Nd:YAG laser to establish the performance characteristics required for cutting relevant materials, including materials with explosives. These tests determined essential attributes such as laser fluence, wavelength, pulse energy, and repetition rates. Based on these findings, a tailored laser system was specified. The development of subsystems was the next crucial step, which included sensing and cutting monitoring. Key developments included creating a sensor-equipped tube for monitoring and gas extraction, which was essential for capturing and analyzing cutting process data in real-time. The integration of these subsystems with the laser cutting system was a significant milestone, ensuring comprehensive control and safety. System tests and optimization were conducted to refine the demonstrator's performance. These tests involved cutting various materials, including plastics, metals, and composites, to evaluate the system's effectiveness. While initial tests showed promising results, further optimization was necessary. The system demonstrated significant potential for safe and effective cutting of explosive containing objects. The final phase focused on testing and evaluating the system's performance under real-world conditions. The investigations provided valuable insights and established a solid foundation for future advancements in this field. Further efforts are ongoing to secure funding for continued development and real-world testing to realize the system's full potential.

The cuttability of various materials using a nanosecond-pulsed laser system at a wavelength of 515 nm depends on the energy coupling into the material. Good results were achieved with most plastics, wood, cardboard, thin glass, and metal. The system also effectively cut cables or avoided cutting based on sensor responses, which is valuable for bomb disposal operations. However, thicker metal sheets, translucent plastics, and white glass showed poor cuttability, with cutting progress stagnating at deeper layers.

However, the reliability of breakthrough detection was not fully assessed. A thorough evaluation, especially in simulated applications during final testing, was not conducted. The tests carried out show the possibilities of sensory cut depth monitoring and offer a field in the fight against IEDs. For the application on real objects, a larger number of tests are required for which fine-tuning must be carried out. Research into miniaturisation and adaptation/optimisation of the

system is continuing. For example, the use of ultrashort pulse (USP) lasers could open up further dimensions in cutting, although these are currently still too large. The cuttability of the materials has already been tested with the USP laser and delivered promising results, so that further research needs to be carried out into the cuttability of other materials (suitable cutting times) and the appropriate sensor technology.

Acknowledgements

This work was supported by the German *Federal Ministry of Education and Research* via *VDI Technologiezentrum* under grant number 13N14491. We would also like to acknowledge our project partners at *Landeskriminalamt Nordrhein-Westfalen*, *ELP GmbH European Logistic Partners* and the associated partners *Bundeskriminalamt Wiesbaden* and *Bundespolizei Entschärfungsdienst Düsseldorf* for their invaluable contributions to this work. The laser system was provided by *Laser Zentrum Hannover e.V.*.

References

References

[1] Ian Jupp, Anthony Cater, Geraint Dermody, Ian Pleasants, and David Burrows. “Systems and methods for using x-rays”. US20130094627A1. Apr. 2013.

[2] Lodewijk Albert Gerrit Berenschot and Hennie Franciscus Hendrik Leemans. “Method and device for inspecting an object”. NL2009049C2.

[3] Eric Roy Filkins, Erwin Hermans, Robert Schnurer, and Robert W. Smith. “Object scanning using multi-view x-ray images”. US10228486B2. Mar. 2019.

[4] Suresh C. Koppolu, Srinivas Sampathkumaran, Harry M. Markowicz, and Leonid M. Reznik. “System and method for automatic detection of contraband using multi-energy computed tomography”. US8428217B2. Apr. 2013.

[5] Kouichi Fukunaga and Mitsuru Suzuki. “Inspection device and method”. JP2011020228A.

[6] Stanislav Lichorobiec and Karla Barčová. “Possible IED Threat to Airport Premises During Security X-Ray Inspection”. In: *Transactions of the VŠB - Technical University of Ostrava, Safety Engineering Series* X.1 (2015), pp. 31–37. DOI: 10.1515/tvsbses-2015-0005.

[7] Jack L. Glover, Praful Gupta, Nicholas G. Paulter Jr., and Alan C. Bovik. “Study of Bomb Technician Threat Identification Performance on Degraded X-ray Images”. In: *Journal of Perceptual Imaging* 4.1 (2021), pp. 010502-1–010502-13. DOI: 10.2352/J.Percept.Imaging.2021.4.1.010502.

[8] Martin J. Seiffert Timothy G. Pickford and Alexander W. Oslund. “Bomb suit with enhanced blast protection”. US20140260939A1. Sept. 2014.

[9] Jeff Levine, Clint Hedge, Gordana Jeftic-Stojanovski, Matthew Keown, Dan Reddin, Magda Slobozianu, Rob Beland, Sören Buchholtz Nielsen, William Dicke, Matthew Watson, and Shaik Kalaam. “Method and system for protecting personnel from explosive devices”. EP3147624A1. European Patent Application. Mar. 2017.

[10] John Kemp, Elena I. Gaura, and James Brusey. “Instrumenting Bomb Disposal Suits with Wireless Sensor Networks”. In: *Proceedings of the 5th European Workshop on Wireless Sensor Networks*. Coventry, UK: Coventry University, 2008, pp. 17–22.

[11] Inventors: N/A. “Water jet cutting system”. DE10358816A1.

[12] William T. Brooks and Thomas J. O’Brien. “Water jet cutting apparatus”. US20090178548A1. July 2009.

[13] Cheng-Wei Hung, Bor-Cherng Shen, and Min-Han Chiu. “Design and Implementation of Water Jet Device”. In: *Journal of Applied Science and Engineering* 28.4 (2024), pp. 681–690. DOI: 10.6180/jase.202504_28(4).0002.

[14] Veeraphat Tangtongkid, Kerati Suwanpakpraek, and Baramee Patamaprohm. “Design of Lightweight Composite Barrel for Water Jet Disruptor Unit in Bomb Disposal Robot”. In: *International Journal of Mechanical Engineering and Robotics Research* 11.3 (2022), pp. 138–144. DOI: 10.18178/ijmerr.11.3.138-144.

[15] Michael D. Perry, Brent C. Stuart, Paul S. Banks, and Joseph A. Sefcik. "Laser Machining of Explosives". US6150630A. U.S. Patent. Nov. 2000.

[16] John A. Sanchez Ross E. Muenchausen Thomas Rivera. "Method for Laser Machining Explosives and Ordnance". US6559413B1. U.S. Patent. May 2003.

[17] HJ Booth. "Recent applications of pulsed lasers in advanced materials processing". In: *Thin Solid Films* 453-454 (2004), pp. 450–457. DOI: 10.1016/j.tsf.2003.11.130.

[18] Xianshi Jia, Yongqian Chen, Lei Liu, Cong Wang, and Ji'an Duan. "Combined pulse laser: Reliable tool for high-quality, high-efficiency material processing". In: *Optics & Laser Technology* 153 (2022), p. 108209. DOI: 10.1016/j.optlastec.2022.108209.

[19] Tsuneo Kurita, Kazuhisa Komatsuzaki, and Mitsuro Hattori. "Advanced material processing with nano- and femto-second pulsed laser". In: *International Journal of Machine Tools and Manufacture* 48 (2008), pp. 220–227. DOI: 10.1016/j.ijmachtools.2007.08.012.

[20] Urs Zeltner. "Method and Apparatus for Laser Drilling with a Jet Nozzle". US7214904B2. U.S. Patent. May 2007.

[21] Kester Nahen and Alfred Vogel. "Investigations on acoustic on-line monitoring of IR laser ablation of burned skin". In: *Lasers in Surgery and Medicine* 25.1 (1999), pp. 69–78. DOI: 10.1002/(SICI)1096-9101(1999)25:1<69::AID-LSM9>3.0.CO;2-3.

[22] "Laser system for processing and deactivating potentially dangerous objects". WO2010136810A2. World Intellectual Property Organization Patent. Dec. 2010.

[23] G. Chryssolouris. "Sensors in Laser Machining". In: *Annals of the CIRP* 43.2 (1994), pp. 513–519. DOI: 10.1016/S0007-8506(07)60497-1.

[24] Robert H. Schmitt and Guilherme Francisco Mallmann. "Process Monitoring in Laser Micro Machining". In: *Photonik International* (2013), pp. 57–59. URL: https://www.researchgate.net/publication/258521623_Process_monitoring_in_the_laser_micro_machining.

[25] Yang Ji, Alexander W. Grindal, Paul J. L. Webster, and James M. Fraser. “Real-time Depth Monitoring and Control of Laser Machining through Scanning Beam Delivery System”. In: *Journal of Physics D: Applied Physics* 48.15 (2015), p. 155301. DOI: 10.1088/0022-3727/48/15/155301.

[26] Gerhard Holl, Dominik Wild, and C. Theiß. *Lasertechniken zur Beurteilung von Gefahrenlagen mit Objekten mit chemischen und explosiven Gefahrstoffen (LAGEF) : Teilvorhaben: Sichere laserbasierte Probenahme und Analyse : Abschlussbericht zum Verbundprojekt : Zeitraum: Nov. 2014-Okt. 2017*. Report. Freier Zugriff. Hochschule Bonn-Rhein-Sieg, 2017.

Part V

Appendix

List of Abbreviations

Table 7.1: List of Abbreviations

Abbreviation	Meaning
AgN_3	Silver Azide
BIT	Ball Impact Tester
CO_2	Carbon Dioxide (Laser)
DAQ	Data Acquisition
DSC	Differential Scanning Calorimetry
DTA	Differential Thermal Analysis
ECC	Energetic Coordination Compound
EASI-MS	Easy Ambient Sonic-Spray Ionization - Mass Spectrometry
EM	Energetic Material
ESD	Electrostatic Discharge
FS	Friction Sensitivity
FTIR	Fourier Transform Infrared Spectroscopy
HMTD	Hexamethylene Triperoxide Diamine
HNS	Hexanitrostilbene
IED	Improvised Explosive Device
IR	Infrared
LDA	Linear Discriminant Analysis
LIBS	Laser-Induced Breakdown Spectroscopy
MEMS	Micro-Electro-Mechanical Systems
Nd:YAG	Neodymium-Doped Yttrium Aluminium Garnet (Laser)
OZM	Optical Zero Measurement
PCA	Principal Component Analysis
PETN	Pentaerythritol Tetranitrate
PSPME	Planar Solid-Phase Microextraction
PTR-ToF-MS	Proton Transfer Reaction - Time-of-Flight Mass Spectrometry
RDX	Cyclotrimethylene Trinitramine
SNR	Signal-to-Noise Ratio
TATP	Triacetone Triperoxide
VIS	Visible Spectrum
$Pb(N_3)_2$	Lead Azide

List of Publications

Publications

1. Matthias Muhr, Emre Ünal, Phillip Raschke, Thomas Klapötke, Peter Kaul, "Sensor-monitored impact sensitivity investigations on HMTD of different aging stages with accompanying PTR-ToF measurements of the substances" DOI: 10.1080/07370652.2023.2295280
   as published in
   Journal of Energetic Materials 2024, 42, 1-15.

2. Emre Ünal, Matthias Muhr, Jennifer Braun, Thomas M. Klapötke, Peter Kaul,
   "Investigation of Laser-Initiation of Graphite Spray-Coated TATP Accompanied by Sensor-Safe Surveillance and Analytical Monitoring Using Microphone and PTR-ToF-MS"
   Accepted for publication in
   Journal of Energetic Materials, Taylor & Francis, Open Select.

3. Emre Ünal, Matthias Muhr, Thomas M. Klapötke, Peter Kaul,
   "Investigation of Laser Initiation of Graphite-Coated TATP and HMTD With Regard to the Influence of Coating Thickness Accompanied by Sensor-Safe Surveillance Using a Microphone"
   Publication in
   Propellants, Explosives, Pyrotechnics.
   DOI: 10.1002/prep.202400188

4. Emre Ünal, Matthias Muhr, Dominik Wild, Cathrin Theiss, Moritz Schumacher, Gerhard Holl, Peter Kaul,
   "Sensory Monitoring for Breakthrough Detection in Mobile Laser Cutting of Various Materials in the Context of IED Disposal"

Submitted for publication in
IEEE Open Journal of Instrumentation and Measurement.

Conference Poster Presentations

1. Emre Ünal, Matthias Muhr, Thomas Klapötke, Peter Kaul, Investigation of laser-initiation of graphite spray-coated TATP accompanied by sensor-safe surveillance and analytical monitoring using Microphone and PTR-ToF-MS, Proceedings of the SICC Series - CBRNe Conference, Third Edition, 25-29 September 2023, Rome, Italy.

2. Matthias Muhr, Emre Ünal, Peter Kaul, Device development for rapid identification of energetic materials, Proceedings of the International Conference CBRNE Research & Innovation 2024, March 19th - 21st, 2024, Strasbourg, France

3. Emre Ünal, Matthias Muhr, Evaluation of dog training agents with the real substances TATP and HMTD, Poster presentation at the 53rd Annual International Conference of the Fraunhofer ICT, 27 June 2024, Karlsruhe, Germany

Acknowledgements

Zunächst möchte ich mich bei meinem Doktorvater, Herrn Prof. Dr. Klapötke, für die herausragende Betreuung während meiner Promotion bedanken. Von Anfang an haben Sie durch fachliche Diskussionen und wertvollen wissenschaftlichen Input maßgeblich zur Entwicklung dieser Arbeit beigetragen. Ihre unermüdliche Unterstützung, Ihre ständige Verfügbarkeit und Ihre Bereitschaft, wichtige Fragestellungen zu klären, haben die Entstehung und Fertigstellung dieser Dissertation entscheidend geprägt.

Mein besonderer Dank gilt auch Herrn Prof. Dr. Gerhard Holl. Ohne Dich wäre dieses Promotionsprojekt nicht möglich gewesen. Ich danke Dir herzlich für die Initiierung des Projekts, die Vermittlung und Deine umfassende Betreuung. Die anregenden Diskussionen mit Dir haben stets neue Ideen hervorgebracht und der Arbeit eine klare Richtung gegeben. Gerade in Phasen, in denen die Motivation fehlte, haben unsere Gespräche neuen Antrieb und wertvolle Impulse geliefert. Darüber hinaus danke ich Dir für den großen Freiraum, den Du mir für eigene Experimente und kreative Entfaltung ermöglicht hast – stets unterstützt durch die Bereitstellung von Material und Geräten. Auch im persönlichen Bereich habe ich viel von Dir lernen können.

Ebenso möchte ich mich bei Prof. Dr. Peter Kaul bedanken. Deine wissenschaftliche und organisatorische Unterstützung hat diese Promotion maßgeblich geprägt. Du hast mir ermöglicht, an Konferenzen und wissenschaftlichen Veranstaltungen teilzunehmen, was mir wertvolle Erfahrungen und Einblicke beschert hat. Dank Deiner Expertise und Unterstützung konnte ich den praktischen Teil meiner Arbeit mit vielfältigen Möglichkeiten und reibungslosem Ablauf durchführen.

Ein besonderer Dank geht an Matthias Muhr. Während meiner Promotionszeit warst du eine unverzichtbare Stütze. Du hast mir in schwierigen Zeiten zur Seite gestanden, mich motiviert und mir geholfen, Herausforderungen konstruktiv anzugehen. Auch abseits des Wissenschaftlichen warst du ein verlässlicher

Freund und wertvoller Begleiter auf diesem Weg.

Ich möchte auch meiner Frau danken. Dein unerschütterlicher Glaube an mich und deine beständige Motivation haben mir sehr geholfen, meine Ziele zu verfolgen. Ohne deine bedingungslose Unterstützung hätte ich diesen Weg nicht meistern können. Danke, dass du an meiner Seite bist.

Abschließend danke ich meiner Familie. Ihr habt mir die Möglichkeit zur Promotion überhaupt erst eröffnet, mich durch mein Studium begleitet und mich stets motiviert. Ohne eure Unterstützung wäre diese Dissertation nicht entstanden.